Forschungszentrum Karlsruhe
in der Helmholtz-Gemeinschaftt

Wissenschaftliche Berichte
FZKA 7199

Statistical Analysis of Liquid Phase Turbulence Based on Direct Numerical Simulations of Bubbly Flows

M. Ilić

Institut für Reaktorsicherheit
Programm Nukleare Sicherheitsforschung

August 2006

Forschungszentrum Karlsruhe

in der Helmholtz-Gemeinschaft

Wissenschaftliche Berichte

FZKA 7199

Statistical analysis of liquid phase turbulence based on direct numerical simulations of bubbly flows*

Milica Ilić

Institut für Reaktorsicherheit

Programm Nukleare Sicherheitsforschung

*Von der Fakultät für Maschinenbau der Universität Karlsruhe (TH) genehmigte Dissertation

Forschungszentrum Karlsruhe GmbH, Karlsruhe

2006

Forschungszentrum Karlsruhe GmbH
Postfach 3640, 76021 Karlsruhe

Mitglied der Hermann von Helmholtz-Gemeinschaft
Deutscher Forschungszentren (HGF)

ISSN 0947-8620

urn:nbn:de:0005-071995

Abstract

This work presents investigations of liquid phase velocity fluctuations based on direct numerical simulations (DNS) of dilute bubbly flows by the computer code TURBIT-VoF. The investigations are performed by statistical analysis of instantaneous liquid flows generated by the rise of monodisperse bubble-arrays through initially quiescent liquid within a plane semi-infinite channel (phase density ratio 0.5, phase viscosity ratio 1 and bubble Eötvös number 3.065). DNS are conducted for three magnitudes of overall gas volumetric fraction, 0.818%, 4.088% and 6.544%, where one, five and eight ellipsoidal bubbles, respectively, are suspended within a cubic computational domain. Effects of bubble rise velocity, bubble trajectory and bubble shape are analyzed for flow configurations with 8 bubbles with the ratio of liquid viscosity $1 : \sqrt{10} : 10$.

In all the considered bubble-array flows a significant degree of the liquid turbulence anisotropy has been found with the velocity fluctuations in vertical direction being dominant to the horizontal ones. While in very dilute two-phase mixtures the liquid turbulence kinetic energy increases almost linearly with the gas volumetric fraction, in mixtures with the dense bubble packing due to mutual hydrodynamic interactions of bubble wakes a stronger increase of the liquid turbulence kinetic energy with the gas content has been observed.

In order to shed some light on mechanisms governing behaviour of the liquid turbulence kinetic energy in bubble-driven liquid flows, the balance terms in the basic equation for liquid turbulence kinetic energy (k_l equation) are analyzed and the obtained results are used to assess the accuracy of corresponding closure assumptions applied in engineering turbulence models. The main conclusions drawn from these analyzes are as follows.

Evaluations based on rigorous mathematical formulations of balance terms in k_l equation revealed that the fluctuating liquid flow is continuously supplied by energy only through the work of fluctuating liquid stress upon the moving phase interfaces. Since this mechanism is related to the presence of bubbles, the local non-equilibrium between the turbulence generation and turbulence dissipation causes an intensive diffusion transport of liquid turbulence kinetic energy over the flow domain. Especially, the redistribution by the pressure fluctuations is found to be essential.

All currently used engineering approaches strongly overestimate the production term and strongly underestimate the diffusion term. The dissipation term in one-equation models is underestimated in flow regions with high gas volumetric fractions and overestimated in the domains with low gas content. The approximation of the interfacial generation of liquid turbulence kinetic energy by the work of the drag force performs quite well.

Statistische Analyse der Geschwindigkeitsfluktuationen der flüssigen Phase basierend auf direkten numerischen Simulationen von Blasenströmungen

Zusammenfassung
Die vorliegende Arbeit befasst sich mit Untersuchungen der Geschwindigkeitsfluktuationen in der flüssigen Phase basierend auf Ergebnissen der direkten numerischen Simulationen (DNS) von dünnen Blasenströmungen. Die Untersuchungen werden mittels statistischer Analysen der momentanen Flüssigkeitsströmungen durchgeführt, die durch aufsteigende mono-disperse Blasenschwärme in einem halb-unendlichen vertikalen Plattenkanal erzeugt werden (Dichteverhältnis der Phasen 0,5, Viskositätsverhältnis der Phasen 1,0 und Blasen-Eötvös-Zahl 3,065). Die Simulationen umfassen drei Werte des Gasgehalts, 0,818%, 4,088% und 6,544% wobei eine, fünf und acht ellipsoidförmige Blasen in einem kubischen Rechengebiet suspendiert sind. Der Einfluss von Blasenaufstiegsgeschwindigkeit, Blasenbahn und Blasenform wird weiter für Blasenströmungen mit acht Blasen untersucht, bei denen die Viskosität der Flüssigkeit im Verhältnis $1 : \sqrt{10} : 10$ steht.

Alle betrachteten Blasenströmungen zeigen eine signifikante Anisotropie der Flüssigkeitsturbulenz, wobei die Geschwindigkeitsfluktuationen in vertikaler Richtung jeweils über die in horizontaler Richtung dominieren. Während die Turbulenzenergie der Flüssigkeit in sehr dünnen Zweiphasengemischen mit dem Gasgehalt nahezu linear steigt, wird für eine dichtere Packung der Blasen aufgrund der hydrodynamischen Wechselwirkungen der Blasennachläufe ein steilerer Anstieg festgestellt.

Die quantitative Analyse der Bilanzgleichung für die kinetische turbulente Energie der Flüssigkeit (k_l-Gleichung) zeigt, dass dem fluktuierenden Anteil der Flüssigkeitsströmung kontinuierlich Energie durch die Arbeit der flüssigkeitsseitigen fluktuierenden Spannungen an den bewegten Phasengrenzflächen zugeführt wird. Da dieser Mechanismus an die Anwesenheit der Blasen gebunden ist, führt das Nicht-Gleichgewicht zwischen Turbulenz-Erzeugung und Turbulenz-Dissipation zu einem intensiven diffusiven Transport der turbulenten kinetischen Energie innerhalb des Strömungsgebietes. Als wesentlich erweist sich dabei speziell die Umverteilung aufgrund von Druckfluktuationen.

Die DNS basierten Auswertungen der einzelnen Bilanz-Terme in der k_l-Gleichung werden weiterhin verwendet, um Schließungsannahmen in Turbulenzmodellen zu bewerten. Es wird gezeigt, dass alle derzeit verwendeten ingenieurtechnischen Ansätze den Produktionsterm stark überschätzen und den Diffusionsterm stark unterschätzen. Der Dissipationsterm in Eingleichungsmodellen ist unterschätzt in Bereichen mit hohem Gasgehalt und überschätzt in Domänen mit niedrigem Gasgehalt. Dagegen erweisen sich auf der Arbeit der Widerstandskraft basierende Modelle für die grenzflächenbedingte Erzeugung der turbulenten kinetischen Energie der Flüssigkeit als geeignet.

Contents

List of Figures

List of Tables

Nomenclature

Latin characters

a_i	interfacial area concentration
A_i	dimensionless interfacial area concentration, $A_i = a_i l_{ref}$
C_{am}	added-mass coefficient
C_d	drag coefficient
d_b	bubble diameter
$\mathbf{g}$	gravity
Eö_b	bubble Eötvös number
Eö_{ref}	reference Eötvös number
$\mathbf{F}^d$	drag force
f	local liquid volumetric fraction
$\mathbf{I}$	unit tensor
j	superficial velocity
k	turbulence kinetic energy
l_{ref}, l	reference length
l_b	bubble-induced mixing length
l_{si}	shear-induced mixing length
l_{tp}	two-phase mixing length
m	number of mesh cells
M	Morton number
$\mathbf{M}$	interfacial force density
m_{am}	added-mass
$\mathbf{n}$	unit normal vector at phase-interface
n_b	number of bubbles
p	pressure
P	dimensionless pressure (see expression 2.48)
Re_b	bubble Reynolds number
Re_d	bubble drift Reynolds number
Re_{ref}	reference Reynolds number
$\mathbf{T}$	dimensionless stress tensor
$\mathbf{u}$	velocity
u_b	bubble rise velocity
$\langle u_b \rangle$	mean bubble rise velocity

u_d	drift velocity
$\mathbf{u}_r$	relative phase velocity
u_f	friction velocity
u_t	terminal bubble velocity
$\mathbf{U}$	dimensionless velocity
u_{ref}	reference velocity
V	volume
We_b	bubble Weber number
We_{ref}	reference Weber number
$\mathbf{x}$	position vector
x	distance
X	dimensionless distance

Greek characters

α_k	mean volumetric fraction of phase k
$\langle\alpha_g\rangle$	overall gas volumetric fraction
ε	viscous dissipation
η	dimensionless dynamic viscosity, $\eta = \mu/\mu_{ref}$
η_l^K	Kolmogorov length scale for liquid phase turbulence
Γ_μ	phase viscosity ratio
Γ_ρ	phase density ratio
ϕ	redistribution by pressure-strain correlation
Φ_k	indicator function of phase k
κ	curvature
κ	bubble axis aspect ratio
μ	dynamic viscosity
μ_{ref}	reference dynamic viscosity
ν	kinematic viscosity
$\nu^{k\varepsilon}$	eddy viscosity evaluated by $k-\varepsilon$ model
ν^{eff}	effective eddy viscosity
ν^{Diff}	coefficient of diffusion
ν^{Re}	eddy viscosity
ν^b	bubble-induced eddy viscosity
Π	production by mean shear
ϱ	density
ρ	dimensionless density, $\rho = \varrho/\varrho_{ref}$
ϱ_{ref}	reference density
σ	surface tension
τ	stress tensor
ϑ	time
θ	dimensionless time, $\theta = \vartheta u_{ref}/l_{ref}$
Υ	interfacial turbulence terms

Superscripts

$'$	fluctuating
$-$	averaged
$=$	phase averaged
e	ellipsoidal bubble
L	line-averaged
P	plane-averaged
rms	root-mean-square
s	spherical bubble

Subscripts

1	vertical direction
2	span-wise direction
3	wall-normal direction
am	added-mass
b	bubble
d	drag
d	drift
f	friction
k	phase
g	gas
i	interfacial
l	liquid
pt	evaluated by potential flow theory
r	relative
ref	reference
sp	single-phase domain
t	terminal
tp	two-phase mixture / domain
α, β, γ	Cartesian coordinate directions

Chapter 1

Introduction

The two-phase flow pattern where a population of gas bubbles is immersed in a liquid continuum is called *bubbly flow*. Bubbly flows are encountered in a number of natural phenomena such as propagation of sound in oceans, exchange of gases and heat between oceans and the atmosphere and explosive volcanic eruptions. Various types of bubbly flows are also widely used in engineering systems such as power generation, chemical engineering, petro-chemical plants and metallurgical facilities. The applied bubbly flow regimes in these systems span from very slow buoyancy driven flows in bubble columns and air-lift reactors to forced flows in pipes and ducts. Whatever the regime under consideration, low- or high Reynolds number, all bubbly flows have a common characteristic - the relative motion of bubbles induces perturbations of the continuous liquid phase. These fluctuations of the liquid phase pressure and velocity are caused by various mechanisms: random stirring of the liquid by moving bubbles, vortex shedding in the bubble wakes and deformations of gas-liquid interfaces. To emphasize the different nature of such fluctuations from those existing in single-phase flows, the phenomenon is called *bubble-induced turbulence*.

Despite the same fluctuating character the bubble-induced and the shear-induced liquid turbulence interact in a complex manner. In low-sheared flows bubbles enhance the intensity of liquid phase fluctuations [55] [25] [51] [8] [76] [12], whereas in flows with high Reynolds numbers the shear-induced liquid turbulence is often locally suppressed by bubbles [69] [49] [68] [16] [45]. Augmented or attenuated, the resulting liquid phase turbulence is recognized as the key parameter that determines the spatial phase distribution and exchange mechanisms in bubbly flows. A prominent example is provided by the wall void peaking in upward bubbly flows where lift effects are associated with the liquid turbulent entrainment [88] [39] [67]. Another case of practical interest is encountered in stirred vessels and chemical reactors where the dispersed phase tendency to break up the large eddies and create small vortical structures in bubble wakes causes strong mixing beneficial for mass and heat transfer in many industrial processes [74] [23] [37].

A few aforementioned examples imply that the realistic description of the liquid turbulence structure is one of the fundamental requests for accurate predictions of physical processes in bubbly flows. However, contrary to the domain of single-phase flows, where turbulence modelling has already reached a certain level of maturity, models for the liquid turbulence in bubbly flows are still at the infancy [72]. Among several engineering approaches currently used to predict the liquid turbulence, far the most popular concept is based on *balance equation for turbulence kinetic energy of the liquid phase* (hereafter called k_l equation). Balance terms in this equation are formulated by an extension of corresponding closure assumptions well-established for single-phase turbulent flows where the effects of suspended bubbles are either completely ignored or implemented through more or less empirically derived relations. In this context, many proposals available in the literature are contradictory with model parameters mainly fitted to the particular problem under consideration.

Most of the difficulties faced in the development of improved closure assumptions for balance terms in k_l equation concern an extremely poor understanding of mechanisms in which bubbles alter the liquid phase turbulence. Mathematically, these mechanisms were rigorously formulated by derivation of basic balance equations for turbulence kinetic energy in gas-liquid flows [32]. However, although known for more than a decade, these equations could not be exposed to an appropriate quantitative analysis because highly resolved data about the flow field and the phase interface structure required for such an analysis have not been available.

These information cannot be obtained experimentally since even the most advanced techniques such as particle-image-velocimetry yield at best two-dimensional projections of the flow at a given instant in time [7].

Recent improvements in computer performances and positive experience from single-phase flows suggest use of *direct numerical simulations* (DNS). Based on computational grids sufficiently fine to resolve all flow scales and auxiliary algorithms to track gas-liquid interface, DNS of bubbly flows provide complete information on instantaneous three-dimensional flow field and phase-interface topology. In spite of serious limitations concerning the magnitude of liquid Reynolds number and the number of bubbles that can be tracked, DNS approach opens a new promising way to gain a detailed insight into mechanisms governing the liquid turbulence in bubbly flows of practical importance. Various industrial processes, namely, involve slow very dispersed gas-liquid flows where no shear-induced turbulence occurs and where the main flow features such as distribution of phases and mixing are controlled by the bubble agitation of the liquid phase. Among these, the simplest case concerns a confined multi-phase flow where the gas phase is through a distributor sparged into a quiescent liquid medium. A prominent example of such a flow is encountered in flat bubble columns widely used in chemical industries.

Current DNS based liquid turbulence analyses employ the concept of a fully periodic com-

putational domain where an unbounded gas-liquid flow with uniformly sized bubbles and no bubble coalescence is approximated by infinite monodisperse bubble-arrays rising through otherwise quiescent liquid [9] [24]. As the bubbles originally inside the domain leave through one boundary, new ones come in through the opposite boundary. In this way a homogeneous bubbly flow, that allows use of the volume averaging, is put into consideration. Such a flow configuration is, however, not appropriate for the aforementioned quantitative analysis of mechanisms governing the liquid turbulence behaviour because the imposed spatial uniformity excludes considerations of the diffusion transport as well as of the transfer of energy between the mean and fluctuating liquid flow. Consequently, reported turbulence investigations are restricted to evaluations of the liquid turbulence kinetic energy and its dissipation rate [10] [11]. On the other hand, to the best knowledge of the author, no DNS of non-homogeneous multiple bubble systems are reported in the literature.

At the Institute for Reactor Safety of the Research Centre Karlsruhe, where this work is done, *the computer code TURBIT-VoF* for direct numerical simulations of incompressible gas-liquid flows is developed [63] and extensively used for the various analyses of single bubble rise [85] [84] [83] [21]. Different to other DNS codes, TURBIT-VoF is designed to perform computations of a gas-liquid flow within the domain confined with two rigid walls. In relation to this, DNS of multiple bubble systems by TURBIT-VoF can quite realistically approximate a non-homogeneous developed gas-liquid flow within a flat bubble column with the moderate ratio of the bubble diameter to the column depth and, in this way, provide an appropriate data basis for the corresponding analyses of mechanisms governing the behaviour of liquid turbulence kinetic energy.

The fascinating issue of turbulence phenomena in bubbly flows, the popularity of liquid turbulence models based on k_l equation and the availability of TURBIT-VoF code motivated the research to be presented in this work. The objective of the research concerns investigations of liquid phase velocity fluctuations by DNS of bubbly gas-liquid flows. The main goals of the research are:

1. to conduct DNS of non-homogeneous bubble-column-like flows and provide input data basis for sophisticated analyses of liquid phase turbulence behaviour on the level of its rigorous mathematical formulation,

2. to perform statistical analyzes of bubble-induced liquid velocity fluctuations with the special emphasis focused on the distribution of liquid turbulence kinetic energy and its interplay with flow parameters such as velocity field, phase distribution and phase interface topology,

3. to elucidate mechanisms of generation, redistribution and dissipation of liquid turbulence kinetic energy by quantitative analysis of balance terms in k_l equation on the basis of their basic mathematical formulation and

4. to estimate the accuracy of closure assumptions for balance terms in k_l equation and to discuss possibilities for improvement of their performance.

The presentation of the performed research is organized as follows.

The chapter 2 reports the background information needed for the investigation of liquid phase turbulence by DNS of bubbly flows. In this context, the rigorous mathematical description of liquid phase turbulence is presented, currently used engineering models for the liquid turbulence in bubbly flows are reviewed and the methodology implemented in the computer code TURBUT-VoF is outlined.

In the chapter 3 the bubbly flow pattern to be simulated is described, the detailed specification of computational set-up for DNS by computer code TURBIT-VoF is presented and the computed motion of bubbles is analyzed in detail.

The statistical analyzes of the computed liquid motion is presented in the chapter 4, where the data about the instantaneous liquid flow are completed evaluating the interfacial liquid velocity and pressure, appropriate averaging techniques are adopted and computed statistical characteristics of the mean and fluctuating liquid flow are discussed. A special attention is paid to the analyzes of liquid turbulence kinetic energy by considering effects of the suspended gas content and the liquid phase viscosity.

The chapter 5 focuses on the quantitative analysis of balance equation for liquid turbulence kinetic energy. Using DNS data the diffusion transport, viscous dissipation, interfacial generation and transfer of turbulence kinetic energy between the mean and fluctuating liquid flow are evaluated on the basis of their rigorous mathematical formulations and the obtained results are discussed in detail. The relation between different mechanisms governing the liquid turbulence in simulated bubbly flows is analyzed considering the budget of k_l equation.

The objective of the chapter 6 is the assessment of closure assumptions for balance terms in k_l equation. In relation to this, performance of commonly used closure assumptions is tested against the corresponding balance terms evaluated in the chapter 5.

The work is completed by conclusions.

Chapter 2

Background information for investigating liquid turbulence by direct numerical simulations of bubbly flows

This chapter reports the background information that motivated the investigation of liquid phase turbulence by direct numerical simulations of bubbly flows. The chapter is organized as follows. The first section presents the basic balance equations for the liquid phase turbulence where the mathematical formulation of turbulence phenomena is rigorous. The section 2 reviews the current status of liquid turbulence models applied in engineering modelling of bubbly flows. The methodology implemented in the computer code TURBIT-VoF for direct numerical simulations of gas-liquid bubbly flows is outlined in section 3.

2.1 Mathematical formulation of liquid turbulence in bubbly-flows: a review

The relative motion of bubbles induces fluctuations of liquid phase quantities giving rise to Reynolds stresses and other phenomena inherent to the turbulence. Mathematically, these phenomena were rigorously formulated by Kataoka and Serizawa [32] and Kataoka et al. [31] who derived conservation equations for the turbulence kinetic energy and Reynolds stresses in gas-liquid flows. Based on these two references this section presents basic equations for the liquid phase turbulence in bubbly flows.

The basic equations for turbulence in gas-liquid mixtures are derived for an adiabatic,

incompressible two-phase flow without mass transfer between the phases. The starting point in the derivation method represent local instant conservation equations for mass and momentum of the liquid phase, respectively given by:

$$\Phi_l \frac{\partial \hat{u}_{l\beta}}{\partial x_\beta} = 0 \tag{2.1}$$

$$\Phi_l \frac{\partial \hat{u}_{l\alpha}}{\partial \vartheta} + \Phi_l \frac{\partial}{\partial x_\beta}(\hat{u}_{l\alpha}\hat{u}_{l\beta}) = -\Phi_l \frac{1}{\varrho_l}\frac{\partial \hat{p}_l}{\partial x_\alpha} + \Phi_l \frac{1}{\varrho_l}\frac{\partial \hat{\tau}_{l\alpha\beta}}{\partial x_\beta} + \Phi_l g_\alpha, \tag{2.2}$$

where the subscripts α, β and γ denote Cartesian coordinate directions, the subscript l indicates the liquid phase[1], ϱ_l denotes the liquid density and g_α stands for the gravity vector. The instantaneous liquid velocity and pressure are indicated by $\hat{u}_{l\alpha}$ and $\hat{p}_l$, respectively, while the instantaneous viscous stress of the liquid phase is defined by:

$$\hat{\tau}_{l\alpha\beta} = \mu_l\left(\frac{\partial \hat{u}_{l\alpha}}{\partial x_\beta} + \frac{\partial \hat{u}_{l\beta}}{\partial x_\alpha}\right), \tag{2.3}$$

where μ_l represents the liquid molecular viscosity. The liquid phase indicator function, Φ_l, is formulated as:

$$\begin{aligned} \Phi_l(\mathbf{x},\vartheta) &= 1 \quad \text{if } (\mathbf{x},\vartheta) \text{ is occupied by the liquid phase} \\ &= 0 \quad \text{otherwise} \end{aligned} \tag{2.4}$$

for any space point $\mathbf{x}$ and time instant ϑ.

Applying appropriate averaging (time, spatial or ensemble) on 2.1 and 2.2 the following conservation equations of averaged mass and momentum, respectively, can be derived:

$$\frac{\partial \overline{\overline{u}}_{l\beta}}{\partial x_\beta} = -\frac{1}{\overline{\overline{\Phi}}_l}\overline{u'_{li\beta} n_{l\beta} a_i} \tag{2.5}$$

$$\begin{aligned} \frac{\partial \overline{\overline{u}}_{l\alpha}}{\partial \vartheta} + \frac{\partial(\overline{\overline{u}}_{l\alpha}\overline{\overline{u}}_{l\beta})}{\partial x_\beta} = &-\frac{1}{\varrho_l}\frac{\partial \overline{\overline{p}}_l}{\partial x_\alpha} + \frac{1}{\varrho_l}\frac{\partial}{\partial x_\beta}(\overline{\overline{\tau}}_{l\alpha\beta} - \varrho_l \overline{\overline{u'_{l\alpha}u'_{l\beta}}}) - \frac{\overline{\overline{u}}_{l\alpha}}{\overline{\overline{\Phi}}_l}\overline{u'_{li\beta} n_{l\beta} a_i} - \frac{1}{\overline{\overline{\Phi}}_l}\frac{1}{\varrho_l}\overline{p'_{li} n_{l\alpha} a_i} \\ &+ \frac{1}{\overline{\overline{\Phi}}_l}\frac{1}{\varrho_l}\overline{\tau'_{li\alpha\beta} n_{l\beta} a_i} + \frac{1}{\overline{\overline{\Phi}}_l}\frac{1}{\varrho_l}\overline{\overline{u'_{l\alpha}u'_{l\beta}}\,\overline{n_{l\beta}a_i}}, \end{aligned} \tag{2.6}$$

where the subscript i denotes the value at the phase interface[2], $n_{l\alpha}$ indicates the outward unit normal vector at the liquid side of the phase interface and a_i represents the local instant interfacial area concentration (interfacial area per unit volume). The single overbar denotes

[1] Einstein's summation rule applies to the subscripts α, β and γ, while the rule does not apply to the subscript l

[2] Einstein summation rule is not applied to this subscript

the averaging, while the double overbar indicates the so-called phase-weighted averaging defined as:

$$\overline{\overline{\Psi}}_l = \frac{\overline{\Phi_l \hat{\Psi}_l}}{\overline{\Phi}_l}, \tag{2.7}$$

where $\hat{\Psi}_l$ represents an arbitrary instantaneous quantity of the liquid phase. Fluctuating parts of liquid quantities within the bulk fluid and at the phase interface are, respectively, given by:

$$\Psi_l^{'} = \hat{\Psi}_l - \overline{\overline{\Psi}}_l \quad \text{and} \quad \Psi_{li}^{'} = \hat{\Psi}_{li} - \overline{\overline{\Psi}}_l. \tag{2.8}$$

The mass conservation equation for fluctuating terms is obtained subtracting 2.5 from 2.1:

$$\Phi_l \frac{\partial u_{l\beta}^{'}}{\partial x_\beta} = -\frac{\Phi_l}{\overline{\Phi}_l} \overline{u_{li\beta}^{'} n_{l\beta} a_i}, \tag{2.9}$$

while subtracting 2.6 from 2.2 gives the momentum conservation equation for fluctuating terms:

$$\begin{aligned} \Phi_l \frac{\partial u_{l\alpha}^{'}}{\partial \vartheta} + \Phi_l \frac{\partial}{\partial x_\beta}(u_{l\alpha}^{'} u_{l\beta}^{'} + u_{l\alpha}^{'} \overline{\overline{u}}_{l\beta} + u_{l\beta}^{'} \overline{\overline{u}}_{l\alpha}) = -\Phi_l \frac{1}{\varrho_l} \frac{\partial p_l^{'}}{\partial x_\alpha} + \Phi_l \frac{1}{\varrho_l} \frac{\partial}{\partial x_\beta}(\tau_{l\alpha\beta}^{'} + \overline{\overline{u_{l\alpha}^{'} u_{l\beta}^{'}}}) \\ + \frac{\Phi_l}{\overline{\overline{\Phi}}_l} \overline{\overline{u}}_{l\alpha} \overline{u_{li\beta}^{'} n_{l\beta} a_i} + \frac{\Phi_l}{\overline{\overline{\Phi}}_l} \frac{1}{\varrho_l} \overline{p_{li}^{'} n_{l\alpha} a_i} - \frac{\Phi_l}{\overline{\overline{\Phi}}_l} \frac{1}{\varrho_l} \overline{\tau_{li\alpha\beta}^{'} n_{l\beta} a_i} - \frac{\Phi_l}{\overline{\overline{\Phi}}_l} \frac{1}{\varrho_l} \overline{\overline{u_{l\alpha}^{'} u_{l\beta}^{'}}}\, \overline{n_{l\beta} a_i}. \end{aligned} \tag{2.10}$$

Multiplying 2.10 by $u_{l\beta}^{'}$ and averaging one obtains the basic conservation equation of liquid Reynolds stress, $\overline{\overline{u_{l\alpha}^{'} u_{l\beta}^{'}}}$. The general form of this equation is given as [31]:

$$\frac{\partial}{\partial \vartheta}(\overline{\Phi}_l \overline{\overline{u_{l\alpha}^{'} u_{l\beta}^{'}}}) + \frac{\partial}{\partial x_\beta}(\overline{\Phi}_l \overline{\overline{u}}_{l\beta} \overline{\overline{u_{l\alpha}^{'} u_{l\beta}^{'}}}) = \text{Diff} + \Pi_{l\alpha\beta} + \phi_{l\alpha\beta} + \varepsilon_{l\alpha\beta} + \Upsilon_{l\alpha\beta}, \tag{2.11}$$

where the first four terms on the right-hand-side represent:

- diffusion

$$\text{Diff} = \frac{1}{\varrho_l} \frac{\partial}{\partial x_\beta}(\overline{\Phi}_l \overline{\overline{\tau_{l\alpha\beta}^{'} u_{l\gamma}^{'}}} + \overline{\Phi}_l \overline{\overline{\tau_{l\gamma\beta}^{'} u_{l\alpha}^{'}}}) - \frac{\partial}{\partial x_\beta}(\overline{\Phi}_l \overline{\overline{u_{l\alpha}^{'} u_{l\beta}^{'} u_{l\gamma}^{'}}}) - \frac{1}{\varrho_l} \frac{\partial}{\partial x_\alpha}(\overline{\Phi}_l \overline{\overline{p_l^{'} u_{l\gamma}^{'}}}) - \frac{1}{\varrho_l} \frac{\partial}{\partial x_\gamma}(\overline{\Phi}_l \overline{\overline{p_l^{'} u_{l\alpha}^{'}}}),$$

- production by mean shear

$$\Pi_{l\alpha\beta} = -\overline{\Phi}_l \left(\overline{\overline{u_{l\alpha}^{'} u_{l\beta}^{'}}} \frac{\partial \overline{\overline{u}}_{l\gamma}}{\partial x_\beta} + \overline{\overline{u_{l\beta}^{'} u_{l\gamma}^{'}}} \frac{\partial \overline{\overline{u}}_{l\alpha}}{\partial x_\beta} \right),$$

- redistribution by pressure-strain correlation

$$\phi_{l\alpha\beta} = \overline{\Phi}_l \frac{1}{\varrho_l} \left(\overline{\overline{p_l^{'} \frac{\partial u_{l\gamma}^{'}}{\partial x_\alpha}}} + \overline{\overline{p_l^{'} \frac{\partial u_{l\alpha}^{'}}{\partial x_\gamma}}} \right) \quad \text{and}$$

- viscous dissipation

$$\varepsilon_{l\alpha\beta} = -\overline{\Phi}_l \frac{1}{\varrho_l}\Big(\overline{\overline{\tau'_{l\alpha\beta}\frac{\partial u'_{l\gamma}}{\partial x_\beta}}} + \overline{\overline{\tau'_{l\gamma\beta}\frac{\partial u'_{l\alpha}}{\partial x_\beta}}}\Big).$$

Except for being multiplied by $\overline{\Phi}_l$ these terms are analogous to those in the Reynolds stress equation for single-phase turbulence and are, therefore, named single-phase-like terms. The last term on the right-hand-side of equation 2.11 is given by:

$$\Upsilon_{l\alpha\beta} = -\frac{1}{\varrho_l}(\overline{p'_{li}u'_{li\gamma}n_{l\alpha}a_i} + \overline{p'_{li}u'_{li\alpha}n_{l\gamma}a_i}) + \frac{1}{\varrho_l}(\overline{\tau'_{li\alpha\beta}u'_{li\gamma}n_{l\beta}a_i} + \overline{\tau'_{li\gamma\beta}u'_{li\alpha}n_{l\beta}a_i}) \tag{2.12}$$

and represents the peculiarity of gas-liquid flows. This term, namely, takes into account effects of bubble interfaces on the liquid phase turbulence and is called interfacial term.

From practical point of view the turbulence kinetic energy of the liquid phase,

$$k_l = \frac{\overline{\overline{u'_{l\alpha}u'_{l\alpha}}}}{2}, \tag{2.13}$$

is the fundamental turbulence quantity because it represents the basis for the number of engineering turbulence models[3]. Applying the methodology[4] analogous to the one used to derive 2.11 the basic equation of the liquid turbulence kinetic energy in bubbly flows can be formulated as [32]:

$$\begin{aligned}\frac{\partial}{\partial\vartheta}(\overline{\Phi}_l k_l) + \frac{\partial}{\partial x_\beta}(\overline{\Phi}_l k_l \overline{\overline{u}}_{l\beta}) = &-\frac{1}{\varrho_l}\frac{\partial}{\partial x_\alpha}(\overline{\Phi}_l\overline{\overline{p'_l u'_{l\alpha}}}) - \frac{\partial}{\partial x_\beta}(\overline{\Phi}_l\frac{1}{2}\overline{\overline{u'_{l\alpha}u'_{l\alpha}u'_{l\beta}}}) + \frac{1}{\varrho_l}\frac{\partial}{\partial x_\beta}(\overline{\Phi}_l\overline{\overline{\tau'_{l\alpha\beta}u'_{l\alpha}}})\\ &-\frac{1}{\varrho_l}\overline{\Phi}_l\overline{\overline{\tau'_{l\alpha\beta}\frac{\partial u'_{l\alpha}}{\partial x_\beta}}} - \overline{\Phi}_l\overline{\overline{u'_{l\alpha}u'_{l\beta}}}\frac{\partial\overline{\overline{u}}_{l\alpha}}{\partial x_\beta} - \frac{1}{\varrho_l}\overline{p'_{li}u'_{li\alpha}n_{l\alpha}a_i} + \frac{1}{\varrho_l}\overline{\tau'_{li\alpha\beta}u'_{li\alpha}n_{l\beta}a_i}.\end{aligned} \tag{2.14}$$

Similar to 2.11 on the right-hand-side of 2.14 two groups of terms can be distinguished. The group of single-phase-like terms involves the diffusion (the three first terms), the viscous dissipation (the fourth term) and the production by mean shear (the fifth term), while the interfacial transport of the liquid turbulence kinetic energy is represented by the last term.

2.2 Engineering models for liquid turbulence in bubbly flows: a review

Predictions of liquid phase Reynolds stresses in bubbly flows of practical interest cannot be performed by equation 2.11 since it requires highly resolved data about the instantaneous

[3]The review of engineering models for the liquid turbulence in bubbly flows is given in the next section.

[4]Note that the conservation equation for the liquid turbulence kinetic energy can be obtained by taking the trace of the equation 2.11.

three-dimensional liquid flow and the phase interface topology. Instead, in engineering praxis various modelling approaches are developed to struggle the liquid phase turbulence. This section reviews the current status of the liquid turbulence models.

The important role that the Reynolds stress term, $\overline{\overline{\mathbf{u}_l'\mathbf{u}_l'}}$, plays even in very slow bubble-driven liquid flows has been proven when the modelling of a locally aerated flat bubble column was attempted without taking into account turbulence effects [18] [71]. That such an approach may not be accepted as a reliable one was shown by Sokolochin and Eigenberger [71], who reported an excellent agreement of their numerical results with the one of Delinoij et al. [18], but a strong disagreement with the experimental data obtained by Becker et al. [2] for the same bubble column. Moreover, it was shown that this so-called **laminar** approach strongly depends on the refinement of the imposed numerical grid - the finer the grid, the more resolved vortices.

In majority of references the modelling of the liquid phase turbulence is based on the assumption that Boissinesq eddy-viscosity concept can be extended on two-phase gas-liquid flows. Reynolds stress in this concept is related to the mean velocity of the liquid phase by [78]:

$$\overline{\overline{\mathbf{u}_l'\mathbf{u}_l'}} = \nu_l^{Re}(\nabla\overline{\overline{\mathbf{u}}}_l + \nabla\overline{\overline{\mathbf{u}}}_l^T) - \frac{2}{3}\mathbf{I}k_l, \tag{2.15}$$

where ν_l^{Re} represents the eddy viscosity of the liquid phase, k_l indicates the liquid turbulence kinetic energy as defined by 2.13 and $\mathbf{I}$ denotes the unit tensor. Concerning the way followed to evaluate the eddy viscosity of the liquid phase, ν_l^{Re}, three principally different approaches can be distinguished: so-called algebraic models, one-equation $(k-l)$ models and two-equation $(k-\varepsilon)$ models.

Algebraic models. One of the first proposals for the evaluation of the liquid phase eddy viscosity is given by Sato et al. [65] [64]. They supposed that ν_l^{Re} can be expressed as the sum of the shear-induced eddy viscosity (modelled using relations originally developed for single-phase flows) and the bubble-induced eddy viscosity defined by the following algebraic expression:

$$\nu_l^b = 0.6\alpha_g d_b|\overline{\overline{\mathbf{u}}}_r|, \tag{2.16}$$

where α_g denotes the mean gas volumetric fraction, d_b represents bubble diameter and $\overline{\overline{\mathbf{u}}}_r$ stands for the mean relative velocity between the phases.

Michiyoshi and Serizawa [49] used a similar approach expressing the eddy viscosity induced by bubbles in terms of the terminal bubble velocity, u_t, as:

$$\begin{aligned} \nu_l^b = \quad & 0.06\alpha_g l_0(\frac{y}{r})u_t D(y^+) \quad \text{for } y > d_b \\ & 1.2\alpha_g(\frac{y}{r})u_t D(y^+) \quad \text{for } y^* < y < d_b, \end{aligned} \tag{2.17}$$

where y represents the radial distance from the pipe wall and y^+ denotes the distance from the wall beyond which bubbles cannot penetrate. Parameters l_0 and m are given in terms of

pipe radius, r, and the mean gas volumetric fraction, α_g. The wall damping factor, $D(y^+)$, is defined using van Driest's expression for single-phase flows (see for example [82]).

Contrary to the aforementioned approaches, where only the enhancement of the liquid turbulence due to the bubble agitation can be accounted for, the algebraic model developed by Kataoka et al. [36] provides also the evaluation of the turbulence suppression induced by bubbles. In this model the eddy viscosity is using the coefficient $\beta_1 = 0.56$ related to two-phase mixing length, l_{tp}, by:

$$\nu_l^{Re} = \beta_1 l_{tp} \sqrt{k_l}. \tag{2.18}$$

The two-phase mixing length, l_{tp}, is assumed to be a linear superposition of the mixing length due to shear-induced turbulence, l_{si}, and the mixing length due to bubble-induced turbulence, l_b:

$$l_{tp} = l_{si} + l_b. \tag{2.19}$$

The shear-induced mixing length is given as: $l_{si} = 0.4y$, while the mixing length induced by bubbles is defined by: $l_b = \alpha_g d_b/3$. Radial distribution of the liquid turbulence kinetic energy is evaluated from:

$$k_l = \left[\frac{3}{4}\frac{l_{tp}}{d_b}\frac{\alpha_g C_d}{0.04\alpha_l + \alpha_g l_{tp}/d_b}\right]^{\frac{2}{3}} u_t^2, \tag{2.20}$$

where α_l represents the mean liquid volumetric fraction and C_d denotes the drag force coefficient.

k-l models. Further development of the presented model of Kataoka et al. [36] resulted in the so-called $k-l$ model [34] [33] [35]. In this model the turbulence kinetic energy of the liquid phase is, instead by algebraic expression 2.20, determined by the following transport equation:

$$\frac{\partial \alpha_l k_l}{\partial \vartheta} + \nabla \cdot (\alpha_l k_l \overline{\overline{\mathbf{u}}}_l) = \mathrm{Diff}(k_l) + \Pi_l - \varepsilon_l + \Upsilon_l. \tag{2.21}$$

The three first terms on the right-hand-side of the equation above represent the group of single-phase-like terms, diffusion, production by mean shear and viscous dissipation of the liquid turbulence kinetic energy, respectively, while the last term takes into account effects of bubble interfaces.

The influence of the dispersed gas phase on the turbulence diffusion, production by mean shear and dissipation is taken into account introducing the two-phase mixing length defined by 2.19 into the corresponding closure relations originally established for single-phase flows. The mixing length of shear-induced turbulence is evaluated using the following single-phase relation:

$$l_{si} = 0.4y(1 - e^{-\frac{yu_f}{26\nu_l}}), \tag{2.22}$$

where u_f represents the friction velocity and ν_l stands for the kinematic viscosity of the liquid phase. The model for the bubble-induced mixing length, l_b, is based on the assumption that the movement of a bubble across the control surface causes exchange of the liquid in the amount of the bubble volume and is given by:

$$\begin{aligned} l_b &= \frac{1}{3}\alpha_g d_b \qquad \text{for} \quad \frac{3}{2}d_b \leq y \leq r \\ &= \frac{1}{6}\alpha_g[d_b + (y - 0.5d_b)] \quad \text{for} \quad d_b \leq y \leq \frac{3}{2}d_b \\ &= \frac{1}{6}\left[d_b + \frac{\frac{4}{3} - \frac{y}{d_b}}{2 - \frac{4}{3}\frac{y}{d_b}}\right] \quad \text{for} \quad 0 \leq y \leq d_b. \end{aligned} \tag{2.23}$$

The interfacial term, Υ_l, accounts for two effects: the turbulence absorption by bubbles (related to small scales of gas-liquid interface and expressed in terms of the liquid turbulence velocity and the mean gas volumetric fraction) and the turbulence generation by bubbles (related to the relative motion of bubbles and expressed through the work of the drag force).

$\mathbf{k-\varepsilon}$ models. $k-\varepsilon$ models for bubbly gas-liquid flows are derived by an adjustment of transport equations for turbulence kinetic energy and its dissipation rate of the well-established single-phase $k-\varepsilon$ model (see for example [61] or [82]).

In the simplest approach [80] [86] [57] [66] [59] the original form of the balance terms from the single-phase $k-\varepsilon$ model (production, diffusion and dissipation) is kept and the influence of the dispersed phase is taken into account only through the multiplication of the whole equation by the mean liquid volumetric fraction, α_l. Due to its similarity to the single phase $k-\varepsilon$ model, this approach is, usually, called *standard* $k-\varepsilon$ model.

In more complex approaches the effects of suspended bubbles on the liquid phase turbulence are included in model. In this context, two main directions in the development of $k-\varepsilon$ models for bubbly flows can be identified.

In the first one, hereafter called *extended* $k-\varepsilon$ model, transport equations for liquid turbulence kinetic energy, k_l, and its dissipation rate, ε_l, constituting the standard $k-\varepsilon$ model are extended by additional closure terms that account for effects of bubble interfaces [73] [26] [70] [3] [47] [78] [54] [22] [74] [50]. In this context, the structure of the transport equation for the liquid turbulence kinetic energy is identical to the one used in $k-l$ models (see equation 2.21), while the following form of the transport equation for the turbulence energy dissipation rate is applied:

$$\frac{\partial \alpha_l \varepsilon_l}{\partial \vartheta} + \nabla \cdot (\alpha_l \varepsilon_l \overline{\overline{\mathbf{u}}}_l) = \mathrm{Diff}(\varepsilon_l) + \frac{\alpha_l}{\tau}\left[C_{\varepsilon 1}\Pi_l - C_{\varepsilon 2}\varepsilon_l\right] + \Upsilon_l^{\varepsilon}, \tag{2.24}$$

where τ denotes the time scale of turbulence, $\tau = k_l/\varepsilon_l$, Υ_l^{ε} represents the interfacial term and 'standard' constants of the single-phase $k-\varepsilon$ model, $\sigma_\varepsilon = 1.3$, $C_{\varepsilon 1} = 1.44$ and $C_{\varepsilon 2} = 1.92$, are retained.

The evaluation of the liquid phase Reynolds stresses in both, the standard and the extended $k-\varepsilon$ model, is based purely on the Boussinesq hypothesis (equation 2.15). On the other side, when the representative eddy viscosity of the liquid phase is concerned, various approaches can be found in the literature. The basis for all of them represents the eddy viscosity evaluated by corresponding $k-\varepsilon$ model:

$$\nu_l^{k\varepsilon} = C_\mu \frac{k_l^2}{\varepsilon_l}, \tag{2.25}$$

where $C_\mu = 0.09$. However, in addition to $\nu_l^{k\varepsilon}$ some authors take into account the liquid kinematic viscosity, ν_l, and/or the bubble-induced eddy viscosity, ν_l^b, as proposed by Sato et al. [65] [64] (see equation 2.16).

The second approach [47] [46] [73] [42] [53] is based on the assumption that the total turbulence kinetic energy of the liquid phase, k_l, can be decomposed into two statistically independent contributions: a real turbulence part, k_{l0}, induced by mean shear that also contains the turbulence generated in bubble wakes and an irrotational part named pseudo turbulence, k_{lb}, that involves liquid velocity fluctuations generated through the liquid displacement by moving bubbles:

$$k_l = k_{l0} + k_{lb}. \tag{2.26}$$

The real turbulence is modelled by the standard single-phase transport equation multiplied by the mean liquid volumetric fraction:

$$\frac{\partial \alpha_l k_{l0}}{\partial \vartheta} + \nabla \cdot (\alpha_l k_{l0} \overline{\overline{\mathbf{u}}}_l) = \mathrm{Diff}(k_{l0}) + \Pi_l - \varepsilon_{l0}. \tag{2.27}$$

It is noted that the structure of the equation above is only apparent. It is, namely, the result of the assumption that the total dissipation rate, ε_l, can be decomposed into two independent contributions: the one due to cascading, ε_{l0}, and the one in bubble wakes, ε_{lw}. Such an idea originates from Lance and Bataille [43], who observed that in homogeneous bubbly flows turbulence eddies generated in bubble wakes were dissipated by the viscosity before their spectral transfer could take place. Assuming that this result might be extended to a large range of bubbly flows the formulation of the transport equation for k_{l0} is significantly simplified since the closure assumptions for the generation and dissipation of the liquid turbulence kinetic energy in bubble wakes do not have to be specified explicitly. Further, the transport equation for the dissipation rate reduces to its single-phase form since only ε_{l0} remains to be determined. For this purpose the following single-phase-like transport equation is employed:

$$\frac{\partial \alpha_l \varepsilon_{l0}}{\partial \vartheta} + \nabla \cdot (\alpha_l \varepsilon_{l0} \overline{\overline{\mathbf{u}}}_l) = \mathrm{Diff}(\varepsilon_{l0}) + \frac{\alpha_l}{\tau_0}\left[C_{\varepsilon 1}\Pi_l - C_{\varepsilon 2}\varepsilon_{l0}\right], \tag{2.28}$$

where the time constant due to the eddy stretching is given by:

$$\tau_0 = \frac{k_{l0}}{\varepsilon_{l0}}. \tag{2.29}$$

The pseudo turbulence transport is, formally, modelled by the following first-order relaxation type equation [47]:

$$\frac{\partial \alpha_l k_{lb}}{\partial \vartheta} + \nabla \cdot (\alpha_l k_{lb} \overline{\overline{\mathbf{u}}}_l) = \mathrm{Diff}(k_{lb}) + \frac{1}{\tau_b}(k_{lb}^a - k_{lb}), \tag{2.30}$$

that contains the diffusion term and the source term taking into account added mass effects. However, in practical applications k_{lb} is set equal to its asymptotic value k_{lb}^a given by:

$$k_{lb}^a = \frac{1}{2}\alpha_g C_{am} |\overline{\overline{\mathbf{u}}}_r| \tag{2.31}$$

where C_{am} represents the coefficient of the added mass force.

It is noted that in addition to the characteristic time scale of turbulent eddy stretching, τ_0, as defined by 2.29, this approach involves the time scale related to the relative motion of bubbles:

$$\tau_b = C_R \frac{d_b}{|\overline{\overline{\mathbf{u}}}_r|}, \tag{2.32}$$

where C_R is a constant. For that reason, the models based on the aforementioned methodology are named *two-time-scale* $k - \varepsilon$ models.

Reynolds stress in two-time-scale $k - \varepsilon$ models is evaluated as the sum of a turbulent contribution evaluated by the Bousinesq expression 2.15 and a pseudo turbulent term, $2Ak_{lb}$, where A represents the anisotropy matrix. Theoretically, this matrix is a function of the bubble shape and the bubble trajectory, but in practice it is approximated with the diagonal matrix $A = [4/10, 3/10, 3/10]$ derived for the case of a potential flow around a spherical bubble. The liquid phase eddy viscosity in the Bousinesq expression is, principally, evaluated employing the standard $k - \varepsilon$ formula:

$$\nu_{l0}^{k\varepsilon} = C_\mu \frac{k_{l0}^2}{\varepsilon_{l0}}, \tag{2.33}$$

but, like in the case of the extended $k - \varepsilon$ model, magnitude of $\nu_{l0}^{k\varepsilon}$ is, in some references, increased by adding ν_l and / or ν_l^b as given by 2.16.

Beyond the Boussinesq's hypothesis two types of models for the liquid phase turbulence have been developed: algebraic stress models and differential stress models.

Algebraic stress models. Modelling of the liquid phase turbulence by use of an algebraic stress model (ASM) represents the further development of the two-time-scale $k - \varepsilon$ model. In ASM the pseudo turbulent Reynolds stress is evaluated in the same way as in the two-time scale $k - \varepsilon$ model, but in the evaluation of the turbulent Reynolds stress part the Bousinesq hypothesis is replaced by an algebraic stress law. It is, however, noted that no specific two-phase algebraic stress law has been developed, but well-established single-phase formulations are employed. Thus, while Lahey et al. [42] [40] [38] [41] applied the

approximation proposed by Rodi [61], Afshar and Baliga [1] used the algebraic stress law of Gataski and Speziale [20].

Differential stress models. In order to allow for the different development of various Reynolds stresses, differential stress models employ balance equations for the individual components, $\overline{\overline{u'_{l\alpha}u'_{l\beta}}}$. Similar to considerations of the liquid turbulence kinetic energy, two different approaches are applied to establish transport equations for liquid Reynolds stresses.

In the first one, applied by Lopez de Bertodano et al. [48] and Lance et al. [44], the balance of the total Reynolds stress in the liquid phase, $\overline{\overline{u'_{l\alpha}u'_{l\beta}}}$, is considered. Lopez de Bertodano et al. extended the single phase form of transport equations for $\overline{\overline{u'_{l\alpha}u'_{l\beta}}}$ with an interfacial term defined as:

$$\Upsilon_l = C_i F_\alpha^d \overline{\overline{u}}_{r\alpha}, \tag{2.34}$$

where F_α^d represents the drag force exerted by bubbles to the liquid and the parameter $C_i \leq 1.0$ takes into account that the turbulence induced by bubbles is of smaller length scale than the shear-induced turbulence. This source is, further, assumed to be shared only among normal Reynolds stresses:

$$\Upsilon_{l\alpha\beta} = [4/5, 3/5, 3/5]\Upsilon_l. \tag{2.35}$$

Lance et al. [44], however, kept such a structure only apparently adopting the mentioned hypothesis of production-dissipation equilibrium in bubble wakes under which interfacial effects on the turbulence generation / dissipation are not explicitly specified in the transport equations.

In the other approach followed by Chahed et al. [15] [13] [14] the total Reynolds stress of the liquid phase is decomposed into two contributions that can be linearly superimposed: a turbulent part, $\overline{\overline{u'_{l\alpha}u'_{l\beta}}}^0$, and a non-dissipative pseudo-turbulent part, $\overline{\overline{u'_{l\alpha}u'_{l\beta}}}^b$, induced by the liquid displacement by moving bubbles. The hypothesis of the equilibrium of the turbulence generation-dissipation in bubble wakes is here also adopted implying that the differential equations for $\overline{\overline{u'_{l\alpha}u'_{l\beta}}}^0$ reduce to its single-phase form. Transport equations for $\overline{\overline{u'_{l\alpha}u'_{l\beta}}}^b$ include the diffusion term, the interfacial turbulence production by added mass force:

$$\Upsilon^b_{l\alpha\beta} = 0.5\frac{D}{D\vartheta}\alpha_g \overline{\overline{u}}_{r\alpha}\overline{\overline{u}}_{r\alpha}, \tag{2.36}$$

where $D/D\vartheta$ denotes material derivative, and the term that accounts for the liquid turbulence redistribution by the pressure strain correlation:

$$\Phi^b_{l\alpha\beta} = \frac{3}{10}\Upsilon^b_{l\gamma\gamma}\delta_{\alpha\beta} - \frac{9}{10}\Upsilon^b_{l\alpha\beta}, \tag{2.37}$$

where $\delta_{\alpha\beta}$ represents the unit tensor.

While Lopez de Bertodano et al. directly applied the single-phase Daly-Harlow diffusion model (see for examle [61]), Chahed et al. used the following form of the diffusion term:

$$\mathrm{Diff}(\psi) = \frac{C_{s\psi}}{\alpha_l}\frac{\partial}{\partial x_\alpha}\left[\alpha_l\left(\tau_0\overline{\overline{u_{l\alpha}^{'}u_{l\beta}^{'}}}^{0} + \tau_b\overline{\overline{u_{l\alpha}^{'}u_{l\beta}^{'}}}^{b}\right)\frac{\partial\psi}{\partial x_\beta}\right], \tag{2.38}$$

where ψ stands for the turbulent, $\overline{\overline{u_{l\alpha}^{'}u_{l\beta}^{'}}}^{0}$, i.e. the pseudo turbulent, $\overline{\overline{u_{l\alpha}^{'}u_{l\beta}^{'}}}^{b}$, part of liquid Reynolds stress, $C_{s\psi} = 0.11$ and the time scales τ_0 and τ_b are defined in the same way as in the two-time constant $k-\varepsilon$ model (by 2.29 and 2.32, respectively).

Similar to single-phase flows the pressure-strain correlation is decomposed into two contributions: the slow term and the rapid term. Lance et al. and Chahed et al. assumed that the motion of bubbles is not relevant to the rapid term and that its single-phase functional form is valid for dilute bubbly flows. On the other side, the authors did modifications of the slow term attempting to incorporate effects of experimentally observed increased tendency towards isotropy in bubbly flows [43]. For this purpose the time scale of turbulent stretching in the single-phase formulation of Launder (see for example [61]) is modified. Therefore, while Lance et al. formulated the slow term considering the entire turbulence in the liquid phase:

$$\phi_{l\alpha\beta}^{st} = (C_1\frac{k_l}{\varepsilon_{l0}} + C_3\frac{|\overline{\overline{\mathbf{u}}}_r|}{d_b})\left(\overline{\overline{u_{l\alpha}^{'}u_{l\beta}^{'}}} - \frac{2}{3}k_l\right), \tag{2.39}$$

where $C_1 = 2.2$ and $C_3 = 8$, Chahed et al. took into account only the turbulent part of the Reynolds stress in order to avoid inappropriate redistribution rates when the pseudo-turbulence is high:

$$\phi_{l\alpha\beta}^{st} = C_1(\tau_0^{-1} + \alpha_g\tau_b^{-1})\left(\overline{\overline{u_{l\alpha}^{'}u_{l\beta}^{'}}}^{0} - \frac{2}{3}k_{l0}\right), \tag{2.40}$$

where $C_1 = 1.8$.

Lopez de Bertodano et al. followed a different approach. Therefore, they kept original form of Launder's expression for both the slow and the rapid term, and took into account the bubble presence introducing the following additional term:

$$\phi_{l\alpha\beta}^{b} = -C_2\big(\Upsilon_{l\alpha\beta} - \frac{\Upsilon_{l\gamma\gamma}}{3}\delta_{\alpha\beta}\big), \tag{2.41}$$

where $\Upsilon_{l\alpha\beta}$ represents the interfacial source of turbulence as defined by 2.35.

2.3 Computer code TURBIT-VoF for direct numerical simulations of bubbly flows

The computer code TURBIT-VoF developed[5] at the Institute for Reactor Safety of the Research Centre Karlsruhe is used to perform direct numerical simulations (DNS) of bubbly gas-liquid flows to be presented in this work. For an easy reference the methodology applied in TURBIT-VoF is here briefly presented. More details can be found in [62], [63] and [21].

The attention is focused on an adiabatic flow of two incompressible immiscible Newtonian fluids without phase change. Theoretically, such a flow is formulated by local instantaneous conservation equations for mass 2.1 and momentum 2.2. A numerical simulation of two-phase flows on the basis of these equations would require computational grids with an extent of refinement which provides not only that no cell contains two-phase mixture, but also that the boundary layer at the phase interface is resolved. Imposing such grids on a two-phase flow domain is not practical due to high computational costs as well as the deterioration of the accuracy and stability of the numerics with the increased complexity of the interfacial topology. Instead, in DNS of gas-liquid flows local instant equations 2.1 and 2.2 are firstly locally averaged and then discretized on grids with a currently acceptable resolution.

In TURBIT-VoF the averaging of an arbitrary instantaneous phase quantity $\hat{\Psi}_k$ is performed applying the following operators:

$$\Psi_k = \frac{1}{V}\int_V \hat{\Psi}_k \Phi_k(\mathbf{x},\vartheta)dV \quad \text{and} \quad \Psi_{k,k} = \frac{1}{V_k}\int_V \hat{\Psi}_k \Phi_k(\mathbf{x},\vartheta)dV, \tag{2.42}$$

where the subscript k indicates the phase ($k = l$ for the liquid and $k = g$ for the gas), Φ_k indicates phase indicator function, V represents the volume of mesh cell and V_k stands for the volume of mesh cell occupied by the phase k. In the text hereafter, this type of averaging is named local in order to distinguish it from the one applied in the later turbulence analysis.

Applying the local averaging on the liquid phase indicator function, Φ_l, a new quantity named the local liquid volumetric fraction:

$$f = \frac{1}{V}\int_V \Phi_l(\mathbf{x},\vartheta)dV, \tag{2.43}$$

is introduced. Physically, f represents the fraction of cell volume occupied by the liquid phase and, different to the stepwise liquid phase indicator function, Φ_l, takes a continuous value between zero and unity.

[5]The code is originally developed by Sabisch [62] for the purpose of DNS of adiabatic dilute bubbly flows in plane channels. Further, it was significantly improved by Ghidersa [21], who considered slug flow in small rectangular channels and included procedures for simulation of heat transfer phenomena.

Using the local liquid volumetric fraction to define mixture material properties such as density and viscosity:

$$\varrho = f\varrho_l + (1-f)\varrho_g \text{ and } \mu = f\mu_l + (1-f)\mu_g \tag{2.44}$$

and mixture flow properties such as center-of-mass velocity and pressure:

$$\mathbf{u} = \frac{f\varrho_l\mathbf{u}_{l,l} + (1-f)\varrho_g\mathbf{u}_{g,g}}{f\varrho_l + (1-f)\varrho_g} \text{ and } p = fp_{l,l} + (1-f)p_{g,g}, \tag{2.45}$$

the behaviour of both phases, the liquid and the gas, as well as the dynamic boundary condition at the phase interface can be described by a single set of governing equations that express conservation of mass and momentum within the entire computational domain. In TURBIT-VoF these equations are given in the following dimensionless form:

mass:

$$\nabla \cdot \mathbf{U} = 0 \tag{2.46}$$

momentum:

$$\frac{\partial \rho \mathbf{U}}{\partial \theta} + \nabla \cdot (\rho \mathbf{U}\mathbf{U}) = -\nabla P + \frac{1}{\mathrm{Re}_{ref}}\nabla \cdot \mathbf{T} - \frac{(1-f)\mathrm{E\ddot{o}}_{ref}}{\mathrm{We}_{ref}}\frac{\mathbf{g}}{|\mathbf{g}|} + \frac{\kappa A_{in}}{\mathrm{We}_{ref}}\mathbf{n}, \tag{2.47}$$

where the following scaling applies:

$$\theta = \frac{\vartheta u_{ref}}{l_{ref}},\ \rho = \frac{\varrho}{\varrho_{ref}},\ \mathbf{U} = \frac{\mathbf{u}}{u_{ref}},\ \mathbf{T} = \frac{l_{ref}}{\mu_{ref}u_{ref}}\tau,\ P = \frac{p - \varrho_l\mathbf{g}\cdot\mathbf{x}}{\varrho_{ref}u_{ref}^2} \text{ and } A_{in} = l_{ref}a_{in}, \tag{2.48}$$

with the material properties of the liquid phase taken to be reference values ($\varrho_{ref} = \varrho_l$ and $\mu_{ref} = \mu_l$) and the reference length, l_{ref}, and reference velocity, u_{ref}, to be specified. The reference Reynolds, Weber and Eötvos number appearing as the result of scaling are, respectively, given by:

$$\mathrm{Re}_{ref} = \frac{\varrho_l u_{ref} l_{ref}}{\mu_{ref}},\quad \mathrm{We}_{ref} = \frac{\varrho_l u_{ref}^2 l_{ref}}{\sigma} \quad \text{and} \quad \mathrm{E\ddot{o}}_{ref} = \frac{(\varrho_l - \varrho_g)|\mathbf{g}|l_{ref}^2}{\sigma}, \tag{2.49}$$

where σ represents the surface tension. The third term on the right-hand-side of the momentum equation 2.47 represents the buoyancy term, while the last term expresses the contribution of the surface tension force (κ stands for twice the mean dimensionless interface curvature and $\mathbf{n}$ represents the unit normal vector at the phase interface pointing from the gas to the liquid phase).

Employing the transport equation for the local liquid volumetric fraction:

$$\frac{\partial f}{\partial \theta} + \mathbf{U} \cdot \nabla f = 0, \tag{2.50}$$

flow regions containing pure liquid ($f = 1$) are distinguished from the pure gas ones ($f = 0$). If $0 < f < 1$, an interface exists within the computational cell. In such cells the model of a homogeneous two-phase mixture is applied where the equality of phase velocities and pressures is assumed.

The equation 2.50 is numerically solved employing a Volume-of-Fluid (VoF) procedure. The interface orientation and location inside each mesh cell is first reconstructed using a rather geometrical method EPIRA (Exact Plane Interface Reconstruction Algorithm) which yields a linearly-accurate interface reconstruction on a three-dimensional structured orthogonal non-equidistant fixed grids. The algorithm belongs to the class of PLIC (Piecewise Linear Interface Calculation) methods which employ straight oblique lines to reconstruct the interface and provide more accurate allocation of fluid properties and interfacial area. Once the updated interface information is known liquid fluxes across the faces of the mesh cell can be computed and the local liquid volumetric fraction can precisely be advected.

The Navier-Stokes equations are solved by a standard finite difference projection method on the staggered three-dimensional Eulerian grid. All spatial derivatives are evaluated by second order centered differences, while the integration over time is performed by an explicit third order Runge-Kutta scheme.

The methodology is verified comparing numerical results with experimental data for the rise of an ellipsoidal bubble and an oblate ellipsoidal cap bubble [63].

Chapter 3

Direct numerical simulations of bubble-array flows with computer code TURBIT-VoF

This chapter deals with direct numerical simulations (DNS) of dilute bubbly flows performed in order to provide an input data basis for statistical analyses of the liquid phase turbulence. The chapter is organized as follows. In the first section the bubbly flow pattern to be simulated is described and different simulation scenarios are outlined. The section 2 presents the detailed specification of computational setup for DNS by the computer code TURBIT-VoF. The analyses of DNS results presented in this chapter mainly concern the dynamics of bubbles. In this context, the section 3 focuses on the analyses of bubble trajectories and bubble velocities as well as on the parameters concerning the bubble shape and the bubble orientation. Peculiarities of the bubble-induced liquid flow are, due to its relevance to the liquid phase turbulence characteristics, presented in the next chapter.

3.1 Definition of bubble-array flow

This section describes bubbly flow configurations for which direct numerical simulations (DNS) by the computer code TURBIT-VoF are performed.

The simulated flow pattern is named *bubble-array flow*. The term 'bubble-array flow' refers to the flow regime where monodisperse arrays of bubbles rise through otherwise stagnant liquid within a plane infinite channel. The simplest case of such a flow is depicted in Figure 3.1. For the sake of clarity, only one array of bubbles is displayed. The whole bubble-array flow can be imagined as an entity where the array presented in Figure 3.1 is

indefinite number of times periodically repeated in the lateral non-wall direction. From the geometrical and hydrodynamical point of view such a flow domain can fully be represented by a fixed doubly periodic unit cell highlighted on the right-hand-side of Figure 3.1. In this context, two types of bubble-array flow can be distinguished.

Fixed bubble-array flow corresponds to the flow pattern presented in Figure 3.1 where only one bubble is suspended within the periodic cell. Such a definition of the flow configuration implies that all the bubbles within the whole channel are of an identical shape, move with the same velocity and are at constant distances from their neighbours.

Free bubble-array flow represents a flow pattern where the periodic cell contains a swarm of several freely interacting bubbles. The number of bubbles within the swarm is specified to be constant by preventing the bubble coalescence. As the bubble population in this flow configuration is denser than in the case of the fixed bubble-array flow, the rise of an individual bubble is through the mutual interactions of bubble wakes influenced by the motion of other bubbles. Therefore, despite the same equivalent diameter, the bubbles within a free bubble-array are, in principle, not of an identical shape and do not rise with the same velocity.

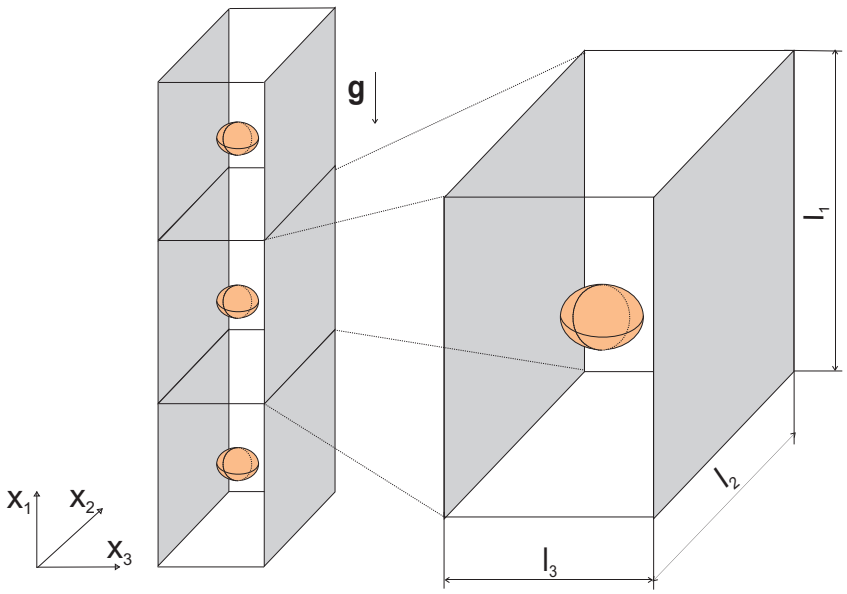

Figure 3.1: Fixed bubble-array flow with extracted unit cell.

Although the developed flow regime in flat bubble columns is more realistically described by the concept of free bubble-arrays than by the pattern consisting of fixed bubble-arrays,

the latter is for the following two reasons used as the first approximation. First, due to its simplicity (only one phase interface within computational domain, less agitated liquid flow) this flow configuration was more convenient for developing and testing the computational tool needed for statistical analysis of the bubble-induced liquid phase fluctuations. Second, comparing characteristics of liquid phase perturbations generated by fixed bubble-arrays with the ones driven by free bubble-arrays the effects of the bubble relative motion can be distinguished from the effects of hydrodynamic interactions between bubble wakes.

In order to examine how the magnitude of overall gas content and the distribution of suspended bubbles influence the liquid velocity fluctuations, the motion of monodisperse bubble populations involving different number of suspended bubbles is simulated.

Finally, the influence of physical properties of gas-liquid system on the agitation of the liquid phase by moving bubble swarms is considered. In this purpose, the motion of geometrically identical free bubble-arrays through the liquids with different viscosity is computed.

3.2 Computational set-up for direct numerical simulations of bubble-array flows

Employing the computer code TURBIT-VoF in total five numerical experiments with bubble-array flows are conducted: one with the fixed bubble-array and four with free bubble-arrays. Computations are performed on a single processor of Fujitsu VPP 5000 parallel vector computer. Since the analyses of the liquid turbulence structure require the knowledge on steady state flow characteristics, numerical runs are associated with the long CPU time and high computational costs. This section presents the geometrical, physical and initial parameters of conducted DNS. For an easy reference the details of the computational setup used to specify all the simulations of bubble-array flows are summarized in Table 3.1.

3.2.1 Geometrical parameters of simulations

The computational domain for all the simulations is specified to be a cubic channel bounded with two vertical rigid walls. The size of the domain is $l_1 = l_2 = l_3 = l = l_{ref}$. The domain is discretized with 64^3 uniform mesh cells. Imposed boundary conditions are non-slip ones at the lateral rigid walls and periodic ones in stream-wise (x_1) and span-wise (x_2) direction. The equivalent bubble diameter, d_b, in all the simulations is prescribed to be one fourth of the computational domain size and is, thus, resolved with 16 mesh cells.

Since the assumption of incompressibility is adopted for both phases, the overall gas volumetric fraction can be expressed only in terms of geometrical quantities as:

$$\langle \alpha_g \rangle = \frac{n_b d_b^3 \pi}{6 l^3}, \tag{3.1}$$

where n_b represents the number of bubbles contained within the computational domain.

In the case of fixed bubble-array flow the overall gas volumetric fraction is $\langle \alpha_g \rangle = 0.818\%$, i.e. a very dilute bubbly flow is considered.

DNS with free bubble-arrays are performed for two magnitudes of overall gas volumetric fraction. A dilute mixture ($\langle \alpha_g \rangle = 4.088\%$) is simulated with five bubbles suspended within the flow domain, while the lower limit of a moderate bubbly flow ($\langle \alpha_g \rangle = 6.544\%$) is achieved in the numerical experiment where the swarm consists of eight bubbles. The flow configuration with 8 bubbles is not chosen arbitrarily, but seems to be the densest one that the current version of TURBIT-VoF can successfully track during the long time period needed to reach the steady flow regime and under the request of no bubble coalescence. The population consisting of 5 bubbles is also chosen on purpose. Hence, when a swarm with an odd number of bubbles rises within a channel confined with two vertical walls, the phase distribution is suspected to differ significantly from the one where the swarm involves an even number of bubbles - the dispersion of bubbles towards lateral channel walls almost symmetrically with respect to the channel axis is expected in the scenario with 8 bubbles, but not in the scenario with 5 bubbles. In this context, comparing perturbations of the liquid phase induced by the rise of 5 bubbles with the ones generated by the motion of 8 bubbles one can analyze, not only the influence of the overall gas volumetric fraction, $\langle \alpha_g \rangle$, but also the effects of the bubble distribution on the liquid phase turbulence.

3.2.2 Physical parameters of fluids

The influence of physical parameters on the rise of gas bubbles with the equivalent diameter d_b and the density ϱ_g through the liquid with the density ϱ_l and the viscosity μ_l is taken into account by bubble Eötvös number and Morton number respectively defined as:

$$\mathrm{E\ddot{o}}_b = |\mathbf{g}| d_b^2 \frac{(\varrho_l - \varrho_g)}{\sigma} \text{ and } \mathrm{M} = |\mathbf{g}| \mu_l^4 \frac{\varrho_l - \varrho_g}{\varrho_l^2 \sigma^3}, \tag{3.2}$$

where $\mathbf{g}$ represents the gravity and σ stands for the surface tension.

In all the performed simulations of bubble-array flows $\mathrm{E\ddot{o}}_b = 3.065$ is specified. The simulation of the fixed bubble-array flow (further called scenario 1BM6[1]) and free bubble-array flow with 5 bubbles (scenario 5BM6) are performed specifying $\mathrm{M} = 3.06 \cdot 10^{-6}$. In

[1]Bubble-array scenarios are named following the pattern 'n_bBMm' where n_b represents the number of bubbles suspended within the computational domain and m indicates the order of magnitude of specified Morton number.

this way all the parameters of the simulation scenario 1BM6 are chosen to be the same as in [63], where the ability of TURBIT-VoF to accurately predict the shape, the path and the rise velocity of a single bubble moving within an initially quiescent liquid was validated through the comparison of numerical results with experimental data.

In order to analyze the influence of bubble shape and bubble rise velocity on characteristics of generated liquid flow, free bubble-array flow simulations with 8 bubbles are performed for three different values of Morton number. In Figure 3.2 specified physical parameters of two-phase systems are highlighted in the diagram of Clift et al. [17].

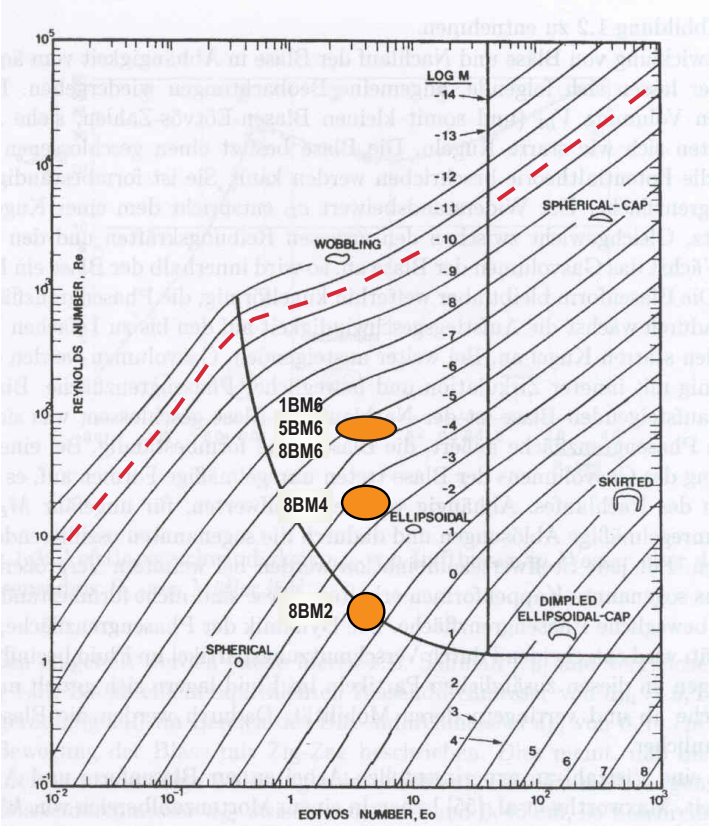

Figure 3.2: Diagram of Clift et al. [17] used for the preliminary estimation of bubble shape and bubble rise velocity. Dashed red line represents air bubbles in water.

It is noted that this diagram is established for the case of a single bubble rising within an unbounded domain filled with quiescent liquid and can, thus, provide only a rough estimate of bubble parameters for rather different flow conditions prescribed here (doubly periodic flow domain confined with two rigid walls, multiple bubble flow with intensive bubble-wake interactions). Nevertheless, it is expected that a decrease of Morton number

from $\mathrm{M} = 3.06 \cdot 10^{-2}$ (scenario 8BM2) to $\mathrm{M} = 3.06 \cdot 10^{-4}$ (scenario 8BM4) will cause change in the bubble shape from spherical to slightly ellipsoidal. A further decrease of Morton number to $\mathrm{M} = 3.06 \cdot 10^{-6}$ (scenario 8BM6) should result in an increase of the ellipsoid axis aspect ratio. Physically, such a decrease of Morton number while keeping Eötvos number constant can be achieved by choosing the liquid phase of a lower viscosity.

In Figure 3.2 it can be seen that the specified values of bubble Eötvös number and Morton number are rather far from that, for practice more interesting, case of air bubbles in water. Such a choice is dictated by the expected bubble deformation and bubble Reynolds number:

$$\mathrm{Re}_b = \frac{\varrho_l d_b u_b}{\mu_l}, \tag{3.3}$$

where u_b denotes the bubble rise velocity. The current numerical scheme and limited computer resources, namely, make it difficult to perform long-time three dimensional computations of bubble swarms consisting of bubbles that exhibit complex unsteady motion characterized by wobbling and rocking, vortex shedding and shape oscillations. This constrain is not associated only with TURBIT-VoF, but is more a general problem associated with DNS of bubbly flows. Moreover, while a number of authors have simulated the motion of a single bubble, for multiple bubble systems the literature is quite limited. To the best knowledge of the author the most complex simulations of free bubble-array flows are carried out by Bunner and Tryggvason. In [9] and [10] they considered even 216 bubbles. However, specified parameters of the simulation (fully periodic computational domain, $\mathrm{Eö}_b = 1, \mathrm{M} = 1.543 \cdot 10^{-4}$) resulted in a rather academic flow configuration with a spherical bubble shape and almost rectilinear bubble trajectories. Their most recent paper [11] reports the simulation of free arrays consisting of ellipsoidal bubbles. Although 27 bubbles were tracked, due to the larger computational domain, the overall gas volumetric fraction in [11] is the same as in here presented simulation scenarios with 8 bubbles, $\langle \alpha_g \rangle = 6.544\%$. However, when the agitation of the liquid phase is concerned the ellipsoidal bubbles in here specified numerical experiment 8BM6 are expected to be more aggressive than the ones simulated in [11]. This statement is based on the higher magnitude of expected bubble Reynolds number in the simulation run 8BM6 (see Figure 3.2) than $\mathrm{Re}_b \sim 25$ achieved in the computations reported by Bunner and Tryggvason [11].

The ratios of phase densities and viscosities:

$$\Gamma_\varrho = \frac{\varrho_g}{\varrho_l} \text{ and } \Gamma_\mu = \frac{\mu_g}{\mu_l} \tag{3.4}$$

are physical parameters that also have to be specified. Although these ratios are very low in most bubbly flows, for computational reasons the simulations are performed for the following values: $\Gamma_\varrho = 0.5$ and $\Gamma_\mu = 1$. The choice of these parameters was motivated by results reported by Wörner [84] [83], who using TURBIT-VoF investigated the influence of the density ratio on the rise of a single ellipsoidal bubble with parameters $\mathrm{Eö}_b = 3.065$, $\mathrm{M} = 3.06 \cdot 10^{-6}$ and $\Gamma_\mu = 1$. Comparing results of numerical simulations for Γ_ϱ =0.5,

0.2, 0.1 and 0.02 he found that the phase density ratio, Γ_ϱ, has a notable influence on the initial acceleration of the bubble, but does not affect the bubble shape and bubble Reynolds number when the bubble terminal velocity was reached. Moreover, the liquid velocity scaled by the bubble rise velocity turned out to be virtually independent on Γ_ϱ when the steady flow regime was reached.

The fluids are taken to be free of contaminants so that the tangential stress is continuous across the phase interface.

3.2.3 Initial conditions and time step width

The fixed bubble-array flow is simulated starting from an initial situation where one spherical bubble is positioned in the centre of the channel filled with stagnant liquid.

In numerical experiments with free bubble-arrays 5BM6, 8BM6 and 8BM2 spherical bubbles are placed inside the quiescent liquid and arranged by slight perturbations of a regular pattern in each coordinate direction. In order to save computational time, initial conditions for the scenario 8BM4 are derived from the computed steady flow regime of the simulation run 8BM2.

The time step width is estimated considering the criteria imposed by the convective, viscous, capillary and buoyancy force, respectively formulated as [83]:

$$\Delta\theta_c = \frac{\triangle x}{\max|u_n|}, \quad \Delta\theta_\mu = \frac{1}{6}\triangle x^2 \mathrm{Re}_{ref} \min\left(\frac{\Gamma_\varrho}{\Gamma_\mu}\right), \quad \Delta\theta_\sigma = \sqrt{\frac{\triangle x^3}{4\pi}\mathrm{We}_{ref}(1+\Gamma_\varrho)}$$
$$\text{and} \quad \Delta\theta_g = 2\triangle x\left\{\max|u_n| + \sqrt{\left(\max|u_n|\right)^2 + \frac{4\triangle x}{\Gamma_\varrho}\left|\frac{\mathrm{Eö}_{ref}}{\mathrm{We}_{ref}}\right|}\right\}, \qquad (3.5)$$

where Δx represents the mesh cell size of a uniform grid and the subscript $n = 1, 2, 3$ indicates Cartesian coordinate directions. The reference Reynolds, Eötvös and Weber number are computed from:

$$\mathrm{Eö}_{ref} = \left(\frac{l_{ref}}{d_b}\right)^2 \mathrm{Eö}_b, \quad \mathrm{We}_{ref} = \frac{\mathrm{Eö}_{ref}}{1-\Gamma_\varrho}\frac{u_{ref}^2}{|\mathbf{g}|l_{ref}^2} \quad \text{and} \quad \mathrm{Re}_{ref} = \left(\frac{\mathrm{Eö}_{ref}\mathrm{We}_{ref}^2}{\mathrm{M}}\right)^{0.25},$$

with the reference length and the reference velocity respectively specified as $l_{ref} = 4m$ and $u_{ref} = 1m/s$.

The width of the dimensionless time step actually used in computations, $\Delta\theta$, is determined when the minimal value evaluated by 3.5, $\min(\Delta\theta_c, \Delta\theta_\mu, \Delta\theta_\sigma, \Delta\theta_g)$, is multiplied by a safety factor. In the simulation of the fixed bubble-array flow this safety factor is taken to be 0.2, while in the more dynamic cases of free bubble-array flows even more rigid value of 0.1

turned out to be necessary. The magnitudes of the time step width specified for different simulation cases are presented in Table 3.1.

3.2.4 Prevention of bubble-wall interaction

An inspection of the momentum equation 2.47 shows that an additional body force, $-\varrho_l \mathbf{g}$, is imposed on both fluids. This force is equivalent to the pressure gradient generated by the base of a flow container which prevents the gravitational force to cause the acceleration of the entire flow field in the downward vertical direction. As a consequence, the velocity field in the whole domain will be oriented upwards. Such a flow situation could be acceptable for DNS of the fixed bubble-array flow because in that case the bubble rises rectilinearly upwards through the central part of the channel and makes no interaction with lateral channel walls. However, when a free bubble-array flow is concerned, due to the denser bubble population as well as lateral bubble movements, the liquid velocity profile in the vicinity of channel walls decides the destiny of simulations.

Ellipsoidal bubbles in an upward liquid flow are, namely, exposed to the action of lift force [88] that makes them move towards the wall (see Figure 3.3a). On the other side, repelling action of the wall force ensures the existence of the liquid layer along the channel walls that prevents bubbles touch the wall. However, since this liquid film is very thin, it cannot be resolved by TURBIT-VoF.

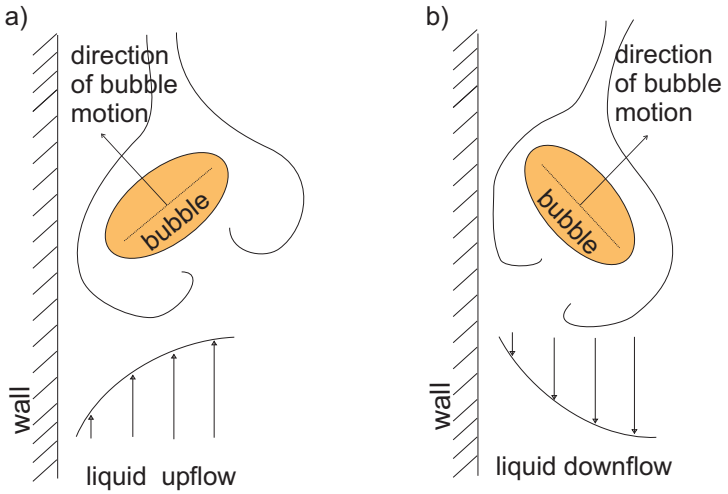

Figure 3.3: Preferential direction of bubble motion in the vicinity of rigid wall within an upward (a) and a downward (b) liquid flow.

Therefore, in its approaching to the wall the bubble touches it. As the methodology currently implemented in TURBIT-VoF is not able to resolve phase interface in such a

situation, the simulation has to be stopped. On the other hand, when the liquid flow is oriented downwards, the direction of the lift force changes and, instead towards the wall, an ellipsoidal bubble is pushed towards the core region of the channel (see Figure 3.3b).

In order to provide a downward flow of the liquid phase in the vicinity of the channel walls, the magnitude of the additional body force from the equation 2.47 had to be decreased. Therefore, in the simulations of bubble-array flows presented here the additional body force is specified as $-\langle\varrho\rangle\mathbf{g}$, where $\langle\varrho\rangle = \varrho_l + \langle\alpha_g\rangle(\varrho_g - \varrho_l)$ represents the mean density of the two-phase mixture. Consequently, the buoyancy term in the momentum equation 2.47 takes the following form:

$$-\frac{(1-f-\langle\alpha_g\rangle)\mathrm{E\ddot{o}}_{ref}}{\mathrm{We}_{ref}}\frac{\mathbf{g}}{|\mathbf{g}|}, \tag{3.6}$$

where f represents the local liquid volumetric fraction.

Table 3.1: Computational set-up specified in DNS of bubble-array flows with code TURBIT-VoF

type of bubble-array flow	fixed	free			
simulation scenario	1BM6	5BM6	8BM6	8BM4	8BM2
reference length	$4m$	$4m$	$4m$	$4m$	$4m$
reference velocity	$1m/s$	$1m/s$	$1m/s$	$1m/s$	$1m/s$
computational domain size[a]	1x1x1	1x1x1	1x1x1	1x1x1	1x1x1
number of grid points	64^3	64^3	64^3	64^3	64^3
bubble equivalent diameter[a]	0.25	0.25	0.25	0.25	0.25
number of bubbles	1	5	8	8	8
overall gas volume fraction	0.818%	4.088%	6.544%	6.544%	6.544%
phase density ratio	0.5	0.5	0.5	0.5	0.5
phase viscosity ratio	1	1	1	1	1
Morton number	$3.06 \cdot 10^{-6}$	$3.06 \cdot 10^{-6}$	$3.06 \cdot 10^{-6}$	$3.06 \cdot 10^{-4}$	$3.06 \cdot 10^{-2}$
bubble Eötvös number	3.065	3.065	3.065	3.065	3.065
reference Eötvös number	49.05	49.05	49.05	49.05	49.05
reference Weber number	2.5	2.5	2.5	2.5	2.5
reference Reynolds number	100	100	100	31.6	10
time step width[a]	10^{-4}	$0.5 \cdot 10^{-4}$	$0.5 \cdot 10^{-4}$	$0.5 \cdot 10^{-4}$	$0.5 \cdot 10^{-4}$
initial conditions	stagnant	stagnant	stagnant	8BM2[b]	stagnant

[a] scaled

[b] steady state flow regime from scenario 8BM2 is used to specify initial conditions for scenario 8BM4

3.3 Analyses of computed three-dimensional motion of bubble-arrays

Our intuition suggests that the bubble-induced velocity fluctuations of the liquid phase are strongly related to the dynamics of bubbles. This is, particulary, expected in free bubble-array flows where, owning to the proximity of other bubbles, the motion of an individual bubble is more complex. For the later turbulence analysis it is, therefore, advantageous to determine bubble trajectories and bubble velocities as well as characteristics of bubble shape and orientation. In this context, this section presents a detailed analysis of three-dimensional bubble-array evolution for all the simulation cases. For an easy reference main characteristics of bubble motion are summarized in Table 3.2.

3.3.1 Methodology for analyses of bubble-array motion

To obtain a first overall impression on the bubble-array dynamics, simulation results are visualized using AVS software. For more detailed analysis the methodology to be presented in this subsection is developed and implemented in the evaluation part of TURBIT-VoF.

Since the flow is incompressible the centre-of-mass of the m^{th} bubble[2] can be evaluated by:

$$\mathbf{r}_b^m = \frac{\int_{V_b^m} \mathbf{r} Ind(\mathbf{r}) dV}{\int_{V_b^m} Ind(\mathbf{r}) dV}, \tag{3.7}$$

where $\mathbf{r}$ represents the centroid position of the mesh cell belonging to the m^{th} bubble. In order to avoid an interference of individual bubbles within a free bubble-array, cells belonging to a certain bubble are marked introducing a bubble indicator function, $Ind(\mathbf{r})$. This function is defined to have a zero value if the considered cell is fully occupied with the liquid phase and a constant value m if the cell is a part of the bubble with the ordinal number m.

The relation 3.7 for evaluating $\mathbf{r}_b^m$ is based on the assumption that $\mathbf{r}$ overlaps with the geometrical centre of computational cell. Although such an assumption does not hold for interfacial cells being only partially filled with the gas phase, due to very fine computational grid the evaluation of bubble trajectories may be accepted as sufficiently accurate.

As all the bubbles within a considered swarm of bubbles have the same volume, the tra-

[2]The notation used in the presentation of the applied methodology concerns more general case of the free bubble-array flow where an individual bubble within the considered swarm of bubbles is associated with its ordinal number m ($m = 1, n_b$). To apply corresponding formulae on the case of the fixed bubble-array flow one should simply put $m = 1$.

jectory of the swarm as an entity can be determined by the simple average:

$$\langle \mathbf{r} \rangle = \frac{1}{n_b} \sum_{m=1}^{m=n_b} \mathbf{r}_b^m. \tag{3.8}$$

The velocity of the bubble centroid is evaluated either by:

$$\mathbf{u}_b^m = \frac{\int_{V_b^m} \mathbf{u} Ind(\mathbf{r}) dV}{\int_{V_b^m} Ind(\mathbf{r}) dV}, \tag{3.9}$$

where $\mathbf{u}$ represents velocity computed by TURBIT-VoF, or differentiating the bubble path:

$$\mathbf{u}_b^m = \frac{d\mathbf{r}_b^m}{d\vartheta}. \tag{3.10}$$

It has been verified numerically that these two formulae give identical results. The former is used for the initial time step ($\vartheta = 0$), while the latter is applied when positions of the bubble centroid are known for two subsequent time steps ($\vartheta > 0$).

The rise velocity of the swarm (further called mean bubble rise velocity) is computed as the arithmetic mean of the individual bubble rise velocities:

$$\langle u_g \rangle = \frac{1}{n_b} \sum_{m=1}^{m=n_b} u_{b1}^m, \tag{3.11}$$

where the subscript 1 denotes vertical (x_1) direction.

In order to be compatible with Bunner and Trygvason [9] [10] [11] the bubble rise is characterized by bubble drift Reynolds number:

$$\mathrm{Re}_d^m = \frac{\varrho_l u_d^m d_b}{\mu_l}, \tag{3.12}$$

where u_d^m indicates bubble drift velocity defined as:

$$u_d^m = u_{b1}^m - j. \tag{3.13}$$

The second term on the right-hand-side of the above equation represents the superficial velocity of two-phase mixture:

$$j = j_l + j_g, \tag{3.14}$$

with superficial velocities of the liquid and gas phase respectively formulated by:

$$j_l = (1 - \langle \alpha_g \rangle)\langle u_l \rangle \quad \text{and} \quad j_g = \langle \alpha_g \rangle \langle u_g \rangle, \tag{3.15}$$

where $\langle u_g \rangle$ is given by 3.11 and the mean velocity of the liquid phase in vertical direction is determined from:

$$\langle u_l \rangle = \frac{1}{1 - \langle \alpha_g \rangle} \int_V f u_1 dV. \tag{3.16}$$

Finally, the drift Reynolds number for the whole swarm of bubbles is computed as:

$$\langle \mathrm{Re}_d \rangle = \frac{1}{n_b} \sum_{m=1}^{m=n_b} \mathrm{Re}_d^m. \tag{3.17}$$

3.3.2 Comparison of bubble-arrays with different number of bubbles

This section presents the three-dimensional evolution of bubble-arrays with the same bubble size and physical properties of fluids, but with different number of suspended bubbles. In this context, the analyses concern characteristics of the bubble motion computed in simulation scenarios 1BM6, 5BM6 and 8BM6, where the magnitudes of overall gas volumetric fraction stand in the following relationship:

$$\langle \alpha_g \rangle^{1\mathrm{BM6}} : \langle \alpha_g \rangle^{5\mathrm{BM6}} : \langle \alpha_g \rangle^{8\mathrm{BM6}} = 0.818\% : 4.088\% : 6.544\%. \tag{3.18}$$

In Figure 3.4 bubble shape and liquid phase velocities are visualized for the fixed bubble-array flow (numerical run 1BM6). It can be seen that bubble takes the shape of an ellipsoid with the major axis parallel to the horizontal plane. The ellipsoid is axisymmetric with the axis aspect ratio $\kappa = 1.555$.

In the central part of the channel the rising bubble induces an intensive upward motion of the liquid phase, while in the peripheral domains of the channel cross-section the liquid slowly flows downwards. The region where the liquid flow changes direction from upwards to downwards is, in the form of the light circular annuli, visible in Figure 3.4b. Due to the motion of neighbouring bubble-arrays the intensity of the downward liquid flow in the vicinity of the periodic lateral boundaries is slightly lower than along the channel walls.

The trajectory of fixed bubble-array may be considered as an approximatively straight path taking into account that during the whole simulation time an individual bubble within the array vertically rose a distance of $19l$ what corresponds to $76d_b$, while the maximal lateral deviation of its trajectory was less than $0.05l$ i.e. $0.2d_b$. Therefore, it can be concluded that the chosen flow configuration ensures that neither laterally neighbouring bubble-arrays nor channel walls influence the shape of the fixed bubble-array rising path.

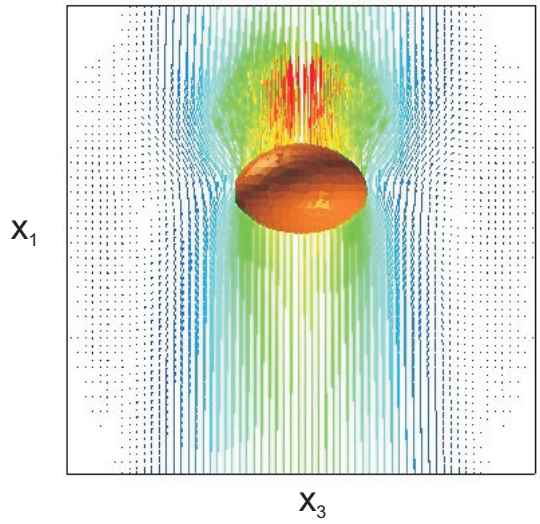

(a) $x_2 = 0.5l$

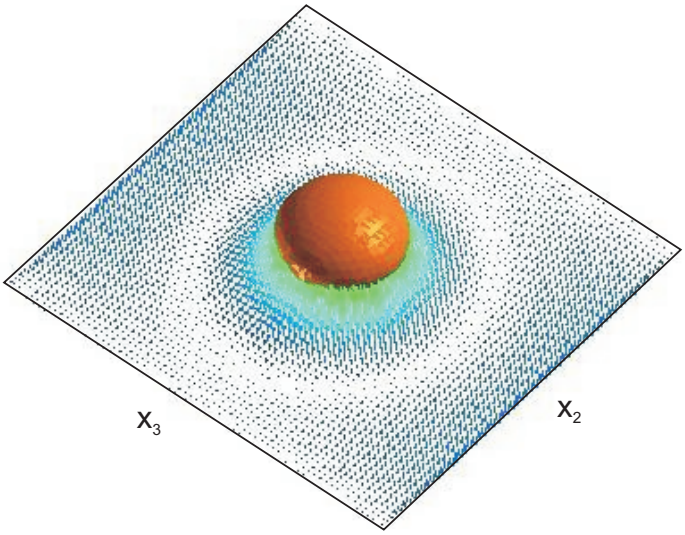

(b) $x_1 = 0.5l$

Figure 3.4: Visualization of bubble-array flow computed in simulation scenario 1BM6.

In order to obtain an overall impression about the effects of other bubbles on the liquid flow structure and individual bubble deformation, simulation results for both free bubble-array flow scenarios, 5BM6 and 8BM6, are visualized in Figure 3.5. For clarity reasons views at all three coordinate planes are presented. The striking difference to the fixed bubble-array flow case is much more agitated liquid flow. Although given only in one section, perturbations of the liquid phase by moving bubbles are evident, not only through

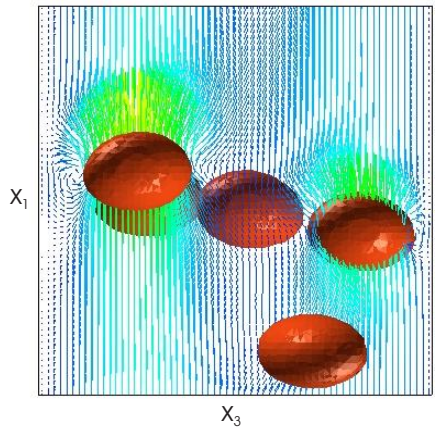

(a) $x_2 = 0.8047l$

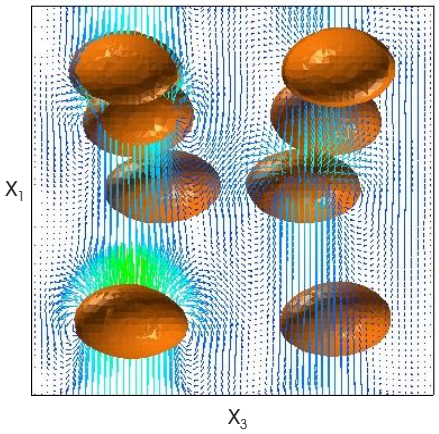

(b) $x_2 = 0.78125l$

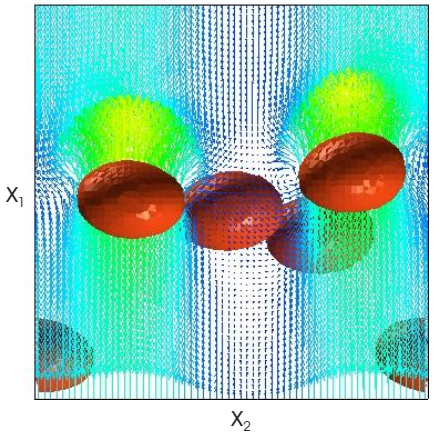

(c) $x_3 = 0.7266l$

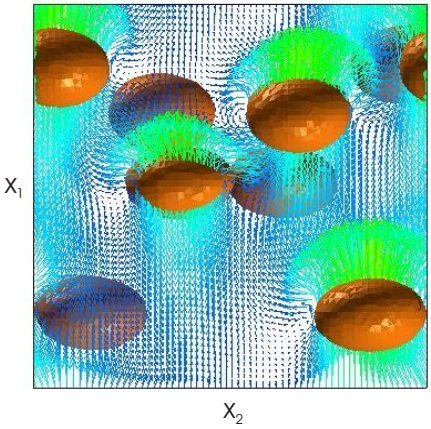

(d) $x_3 = 0.78125l$

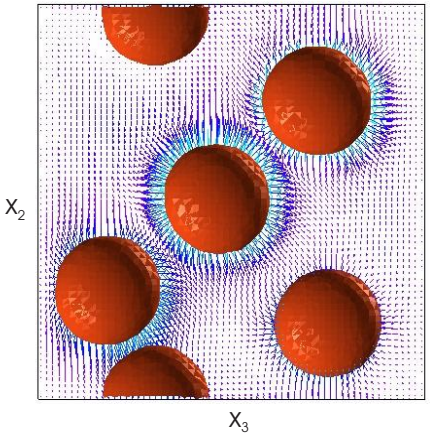

(e) $x_1 = 0.5234l$

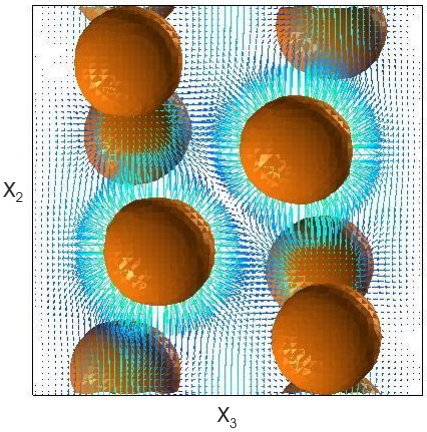

(f) $x_1 = 0.59375l$

Figure 3.5: Visualization of bubble-array flows computed in simulation scenarios 5BM6 (left) and 8BM6 (right).

the bubble-induced displacement of the liquid, but also through the formation and mutual interaction of bubble wakes. Bubbles generally took an ellipsoidal shape with major axis not perfectly aligned with the horizontal plane. Although some differences in the shape of individual bubbles can be observed, in both simulation scenarios they may be considered as negligible and the average ellipsoid axis aspect ratio of $\kappa = 1.535$ and $\kappa = 1.526$ can be estimated for the case 5BM6 and the case 8BM6, respectively.

Individual bubble trajectories in the free bubble-array flows 5BM6 and 8BM6 are presented in Figure A.1 and Figure A.2, respectively (see Apendix A). It can be seen that different to the case of the fixed bubble-array flow, the bubbles move, not only into the adjacent periodic box in the vertical direction through buoyancy, but also in both horizontal directions, wall-normal and span-wise, through the dispersion. These lateral movements of bubbles in the free bubble-array scenario 8BM6 resulted in the formation of two distinctive bubble populations. To analyze the time evolution of this free bubble-array in more detail, a movie has been made. The movie has revealed that bubbles tend to align at approximatively constant distance from the walls making a kind of bubble curtains between the central liquid core and downward flowing liquid layers next to the walls (such a situation can also be observed in Figure 3.5f). In the case 5BM6, however, lateral bubble movements resulted in a more or less uniform bubble distribution over channel cross-section with no distinctive pattern with respect to the channel walls (see Figure 3.5c). Further, while the lateral bubble movements in scenario 8BM6 are approximatively symmetric with respect to the diagonal channel plane, no similarity of individual bubble trajectories is observed in the simulation scenario with 5 bubbles (compare projections of bubble trajectories on $x_2 - x_3$ plane in Figure A.1 and Figure A.2).

Further information about the rise of bubble-arrays with different number of bubbles can be drawn from Figure 3.6, where the time evolution of drift Reynolds number for the entire bubble-arrays as well as for the individual bubbles within the free bubble-arrays is presented. It is evident that, except for a short initial phase of simulation, the acceleration of the fixed bubble-array is stronger than the one of the free bubble-arrays. Such a behaviour is caused by the larger drag due to increased vorticity deposition in the case of thicker bubble population. Even though the individual bubble motion show the transient behaviour owning to mutual bubble wake interactions, the whole swarm of bubbles reaches a well defined steady state quite quickly. In the steady state regime the mean bubble rise velocities computed for the different bubble-array scenarios (see Table 3.2) satisfy the following relation:

$$\frac{\langle u_g \rangle_r^{1\mathrm{BM6}}}{\langle \alpha_g \rangle_r^{1\mathrm{BM6}}} : \frac{\langle u_g \rangle_r^{5\mathrm{BM6}}}{\langle \alpha_g \rangle_r^{5\mathrm{BM6}}} : \frac{\langle u_g \rangle_r^{8\mathrm{BM6}}}{\langle \alpha_g \rangle_r^{8\mathrm{BM6}}} = \frac{1}{1} : \frac{0.725}{5} : \frac{0.674}{8} \tag{3.19}$$

the subscript r indicates relative to the simulation case 1BM6.

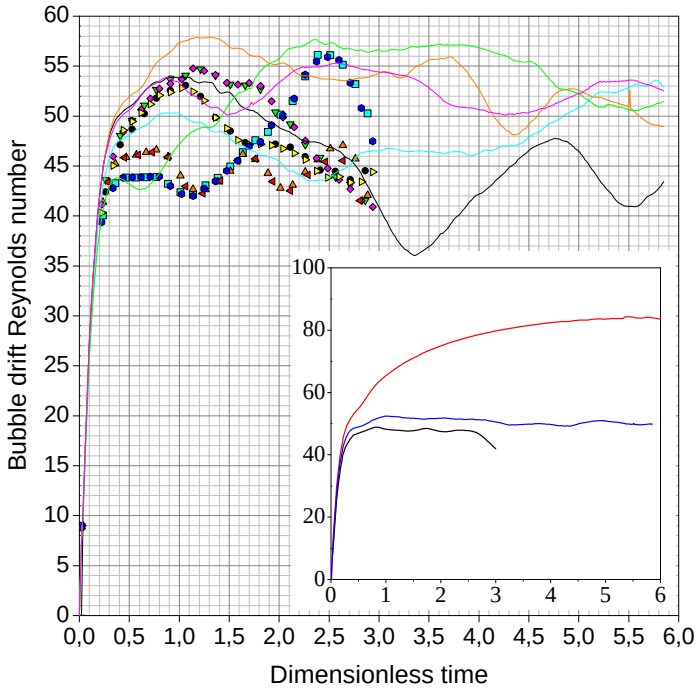

Figure 3.6: Time evolution of drift Reynolds number for bubble-arrays with different number of bubbles. Drift Reynolds number of individual bubbles in free bubble-array flows 5BM6 and 8BM6 is, respectively, depicted with lines (colours compatible with Figure A.1) and symbols (shapes compatible with Figure A.2). Subfigure presents drift Reynolds number of the representative bubble-swarm in bubble-array flow scenarios 1BM6 (red), 5BM6 (blue) and 8BM6 (black).

Contrary to the simulations 1BM6 and 5BM6 that passed smoothly, the simulation run 8BM6 was corrupted. An inspection of the bubble-array evolution has shown that this corruption was caused by a local unsteadiness of the flow. In the free bubble-array flow 8BM6, namely, beside approaching the walls, bubbles also tend to align themselves horizontally (a careful analysis of Figure A.2 shows that throughout the simulation the vertical bubble-bubble distances in the free bubble-array flow scenario 8BM6 decrease). This phenomenon, known as the bubble rafting [11], caused a transient behaviour of the whole two-phase system. Thus, reaching approximatively the same vertical position and owning to the large shape deformations, bubbles occupied significant part of the channel cross-section. Due to the locally increased buoyancy the liquid layer at the channel walls could not retain its downward orientation. As a consequence the lift force changed direction and made one of the bubbles hit the channel wall. Since TURBIT-VoF could not resolve the phase interface in such a flow configuration, the simulation had to be stopped.

Finally, an observation from the aforementioned analysis is pointed out as beneficial for the

later turbulence considerations. Therefore, despite the conspicuously different dynamics of the considered bubble-array flows, only slight differences are observed when the bubble shape and bubble orientation are concerned. Subsequently, in comparisons of liquid phase velocity fluctuations induced by the rise of bubble-arrays with different number of bubbles, effects of the bubble shape do not have to be considered as a parameter of the analysis.

3.3.3 Comparison of bubble-arrays moving in liquids with different viscosity

This subsection focuses on effects of the liquid phase viscosity on the dynamics of geometrically identical bubble-swarms. In this context, the motion of free bubble-arrays computed by TURBIT-VoF in numerical runs 8BM2, 8BM4 and 8BM6 is analyzed. It is reminded that the number of suspended bubbles, individual bubble volume and computational domain size are identical for all the considered simulation cases (see Table 3.1), while the corresponding liquid viscosities relative to the viscosity specified in the case 8BM2 stand in the following relation:

$$\mu_{l,r}^{8\mathrm{BM6}} : \mu_{l,r}^{8\mathrm{BM4}} : \mu_{l,r}^{8\mathrm{BM2}} = 0.1 : 0.316 : 1, \tag{3.20}$$

where the superscripts indicate simulation scenarios and the subscript r indicates the division by $\mu_l^{8\mathrm{BM2}}$.

The visualization of the bubble shape and the liquid phase velocity for free bubble-array flow scenario 8BM2 is presented in Figure 3.7. As expected, in this, the most viscous case, bubble deformation is absent, i.e. bubbles retained their initial spherical shape. The evaluation of bubble trajectories[3] has shown that individual bubbles move almost rectilinearly keeping initially prescribed distances from each other. A detailed inspection of the liquid flow structure revealed no existence of bubble wakes, what leads to the conclusion that the generated liquid motion is the result of pure liquid displacement by moving bubbles.

Figure 3.8 shows a rather different flow configuration in the case 8BM4 - only slightly ellipsoidal bubbles (bubble axis aspect ratio $\kappa = 1.132$) agitate the liquid phase considerably, not only through the liquid displacement, but also through the formation of vortical structures. Comparing to the case 8BM2 larger lateral deviations of individual bubble trajectories can be observed in Figure A.5. On the other hand, when compared to the run 8BM6, these lateral movements are significantly less pronounced. Nevertheless, bubbles show tendency to approach channel walls.

The time evolution of drift Reynolds number computed for the bubble swarms moving

[3]Details on bubble trajectories for each individual simulation scenario with 8 bubbles can be seen in Figure A.2, A.3 and A.4. Lateral bubble movements are highlighted in Figure A.5 for all the simulation cases.

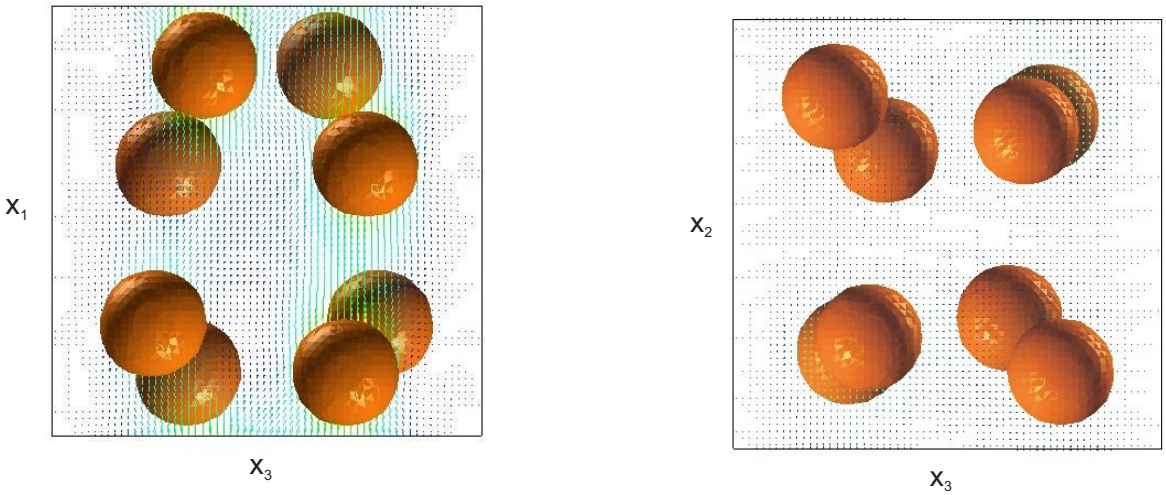

(a) $x_2 = 0.734l$ (b) $x_1 = 0.5l$

Figure 3.7: Visualization of free bubble-array flow computed in numerical run 8BM2.

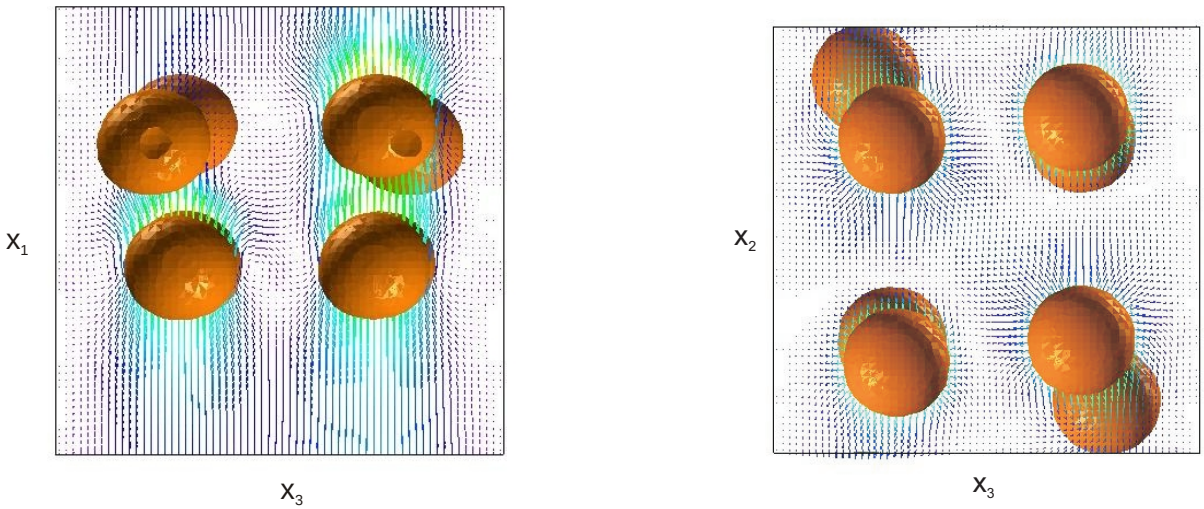

(a) $x_2 = 0.7349l$ (b) $x_1 = 0.5l$

Figure 3.8: Visualization of free bubble-array flow computed in numerical run 8BM4.

through the liquids with different viscosity is presented in Figure 3.9. It can be seen that the steady state for the case with the highest liquid viscosity (scenario 8BM2) is reached within the shortest time period, after which the two-phase system behaves very stable.

The Table 3.2 shows that the liquid viscosity influences the magnitudes of the mean bubble rise velocity strongly and changes the values of the drift bubble Reynolds number dramatically. Therefore, the relationship between the liquid viscosities given by 3.20 results in the following ratios:

$$\langle u_b \rangle_r^{8\mathrm{BM6}} : \langle u_b \rangle_r^{8\mathrm{BM4}} : \langle u_b \rangle_r^{8\mathrm{BM2}} = 5.174 : 2.717 : 1 \tag{3.21}$$

and

$$\langle \mathrm{Re}_d \rangle_r^{8\mathrm{BM6}} : \langle \mathrm{Re}_d \rangle_r^{8\mathrm{BM4}} : \langle \mathrm{Re}_d \rangle_r^{8\mathrm{BM2}} = 55.640 : 9.365 : 1, \tag{3.22}$$

where the subscript r indicates relative to the case 8BM2.

Finally, it is noted that the numerical experiment 8BM2 is the only simulation scenario with 8 bubbles that was not broken due to flow instabilities that occurred after the stationary regime has been reached. An analysis of the history of the simulation runs 8BM4 and 8BM6 revealed an important role that bubble wakes play in the evolution of three-dimensional bubble-array motion. Intuitively, one would expect that the bubble coalescence will occur rather in the numerical experiment 8BM6, where the bubble deformation is large, the bubble rise velocity is high and the bubble lateral movements are significant, than in the simulation scenario 8BM4, where only slightly deformed bubbles rise slowly along paths with small lateral deviations. However, bubble coalescence in the scenario 8BM6 did not occur because approaching of a certain bubble to the other one beyond a critical distance was stopped by repelling effects of bubble wakes. On the other side, in the scenario 8BM4 the acceleration of the trailing bubble in the wake of the leading bubble caused formation of tight bubble clusters and resulted, finally, in the bubble coalescence.

At the end the following is stressed: In all the presented simulations of bubble-array flows a steady flow regime has been reached and kept sufficiently long to provide the data basis required for the statistical analyses of liquid phase velocity fluctuations. In this way it is demonstrated that DNS can successfully be used for the turbulence investigation in dilute bubble-driven liquid flows.

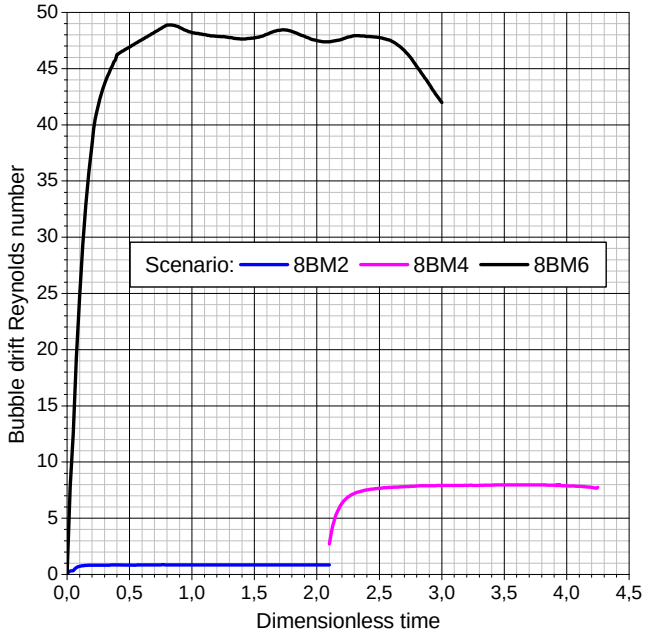

Figure 3.9: Time evolution of drift Reynolds number for simulated bubble-arrays moving through liquids with different viscosity.

Table 3.2: List of main DNS results for the dynamics of simulated bubble-arrays

type of bubble-array	fixed	free			
simulation scenario	1BM6	5BM6	8BM6	8BM4	8BM2
computed time [a]	6	5.85	3	2.15	2.1
rise length [a]	19.10	14.28	6.89	2.26	0.94
lateral bubble motion[c]	negligible	strong	strong	slight	negligible
bubble distribution[b]	core	uniform	wall-aligned	wall-aligned	initial
mean bubble rise velocity [abd]	3.53	2.56	2.38	1.25	0.46
Reynolds number [bd]	88.2	64.1	59.5	9.87	1.15
drift Reynolds number [bd]	84.1	50.3	47.3	7.96	0.85
bubble axis aspect ratio [b]	1.555	1.535	1.526	1.132	1

[a] scaled
[b] in steady state
[c] during the whole simulation period
[d] in free bubble-arrays mean value for the swarm of bubbles

Chapter 4

Statistical analyses of liquid flow induced by motion of bubble-arrays

This chapter presents the statistical analysis of the liquid motion computed by direct numerical simulations (DNS) of bubble-array flows using the computer code TURBIT-VoF. An inspection of the raw DNS data has shown that the information about the instantaneous liquid flow is not complete, since the liquid behaviour at the phase interface is not accurately described by the current version of TURBIT-VoF. In this context, the first section presents the methodology applied to determine the instantaneous velocity and pressure at the liquid side of the phase interface. The section 2 deals with averaging of the instantaneous liquid flow. First, the choice of the most feasible averaging technique is discussed and adopted procedures are described in detail. Further, evaluated statistical characteristics of the mean and fluctuating liquid flow are presented for different bubble-array flow cases. The topic of section 3 is the liquid turbulence kinetic energy itself. This section gives a detailed insight into the distribution of the liquid turbulence kinetic energy evaluated on the basis of DNS data for different bubble-array flow scenarios. Next, effects of the gas content and the liquid viscosity on the behaviour of the liquid turbulence kinetic energy are analyzed. Finally, DNS based results are compared with predictions based on the potential flow theory.

4.1 Determination of instantaneous liquid flow at phase-interface

While the raw data obtained by DNS of bubble-array flows using the computer code TURBIT-VoF fully determine the instantaneous liquid flow within the bulk fluid, the information about the actual liquid flow at the phase interface is not provided. The interfacial liquid flow is, namely, not realistically described by DNS data because the methodology

implemented in TURBIT-VoF assumes a homogeneous two-phase mixture in cells containing gas-liquid interface (further called interfacial cells). On the other hand, in order to quantify effects of bubble interfaces on the balance of liquid turbulence kinetic energy the instantaneous interfacial liquid flow has to be known. In this context, this section presents the methodology applied for the determination of the instantaneous velocity and the instantaneous pressure at the liquid side of the phase interface.

4.1.1 Determination of liquid interfacial velocity

Since in the considered bubble-array flows no phase change occurs, interfacial velocities of both phases, the liquid and the gas, are equal to the velocity of the phase interface [29]:

$$\mathbf{u}_{il} = \mathbf{u}_{ig} = \mathbf{u}_i, \tag{4.1}$$

where l and g indicate the liquid and gas phase respectively, and i denotes the interface. The considerations may, therefore, be confined to the motion of the interfacial surface. The velocity of the interfacial surface, $\mathbf{u}_i$, can, as any vector, be decomposed into two perpendicular components. For an analysis of interfacial effects particularly convenient is the following decomposition [29]:

$$\mathbf{u}_i = \mathbf{u}_{i,t} + \mathbf{u}_{i,n}, \tag{4.2}$$

where $\mathbf{u}_{i,t}$ represents the component that lies in the plane tangential to the interfacial surface and $\mathbf{u}_{i,n}$ denotes the component in the direction of the unit normal vector, $\mathbf{n} = \mathbf{n}_g = -\mathbf{n}_l$, pointing from the gas to the liquid phase (see Figure 4.1).

The tangential component of the interfacial velocity, $\mathbf{u}_{i,t}$, is theoretically defined to be equal to the tangential velocity of a fluid particle lying at the interface [29]. Since interfacial cells are occupied with two-phase mixture, $\mathbf{u}_{i,t}$ is assumed to be equal to the tangential component, $\mathbf{u}_t$, of the mixture velocity, $\mathbf{u}$, computed by TURBIT-VoF:

$$\mathbf{u}_{i,t} = \mathbf{u}_t = \mathbf{u} - (\mathbf{u} \cdot \mathbf{n}) \cdot \mathbf{n}. \tag{4.3}$$

The normal component of the velocity of the interfacial surface is given by [30] [29]:

$$\mathbf{u}_{i,n} = -\frac{\partial F(\mathbf{x}, \vartheta)/\partial \vartheta}{|\nabla F(\mathbf{x}, \vartheta)|} \cdot \mathbf{n}, \tag{4.4}$$

where $F(\mathbf{x}, \vartheta) = 0$ represents the equation of the interfacial surface. In TURBIT-VoF this surface is at any time instant, ϑ, defined via the unit normal vector, $\mathbf{n}$, and a point lying on the interface, $M(\mathbf{b})$ [62]:

$$F(\mathbf{x}, \vartheta) = (\mathbf{b} - \mathbf{x}) \cdot \mathbf{n} = 0. \tag{4.5}$$

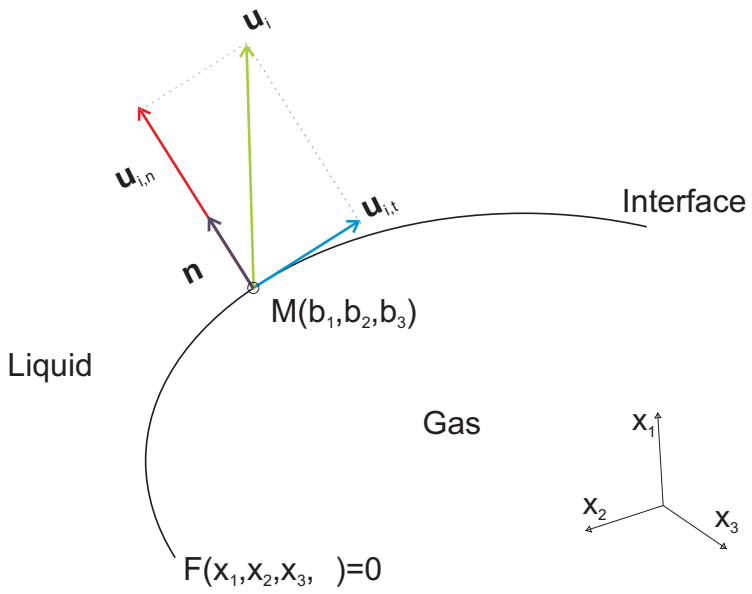

Figure 4.1: Decomposition of interfacial velocity in normal and tangential component

Since the function $F(\mathbf{x}, \vartheta)$ as given by the equation 4.5 is not explicit with respect to time, the methodology for determining $\partial F(\mathbf{x}, \vartheta)/\partial\vartheta$ had to be developed. In the following the applied procedure is presented.

Consider two subsequent time instants ϑ_0 and $\vartheta_0 + \delta\vartheta$ at which the interfacial surface passes through the points $M(\mathbf{b}_0)$ and $M(\mathbf{b}_0 + \delta\mathbf{x})$, respectively (see Figure 4.2). At these time instances the equation of the interfacial surface satisfies:

$$F(\mathbf{b}_0, \vartheta_0) = 0 \tag{4.6}$$

and

$$F(\mathbf{b}_0 + \delta\mathbf{x}, \vartheta_0 + \delta\vartheta) = 0. \tag{4.7}$$

If the distance $\delta\mathbf{x}$ is small, the function F given by equation 4.7 can be extended into the Taylor series:

$$F(\mathbf{b}_0 + \delta\mathbf{x}, \vartheta_0 + \delta\vartheta) = F(\mathbf{b}_0, \vartheta_0) + \frac{\partial F(\mathbf{x}, \vartheta)}{\partial\vartheta}\Big|_{\mathbf{b}_0,\vartheta_0}\delta\vartheta + \nabla F(\mathbf{x}, \vartheta)\Big|_{\mathbf{b}_0,\vartheta_0} \cdot \delta\mathbf{x} + \text{HOT}, \tag{4.8}$$

where HOT stands for higher order terms. Assuming HOT ≈ 0 and subtracting the equation 4.6 from the equation 4.8 the following is obtained:

$$\frac{\partial F(\mathbf{x}, \vartheta)}{\partial\vartheta}\Big|_{\mathbf{b}_0,\vartheta_0}\delta\vartheta = -\nabla F(\mathbf{x}, \vartheta)\Big|_{\mathbf{b}_0,\vartheta_0} \cdot \delta\mathbf{x}. \tag{4.9}$$

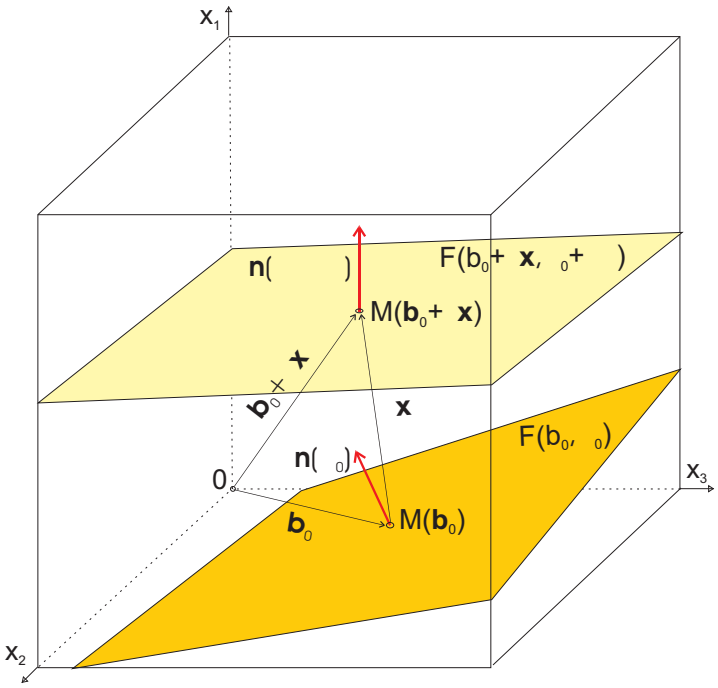

Figure 4.2: Interface position within mesh cell at two subsequent time instances

Dividing the above equation with $\delta\vartheta$ the time derivative of the function $F(\mathbf{x},\vartheta)$ at the position $M(\mathbf{b}_0)$ and time instant ϑ_0 needed in equation 4.4 can be expressed as:

$$\frac{\partial F(\mathbf{x},\vartheta)}{\partial\vartheta}\Big|_{\mathbf{b}_0,\vartheta_0} = -\frac{1}{\delta\vartheta}\nabla F(\mathbf{x},\vartheta)\Big|_{\mathbf{b}_0,\vartheta_0}\cdot\delta\mathbf{x}. \tag{4.10}$$

Further, taking into account the following geometrical relation [30]:

$$\mathbf{n} = \frac{\nabla F(\mathbf{x},\vartheta)}{|\nabla F(\mathbf{x},\vartheta)|}, \tag{4.11}$$

the normal component of the interfacial velocity in the point $M(\mathbf{b}_0)$ and at the time instant ϑ_0 can, finally, be formulated as:

$$\mathbf{u}_{i,n}\Big|_{\mathbf{b}_0,\vartheta_0} = \frac{1}{\delta\vartheta}(\mathbf{n}\Big|_{\mathbf{b}_0,\vartheta_0}\cdot\delta\mathbf{x})\mathbf{n}\Big|_{\mathbf{b}_0,\vartheta_0}. \tag{4.12}$$

The validity of the presented methodology for evaluation of the interfacial velocity is tested for the following flow configuration. A channel of the dimensionless size 1x1x1 is discretized with 64^3 uniform mesh cells. The channel is laterally confined with two rigid walls, while in the vertical and span-wise direction periodic boundary conditions are imposed. Two immiscible fluids of identical physical properties are arranged in the following flow pattern: the fluid 1 occupies a spherical space with the dimensionless diameter 1/4 and the fluid 2 fills the rest of the channel. Both fluids move vertically upwards at constant dimensionless

velocity $U_f = 1$. Under such flow conditions the interface rises together with fluids, i.e. the velocity of fluid-fluid interface is, theoretically, equal to the velocity of fluids, U_f.

The performance of the presented methodology for the evaluation of interfacial velocity in the case of the described flow configuration is illustrated in Table 4.1 for the set of computational cells lying in the span-wise plane $x_2 = 0.4292l$. The comparison of the evaluated interfacial velocity, U_i, with the theoretical value, $U_f = 1$, over the whole fluid-fluid interface has shown that the accuracy of the presented methodology is acceptable. It has, namely, been found that the maximal discrepancy is:

$$\max\left[\frac{|U_i - U_f|}{U_f}\right] = 7.214\%, \tag{4.13}$$

while the mean error computed for N interfacial cells is:

$$\frac{1}{N}\sum_{m=1}^{m=N}\frac{|U_{im} - U_f|}{U_f} = 1.904\%. \tag{4.14}$$

Table 4.1: Evaluated interfacial velocity for the flow configuration where two immiscible fluids with identical physical properties move with constant velocity $U_f = 1.0$. Results are given for span-wise position $x_2 = 0.4292l$.

	k[a]													
i[b]	26	27	28	29	30	31	32	33	34	35	36	37	38	39
40														
39					0.952	0.997	0.999	0.999	0.997	0.952				
38			0.997	0.999	1.000	1.000			1.000	1.000	0.999	0.997		
37		1.071	0.996	1.000							1.000	0.996	1.071	
36		1.012	0.996										1.012	
35	0.988	0.996											0.996	0.988
34	1.003													1.003
33	0.999													0.999
32	1.002													1.002
31	0.999													0.999
30	0.991	1.033											1.033	0.991
29	1.000	1.027											1.027	1.000
28		1.000	1.004									1.004	1.000	
27			0.999	1.016							1.016	0.999		
26				0.993	1.000	1.000	0.999	0.999	1.000	1.000	0.993			
25														

[a] indices of mesh cells in wall-normal direction

[b] indices of mesh cells in vertical direction

When the interfacial velocity evaluated by the presented methodology, $\mathbf{u}_i$, is compared with the velocity of two-phase mixture computed by TURBIT-VoF in interfacial cells, $\mathbf{u}$, dramatic differences are not observed in any of the considered bubble-array flows. Here, as an illustration, the difference between the vertical components, $u_{i1} - u_1$, is presented in Table 4.2 for the fixed bubble-array flow scenario 1BM6.

Table 4.2: Difference between vertical components of the interfacial and mixture velocity, $u_{i1} - u_1(m/s)$, computed for the fixed bubble-array flow (scenario 1BM6). Results are given for span-wise position $x_2 = 0.4292l$ and time instant $\theta = 5.06$. Presented data are multiplied with 10.

	k[a]															
i[b]	25	26	27	28	29	30	31	32	33	34	35	36	37	38	39	40
61					.01	-.41	- .34	- .35	-.35	-.34						
60			-.24	-.36	-.99	2.67	-1.33	-1.73	-1.07	-1.95	.09					
59			-.03	-2.34							-2.49	.19	.07	-.25		
58		-.23	.86										-2.22	.56	-.27	
57	-.52	.56												.76	.28	-.68
56	-.25	.33													.08	-.19
55	.01	-.00													-.00	.01
54	-.12	-.07													-.08	-.01
53	-.06	.08	-.22											-.17	.03	.40
52		.08	.18										- .50	.23	.35	
51			1.32	-.80	.01	-.47					2.40	.04	.027	.61		
50				.01	.13	.94	.06	.20	.19	.04	.99	1.45				
49																

[a] indices of mesh cells in wall-normal direction

[b] indices of mesh cells in vertical direction

4.1.2 Determination of liquid interfacial pressure

The next important point in dealing with the interfacial liquid flow was to determine the instantaneous pressure at the liquid side of the phase interface. As it can be seen in Table 4.2 drastic errors will not be made if one, instead of the interfacial velocity, adopts the velocity of two-phase mixture computed by TURBIT-VoF in interfacial cells. The situation is, however, significantly different when the liquid pressure at the interface is concerned. It is, namely, stressed that the pressure of the *liquid* phase must be used, otherwise a dramatic overestimation of interfacial effects in the balance equation for liquid turbulence kinetic energy will be caused.

Different to considerations of the interfacial liquid velocity, no methodology for the evaluation of the liquid phase interfacial pressure could be developed. Instead, it is assumed

that gradients of the liquid pressure in the vicinity of the phase interface are weak and that the liquid interfacial pressure is equal to the pressure in the closest adjacent cell fully occupied with the liquid phase. Although good results are obtained with such an approach, for certain time instances difficulties appeared. The difficulties are related to the incorrectness of the TURBIT-VoF reconstruction algorithm, i.e. to the existence of interfacial cells that do not have any adjacent cell completely filled with the liquid phase. In such a case, looking for the cell fully occupied with the liquid phase is continued exploring the local liquid volumetric fraction in cells that are neighbours of neighbours.

4.2 Computation of statistical quantities of liquid flow induced by motion of bubble-arrays

In multiphase flow literature the decomposition of the instantaneous flow field in its mean and fluctuating component is, usually, performed applying either time averaging [29] or ensemble averaging [19] [32]. The first part of this section presents a spatial averaging technique that is found as the most appropriate for here performed statistical analysis of the liquid phase motion induced by the rise of bubble-arrays. The evaluated characteristics of the mean and fluctuating liquid flow field are outlined for all the considered bubble-array flow scenarios. When the statistical turbulence quantities are considered, the attention is mainly paid on the general features of bubble-induced liquid perturbations. It is noted that much more information concerning the fluctuating liquid phase flow can be found in the next section, where the distribution of the liquid turbulence kinetic energy in different bubble-array flows is discussed in detail.

4.2.1 Averaging of instantaneous liquid flow

The existing version of TURBIT-VoF code provides a record of instantaneous quantities (velocity components and pressure) at each time step of integration for only one bar of mesh cells in wall-normal direction. An analysis of the basic balance equation for turbulence kinetic energy of the liquid phase (equation 2.14) requires, however, the knowledge of the instantaneous flow field over the whole computational domain. A storage of DNS data for each computed time instant and over the whole computational domain requires, on the other side, a huge memory space. For instance, in the statistical analysis of liquid fluctuations in the free bubble-array flow scenario 8BM6 the steady state regime within the time interval $\theta = 0.6 - 2.5$ should be considered, what for the specified time step width $\Delta\theta = 0.5 \cdot 10^{-4}$ means that 38000 full data sets have to be stored. On the other hand, when the spatial averaging is applied, the detailed information on instantaneous flow field is required for only one instant in time. Therefore, replacing the time averaging by the

spatial one provides a lot of advantages. In the following possibilities for the application of the spatial averaging on flow configurations analyzed in this work are discussed.

In all the considered bubble-array flows the main flow direction is vertical (x_1 direction). Since all the analyses are performed for a developed steady flow regime, the mean velocity in x_1 direction is constant. When in addition, periodic boundary conditions imposed in this direction are taken into account, it may be assumed that the turbulence structure of the liquid phase induced by a steady rise of monodisperse bubble-arrays within an infinite plane channel does not change vertically.

When the span-wise direction, x_2, is concerned the situation is more complex. Although periodic boundary conditions are also applied in this direction, the structure of the liquid flow within one periodical domain strongly depends on the number of suspended bubbles. For instance, in the case of fixed-bubble array flow an intensive upward liquid motion generated in the cental part of the channel is, at a very short distance from the domain where bubble rises, reduced and, finally, reoriented into a slow downward flow. It is, therefore, expected that such a pronounced local character of the span-wise liquid velocity distribution for cases of very dilute bubbly flows (scenario 1BM6 and scenario 5BM6) would lead to an overestimation of fluctuating liquid quantities if averaging along x_2 direction were attempted. On the other hand, the structure of the liquid phase flow generated by arrays with 8 bubbles (scenarios 8BM2, 8BM4 and 8BM6) is quite different. The motion of the liquid phase is, namely, driven by two distinctive densely packed bubble populations that rise approximatively parallel to the channel walls (see Figure 3.5). In such a flow configuration perturbations of the liquid phase might be assumed to depend spatially only on the distance from the channel walls, i.e. the liquid turbulence structure in other two directions, vertical and span-wise, might be considered as homogeneous.

Finally, due to the existence of lateral rigid walls, the fluctuating liquid flow may not, in any case, be assumed as homogeneous in the wall-normal (x_3) direction.

In the context of the above discussions two types of spatial averaging are applied in this work: line averaging and plane averaging.

Based on the assumption of homogeneous liquid turbulence in the main flow direction, *line averaging* is defined over vertical columns of mesh cells (see Figure 4.3a) as:

$$\overline{A}^{L}_{\beta\gamma} = \frac{1}{m_1} \sum_{\alpha=1}^{m_1} A_{\alpha\beta\gamma}, \tag{4.15}$$

where the subscripts α, β and γ denote indices in vertical (x_1), span-wise (x_2) and wall-normal (x_3) direction, respectively, and m_1 represents the number of mesh cells in the vertical direction.

Extending the assumption of homogeneous liquid turbulence on both directions, vertical

and span-wise, *plane averaging* is defined over vertical slabs of mesh cells parallel to channel walls (see Figure 4.3b) by:

$$\overline{A}^{P}_{\gamma} = \frac{1}{m_1 m_2} \sum_{\alpha=1}^{m_1} \sum_{\beta=1}^{m_2} A_{\alpha\beta\gamma}, \tag{4.16}$$

where m_2 stands for the number of mesh cells in span-wise direction. Note that in the text hereafter the superscripts L and P are used to indicate line and plane averaged quantities, respectively.

The averaging as defined above may be applied only on field quantities (quantities defined in all space and time domains under consideration). For instance, the mean liquid volumetric fraction, α_l, is theoretically defined as an average of the liquid indicator function, Φ_l (the definition of Φ_l is given by equation 2.4). Since the concept of DNS assumes that the liquid phase indicator function, Φ_l, may be replaced by the local liquid volumetric fraction, f, mean magnitudes of the liquid volumetric fraction are computed as:

$$\alpha^{L}_{l\beta\gamma} = \frac{1}{m_1} \sum_{\alpha=1}^{m_1} f_{\alpha\beta\gamma} \quad \text{and} \quad \alpha^{P}_{l\gamma} = \frac{1}{m_1 m_2} \sum_{\alpha=1}^{m_1} \sum_{\beta=1}^{m_2} f_{\alpha\beta\gamma}. \tag{4.17}$$

Mean values of non-field liquid phase quantities are defined introducing the so-called phase-weighted averaging, where only domains occupied by the liquid phase are accounted for. Using the local liquid volumetric fraction, f, to indicate mesh cells entirely filled with liquid phase-weighted liquid quantities in this work are computed as:

$$\overline{\overline{A}}^{L}_{l\beta\gamma} = \frac{1}{\alpha^{L}_{l\beta\gamma}} \frac{1}{m_1} \sum_{\alpha=1}^{m_1} f_{\alpha\beta\gamma} A_{\alpha\beta\gamma}, \tag{4.18}$$

and

$$\overline{\overline{A}}^{P}_{l\gamma} = \frac{1}{\alpha^{P}_{l\gamma}} \frac{1}{m_1 m_2} \sum_{\alpha=1}^{m_1} \sum_{\beta=1}^{m_2} f_{\alpha\beta\gamma} A_{\alpha\beta\gamma}. \tag{4.19}$$

Finally, liquid phase fluctuations in the bulk fluid are evaluated as:

$$A'^{L}_{l\alpha\beta\gamma} = A_{l\alpha\beta\gamma} - \overline{\overline{A}}^{L}_{l\beta\gamma} \quad \text{and} \quad A'^{P}_{l\alpha\beta\gamma} = A_{l\alpha\beta\gamma} - \overline{\overline{A}}^{P}_{l\gamma} \tag{4.20}$$

and at the liquid side of phase interface as:

$$A'^{L}_{li\alpha\beta\gamma} = A_{li\alpha\beta\gamma} - \overline{\overline{A}}^{L}_{l\beta\gamma} \quad \text{and} \quad A'^{P}_{li\alpha\beta\gamma} = A_{li\alpha\beta\gamma} - \overline{\overline{A}}^{P}_{l\gamma}, \tag{4.21}$$

where the subscript i denotes a liquid interfacial quantity. It is noted that liquid phase fluctuations A'_l and A'_{li} are also not field quantities. Therefore, when different correlations of liquid fluctuations are computed, the phase-weighted averaging has to be performed. On

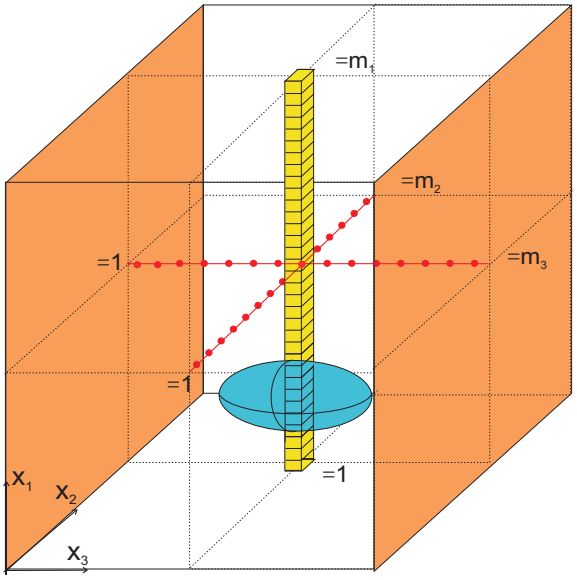

(a) line averaging

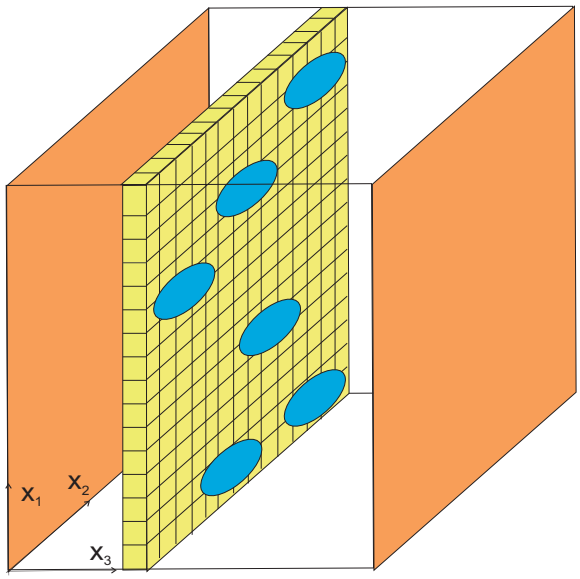

(b) plane averaging

Figure 4.3: Definition of averaging domains. Entities of mesh cells over which averaging is performed are coloured yellow. Blue areas represent suspended gas phase. Notations given in (a) apply to the entire figure.

the other side, correlations involving fluctuations at the phase interface are field quantities since they always involve interfacial area concentration, a_i (interfacial area concentration is field quantity because it is defined via the gradient of the phase indicator function, $\nabla\Phi_l = a_i\mathbf{n}_l$).

The plane averaging is performed in statistical analysis of the liquid motion induced by the rise of free bubble-arrays with 8 bubbles (scenarios 8BM2, 8BM4 and 8BM6). The line averaging is used in the case of fixed bubble-array flow scenario 1BM6 and both free-bubble array flow scenarios with low liquid viscosity (5BM6 and 8BM6). While the choice of the line averaging in cases 1BM6 and 5BM6 was dictated by the local flow structure, in the case 8BM6 this type of averaging is applied in order to provide data comparable with the ones computed in scenarios 1BM6 and 5BM6. A comparison of statistical turbulence quantities evaluated by the line averaging and the plane averaging is, namely, not appropriate. First, because the corresponding profiles obtained by line averaging are two-dimensional, while the ones obtained by plane averaging spatially depend only on the wall-normal coordinate. Second, as the local structure of the liquid flow is in more details recognized by the line than by the plane averaging, evaluated liquid fluctuations are somewhat higher when the latter is concerned. In this context, results obtained applying the line averaging and the plane averaging for the bubble-array flow scenario 8BM6 are not for comparison, too.

The aforementioned averaging techniques can successfully be performed using DNS data for any single time instant within the steady regime[1] of a bubble-array flow. However, in order to obtain smooth profiles of liquid turbulence quantities the following procedure is applied. First, evaluations based on spatial averaging are done for the number of time steps within the interval of fully developed flow regime and then the arithmetic mean of the results obtained for individual time instances is computed. The number of time instances at which this additional time averaging is performed is given in Table 4.3 together with the corresponding time intervals of the developed flow regime for different bubble-array flows.

4.2.2 Computed characteristics of mean and fluctuating liquid flow

Components of the mean liquid velocity for the bubble-array flow scenarios where the plane averaging is applied are presented in Figure 4.4. It can be seen that for all the considered cases the vertical component of the mean liquid velocity, $\overline{\overline{u}}^P_{l1}$, is, at least, an order of magnitude higher than the ones in both horizontal directions, $\overline{\overline{u}}^P_{l2}$ and $\overline{\overline{u}}^P_{l3}$.

Figure 4.5 shows that, despite the same buoyancy force that drives the liquid flow in all

[1]Bubble-array flow is considered as steady when the mean velocity of the two-phase mixture is approximatively constant in time.

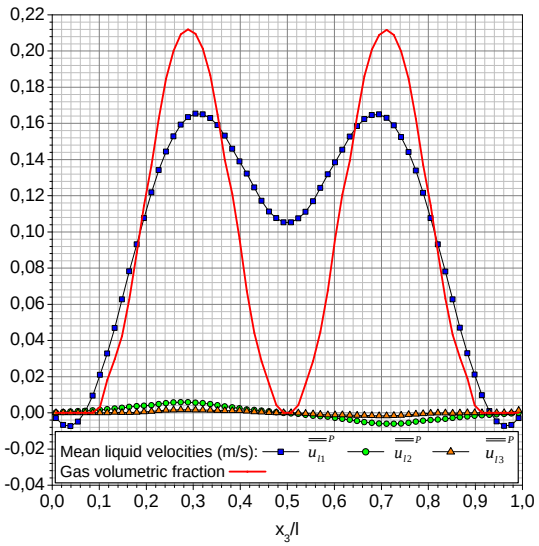

(a) scenario 8BM2

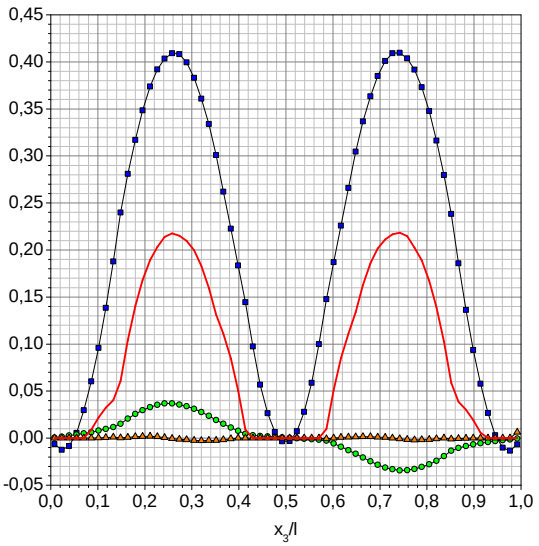

(b) scenario 8BM4

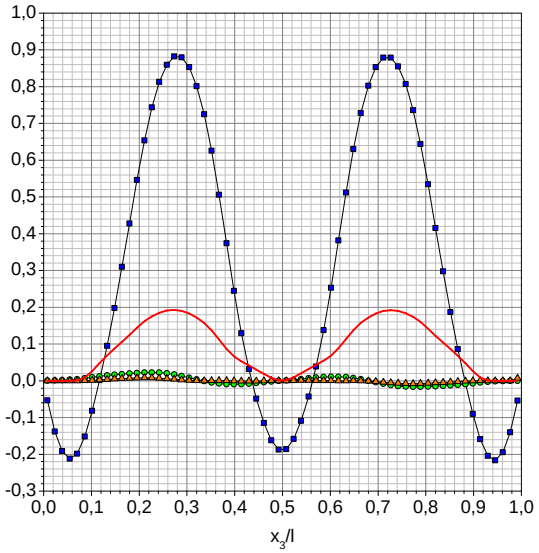

(c) scenario 8BM6

Figure 4.4: Mean liquid velocities and gas volumetric fraction computed by plane averaging for bubble-array flows with different liquid viscosity.

Table 4.3: Averaging set-up for different bubble-array flows.

scenario	averaging	time interval[a]	number of data sets
1BM6	line	$5.5 - 6.0$	20
5BM6		$3.5 - 4.5$	40
8BM6		$0.6 - 2.5$	76
8BM2	plane	$0.2 - 2.1$	76
8BM4		$2.5 - 4.0$	60
8BM6		$0.6 - 2.5$	76

[a] dimensionless time interval where flow is developed

these scenarios, the corresponding profiles of $\overline{\overline{u}}_{l1}^{P}$ remarkably differ, not only in magnitudes, but also in shapes. Although some other parameters such as bubble shape and bubble trajectories certainly influence the mean liquid flow, the observed differences are, in the greatest extent, caused by drastically different magnitudes of the liquid viscosity. Therefore, in the very viscous case 8BM2 the significant portion of the energy transferred to the liquid by rising bubbles is dissipated by viscous stresses, while the rest induces a slow upwards oriented liquid flow in the major part of the channel cross-section. On the other hand, in the low viscous case 8BM6 the internal friction plays a minor role and the liquid flow is mainly governed by the competition of buoyancy and inertial forces. As a result the strong liquid upflow in the domains where bubbles rise occurs, while in the core of the channel and in the vicinity of the lateral walls permanently occupied by the liquid phase the flow is oriented downwards. The bubble-array flow scenario 8BM4 represents an intermediate case where the viscosity is sufficiently strong to prevent the downward liquid flow in the central part of the channel.

Since in bubble-array flow cases where the line averaging is applied (scenarios 1BM6, 5BM6 and 8BM6) two-dimensional averaged quantities are obtained, the presentation of mean liquid velocity components through wall-normal and/or span-wise profiles is not convenient. As in all these cases the horizontal components of the mean liquid flow are very low (see Table 4.4), in Figure 4.5 only contour plots of the mean liquid velocity in the vertical direction are depicted. Figure 4.5 shows that characteristics of the mean liquid flow are governed by the number and the distribution of bubbles. Generally, an upward mean liquid flow is developed behind and in the vicinity of bubbles, while in the rest of the channel liquid flows downwards. However, while in case 5BM6 the mean liquid flow is, mainly, determined by the motion of individual bubbles (positions of individual bubbles can clearly be recognized in Figure 4.5b) in the case 8BM6 mean flow of the liquid phase is driven by two distinctive bubble populations. Finally, due to lower bubble rise velocities the upward mean liquid velocities are locally less intensive in systems with higher gas contents (mean bubble rise velocities for different simulation scenarios can be seen in Table 3.2).

Table 4.4: Range of horizontal mean liquid velocities evaluated by line averaging for bubble-array flow scenarios with different number of bubbles.

simulation scenario	$\overline{\overline{u}}^{L}_{l2}(m/s)$	$\overline{\overline{u}}^{L}_{l3}(m/s)$
1BM6	$-0.036 \div 0.035$	$-0.028 \div 0.041$
5BM6	$-0.094 \div 0.083$	$-0.102 \div 0.115$
8BM6	$-0.060 \div 0.055$	$-0.069 \div 0.070$

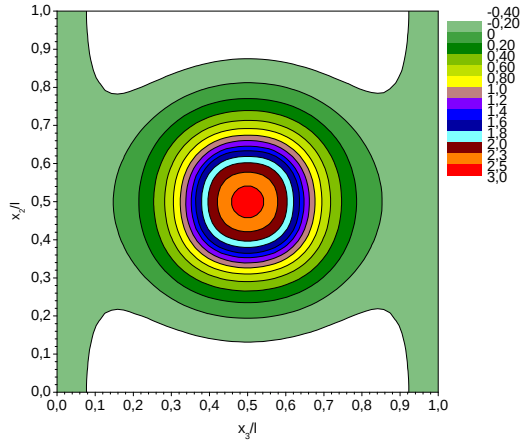

(a) scenario 1BM6

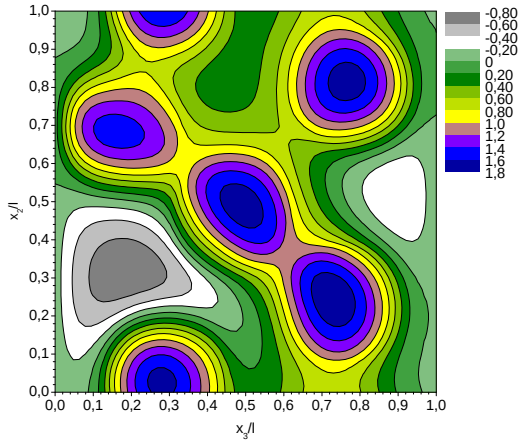

(b) scenario 5BM6

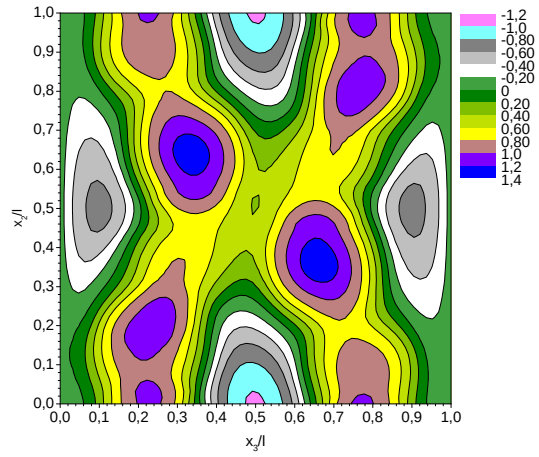

(c) scenario 8BM6

Figure 4.5: Mean liquid velocities in vertical direction computed by line averaging for free bubble-array flows with low liquid viscosity.

The comparison of liquid phase velocity fluctuations generated by the rise of different bubble-arrays is performed by computing the probability density function (p.d.f.).

In order to examine the influence of the suspended gas content on the intensity of induced liquid phase perturbations, in the left part of Figure 4.6 probability density functions of liquid velocity fluctuations are compared for three different magnitudes of the overall gas volumetric fraction: $\langle\alpha_g\rangle = 0.818\%$ (scenario 1BM6), $\langle\alpha_g\rangle = 4.088\%$ (scenario 5BM6) and $\langle\alpha_g\rangle = 6.544\%$ (scenario 8BM6). It can be seen that liquid velocity fluctuations are significantly amplified in multiple bubble cases. However, while the p.d.f. of the horizontal fluctuations is symmetric, the p.d.f. of vertical fluctuations is asymmetric with moderately intense fluctuations ($|u_{l1}^{'}| = 0.1 \div 0.6m/s$) occurring more frequently in the downward direction and very intense fluctuations ($|u_{l1}^{'}| > 0.6m/s$) occurring in the upward direction. The comparison of p.d.f.-s for liquid velocity fluctuations in horizontal directions reveals damping effects of lateral channel walls on the intensity of liquid perturbations for both free bubble-array flow scenarios. However, in the case of fixed bubble-array flow the curves representing corresponding p.d.f.-s totally overlap implying the absence of any wall effect.

The asymmetry of p.d.f. found for liquid velocity fluctuations in the vertical direction and the symmetry of the ones in horizontal directions are in agreement with experimental findings of Risso and Ellingsen [60], who investigated the rise of a monodisperse swarm of ellipsoidal air bubbles within a big tank filled with stagnant tap water. However, contrary to the results of Risso and Ellingsen, the overlapping of p.d.f. curves for liquid velocity fluctuations in here considered bubble-array flows with different number of bubbles could not be obtained by scaling with $\langle\alpha_g\rangle^{0.4}$. This situation is related to the differences in the range of considered gas contents (in [60] $\langle\alpha_g\rangle = 0.64 \div 1.05\%$), to the differences in two-phase flow configuration (bubbly flow in [60] may be assumed as homogeneous) and to the differences in the magnitudes of bubble rise velocity (in [60] $Re_b \sim 800$).

A strong suppression of the liquid velocity fluctuations with an increase of the liquid viscosity can be seen in Figure 4.6-right. Similar to the aforemention observation for the bubble-array flows with different number of bubbles, in all the cases of bubble-array flows with different liquid viscosity the computed p.d.f.-s for horizontal components of liquid velocity fluctuations are symmetric and the one in the vertical direction is asymmetric. The shape of p.d.f.-s for the vertical component of liquid velocity fluctuations, further, significantly changes with change of liquid viscosity. Therefore, intensive velocity fluctuations in the negative direction noticed in the low viscous case 8BM6 are appreciably suppressed in the medium viscous case 8BM4 and almost dampened in the very viscous case 8BM2.

Significantly different magnitudes of liquid velocity fluctuations for three coordinate directions observed in p.d.f.-s (Figure 4.6) imply that the liquid phase turbulence is anisotropic. More details about the anisotropy of the liquid fluctuating field can be drawn from Figures C.1, C.2 and C.3, where components of the root-mean-square (r.m.s.) of liquid velocity fluctuations, $u_{l\alpha}^{rms} = \overline{\overline{u_{l\alpha}^{'} u_{l\alpha}^{'}}}^{0.5}$, are presented. There it can be seen that the fluctuations

in the vertical direction strongly dominate the ones in the horizontal directions in all the bubble-array flow scenarios. Except for fixed bubble-array flow (scenario 1BM6), the magnitudes of r.m.s. of liquid velocity fluctuations in span-wise direction are higher than the one in the wall-normal direction. Moreover, in Figure C.4 it can be seen that this is also true for the fluctuating flow field induced by the motion of free-bubble arrays through the liquids with different viscosity.

The higher magnitudes of liquid velocity fluctuations evaluated by the plane averaging than by the line averaging as discussed in the previous subsection can be observed by comparison of corresponding p.d.f.-s for the scenario 8BM6. However, despite the different magnitudes, the p.d.f.-s of both evaluated liquid fluctuations show the same trend, what supports the use of plane averaging.

4.3 Analysis of the distribution of liquid turbulence kinetic energy in bubble-array flows

The turbulence kinetic energy of the liquid phase is under the assumption of incompressibility defined by [32]:

$$k_l = \frac{1}{2}\overline{\overline{\mathbf{u}_l^{'} \cdot \mathbf{u}_l^{'}}}, \tag{4.22}$$

where $\mathbf{u}_l^{'}$ represents the fluctuating component of the liquid phase velocity and the double overbar indicates the phase-weighted averaging.

For bubble-array flows where the averaging is done over vertical columns of mesh cells (line averaging) the turbulence kinetic energy of liquid phase is evaluated as:

$$k_{l\beta\gamma}^{L} = \frac{1}{2\alpha_{l\beta\gamma}^{L}} \sum_{\alpha=1}^{m_1} f_{\alpha\beta\gamma} u_{\alpha\beta\gamma}^{'} u_{\alpha\beta\gamma}^{'}, \tag{4.23}$$

where the subscripts α, β and γ indicate Cartesian coordinate directions, m_1 represents the number of cells in the column, $\alpha_{l\beta\gamma}^{L}$ denotes the mean liquid volumetric fraction evaluated by line averaging and f stands for the local liquid volumetric fraction.

When averaging is performed over vertical blocks of mesh cells parallel to the channel walls (plane averaging) the liquid turbulence kinetic energy is computed from:

$$k_{l\gamma}^{P} = \frac{1}{2\alpha_{l\gamma}^{P}} \sum_{\alpha=1}^{m_1} \sum_{\beta=1}^{m_2} f_{\alpha\beta\gamma} u_{\alpha\beta\gamma}^{'} u_{\alpha\beta\gamma}^{'}, \tag{4.24}$$

where $\alpha_{l\gamma}^{P}$ represents the mean liquid volumetric fraction evaluated by the plane averaging and m_2 denotes the number of cells in span-wise direction.

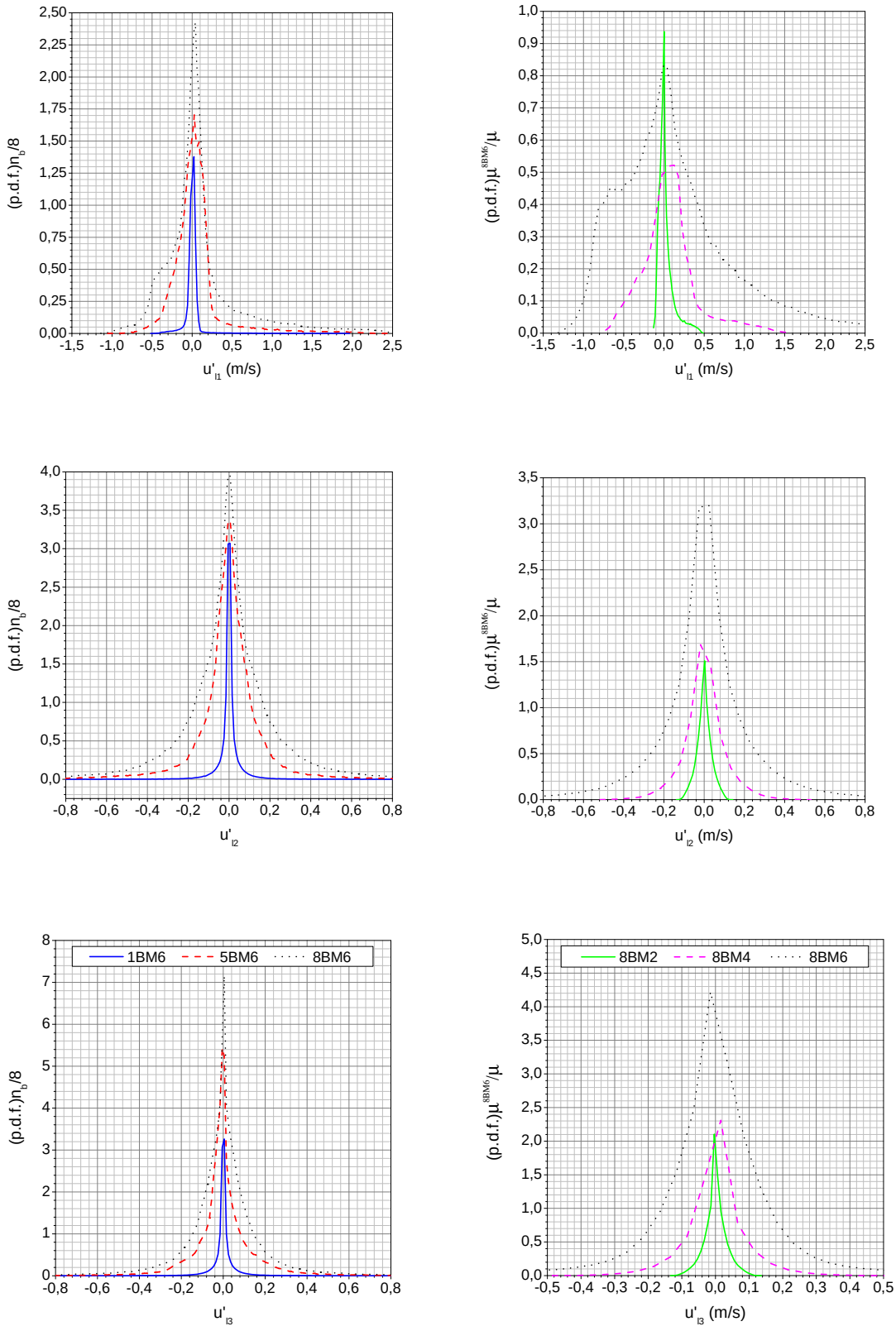

Figure 4.6: Probability density function (p.d.f.) of liquid velocity fluctuations in bubble-array flows computed by line averaging (left) and plane averaging (right).

The evaluated distribution of the liquid turbulence kinetic energy for bubble-array flows where the line averaging applies (scenarios 1BM6, 5BM6 and 8BM6) is, in the form of contour plots, presented in Figure 4.7 and, in the form of wall-normal profiles, in Figure 4.8 for bubble-array flow cases where the plane averaging is performed (scenarios 8BM2, 8BM4 and 8BM6). In these two figures the detailed information about the effects of local flow parameters on the distribution of liquid turbulence kinetic energy for each individual case of considered bubble-array flows (like influence of bubble distribution, effects of rigid walls, etc.) is provided. On the other hand, except for a visual illustration, Figure 4.7 and Figure 4.8 are not convenient either for a corresponding quantitative comparison between different bubble-array flows or an analysis of the effects of global flow parameters on the behaviour of the liquid turbulence kinetic energy (such as influence of liquid viscosity, effects of total gas content, etc.). For that reason in Table 4.5 the following overall data are given:

- overall turbulence kinetic energy of liquid phase evaluated as:

$$\langle k_l^L \rangle = \frac{1}{m_2 m_3} \sum_{\beta=1}^{m_2} \sum_{\gamma=1}^{m_3} \alpha_{l\beta\gamma}^L k_{l\beta\gamma}^L, \tag{4.25}$$

  for cases where the line averaging is applied and by:

$$\langle k_l^P \rangle = \frac{1}{m_3} \sum_{\gamma=1}^{m_3} \alpha_{l\gamma}^P k_{l\gamma}^P, \tag{4.26}$$

  for cases where the plane averaging is applied;

- overall turbulence kinetic energy of liquid phase in two-phase domain, $\langle k_l^L \rangle_{tp}$ and $\langle k_l^P \rangle_{tp}$, evaluated applying equation 4.25 and equation 4.26, respectively, on columns / blocks of cells occupied by two-phase mixture (where the mean liquid volumetric fraction is less than 1), and

- overall turbulence kinetic energy of liquid phase in single phase domain, $\langle k_l^L \rangle_{sp}$ and $\langle k_l^P \rangle_{sp}$, evaluated applying equation 4.25 and equation 4.26, respectively, on columns / blocks of cells fully occupied by the liquid phase (where the mean liquid volumetric fraction is equal 1).

Table 4.5: Overall magnitudes of liquid turbulence kinetic energy (m^2/s^2) for different bubble-array flow scenarios.

	line averaging (A=L)			plane averaging (A=P)		
scenario	1BM6	5BM6	8BM6	8BM6	8BM4	8BM2
$\langle k_l^A \rangle$	$8.813 \cdot 10^{-3}$	$4.535 \cdot 10^{-2}$	$8.552 \cdot 10^{-2}$	$1.658 \cdot 10^{-1}$	$3.917 \cdot 10^{-2}$	$3.992 \cdot 10^{-3}$
$\langle k_l^A \rangle_{tp}$	$7.164 \cdot 10^{-2}$	$7.067 \cdot 10^{-2}$	$1.182 \cdot 10^{-1}$	$1.869 \cdot 10^{-1}$	$4.894 \cdot 10^{-2}$	$4.870 \cdot 10^{-3}$
$\langle k_l^A \rangle_{sp}$	$3.705 \cdot 10^{-3}$	$2.236 \cdot 10^{-2}$	$1.804 \cdot 10^{-2}$	$1.839 \cdot 10^{-2}$	$1.177 \cdot 10^{-2}$	$8.858 \cdot 10^{-4}$

4.3.1 Effects of gas content on distribution of liquid turbulence kinetic energy in bubble-array flows

The contour plot of the liquid turbulence kinetic energy computed for the case of fixed bubble-array flow is presented in Figure 4.7a. As a consequence of the specified flow configuration, where the agitation of the liquid phase is done by only one bubble per computational domain and where the bubble moves along an approximatively rectilinear path, the distribution of k_l^L has a pronounced local character and is closely related to the bubble shape and bubble trajectory. Therefore, while in the channel core high values of k_l^L are noticed, in the peripheral regions of the channel liquid perturbations can be neglected. Surprisingly, in the only centre of the channel, where the highest values of the mean gas volumetric fraction are recorded, magnitudes of liquid turbulence kinetic energy are lower than in the surrounding annular-like domain. An analysis of the instantaneous liquid flow has revealed that the reason for such a distribution of liquid turbulence kinetic energy is the symmetry of the flow pattern that results in very low magnitudes of horizontal liquid velocity fluctuations in the channel core (see Figure C.1). In regions where only liquid phase flows k_l^L decreases so steeply that values an order of magnitude lower than in the channel core are noticed already at a distance of approximatively one half of the bubble size away from the two-phase domain. As the volume of the channel permanently occupied by the liquid phase is significantly larger than the one where bubbles rise (~ 7.5 times), the overall magnitude of the liquid turbulence kinetic energy in the two-phase domain is conspicuously higher than the one in the single-phase region ($\langle k_l^L \rangle_{tp} / \langle k_l^L \rangle_{sp} = 19.336$).

Figure 4.7c shows a quite different distribution of liquid turbulence kinetic energy computed for the case of the free bubble-array flow with the densest bubble population (scenario 8BM6). Although values of the liquid turbulence kinetic energy in domains where bubbles rise are appreciably higher than in the single phase regions ($\langle k_l^L \rangle_{tp} / \langle k_l^L \rangle_{sp} = 6.552$), the liquid flow is disturbed over the whole channel cross-section. The highest values of k_l^L are noticed in regions with the highest magnitudes of the mean gas volumetric fraction and

are caused by a partial alignment of bubbles in the vertical direction. The low values of k_l^L seen in the wall-vicinity are due to damping effects of rigid walls and the downwards oriented liquid flow that prevents bubbles to approach this part of the channel. Patches of low k_l^L values in the central part of the channel are associated with the absence of bubbles. Therefore, it may be concluded that the dense bubble packing in the simulation scenario 8BM6 results in a fully disturbed liquid phase flow where the distribution of liquid turbulence kinetic energy is governed by the collective motion of bubble populations rather than by the motion of each individual bubble.

The distribution of k_l^L computed for the free bubble-array flow scenario 5BM6 (Figure 4.7b) owns some features of both, the rigid fixed bubble-array flow 1BM6 and the fully disturbed free bubble-array flow 8BM6. Although the whole liquid flow is agitated, the distribution of the liquid turbulence kinetic energy in the case 5BM6 still shows a local character and strongly depends on the motion of individual bubbles. Due to the uniform distribution of bubbles over channel cross-section low values of k_l^L are, in this scenario, noticed only in the vicinity of walls and not in the core region like in the case 8BM6. The positions with the highest values of k_l^L in the bubble-array flow 5BM6 are not related to maximal values of the mean gas volumetric fraction like in the case 8BM6, but to the intensive lateral bubble movements.

Finally, if figurative speaking were allowed, the effects of the number of suspended bubbles on the distribution of liquid turbulence kinetic energy could be described as follows. The contour plot of k_l^L for the fixed bubble-array flow 1BM6 makes an impression of a lonely island within a big still ocean, for the free bubble-array flow 5BM6 looks more like an archipelago, while for the simulation scenario 8BM6 reminds to a pair of giant bridges.

When the data are concerned, the effects of the suspended gas content on the bubble-induced perturbations of the liquid phase are illustrated in Figure 4.9a through the relation of the overall liquid turbulence energy, $\langle k_l^L \rangle$, and the overall gas volumetric fraction, $\langle \alpha_g \rangle$. Figure 4.9a shows a non-linear character of the dependance $\langle k_l^L \rangle = f(\langle \alpha_g \rangle)$: for lower gas contents $\langle k_l^L \rangle \propto 1.116 \langle \alpha_g \rangle$ (scenario 1BM6 to scenario 5BM6), while in the range of higher gas volumetric fractions $\langle k_l^L \rangle \propto 1.637 \langle \alpha_g \rangle$ (scenario 5BM6 to scenario 8BM6). The observed dependance of $\langle k_l^L \rangle$ on $\langle \alpha_g \rangle$ is in agreement with experimental results of Lance and Bataille [43], who analyzing fluctuations of water velocity induced by rising air bubbles found a linear variation $\langle k_l^L \rangle \propto 1.05 \langle \alpha_g \rangle$ only for very dilute mixtures ($\langle \alpha_g \rangle < 3\%$), while for higher gas contents the increase of the overall liquid turbulence kinetic energy with the overall gas volumetric fraction was stronger and non-linear.

Taking into account that bubbles in all bubble-array flows considered here are of the same volume and approximatively of the same shape, the following conclusions about the behaviour of $\langle k_l^L \rangle$ with $\langle \alpha_g \rangle$ can be drawn. The almost proportional increase of liquid turbulence kinetic energy with gas content observed in very dilute two-phase mixtures (scenario 1BM6 to scenario 5BM6) implies that the total agitation of the liquid phase can be repre-

sented as a linear superposition of perturbations performed by individual bubbles through the liquid displacement and formation of bubble wakes. However, in mixtures with the dense bubble packing the bubble-bubble distances are sufficiently short to provide the occurrence of mutual hydrodynamic interactions between bubble wakes. Due to this additional agitation fluctuating liquid flow receives a greater amount of kinetic energy, what results in the stronger increase of the overall turbulence kinetic energy with the overall gas volumetric fraction.

4.3.2 Effects of liquid viscosity on distribution of liquid turbulence kinetic energy in bubble-array flows

The distribution of the liquid turbulence kinetic energy, k_l^P, computed on the basis of DNS data for free bubble-array flows with different viscosity of the liquid phase is given in Figure 4.8, while Figure 4.9b presents the dependance of the overall turbulence kinetic energy, $\langle k_l^P \rangle$ on the liquid viscosity[2].

A drastic decrease of the liquid turbulence kinetic energy with the increase of the liquid viscosity can be noticed in both figures. The decrease has a non-linear nature. Therefore, in the range of less viscous flows (scenario 8BM6 to 8BM4) the increase of the liquid viscosity of $\sqrt{10}$ times decreases $\langle k_l^P \rangle$ by the factor of 4.233. However, in the range of more viscous flows (scenario 8BM2 to 8BM4) the same increase of the liquid viscosity ($\sqrt{10}$ times) causes 9.812 times lower values of $\langle k_l^P \rangle$. Taking into account the differences of the considered flow configurations, at least three parameters that are associated with such a behaviour of the liquid turbulence kinetic energy can be identified: the magnitude of the relative bubble velocity, the bubble shape and the formation of bubble wakes. In the following effects of each parameter are discussed.

The simple formulation of the energy in the fluctuating liquid motion produced by the rise of a single bubble [79]:

$$\frac{1}{2} m_{am} \langle u_b \rangle^2, \tag{4.27}$$

implies that the dynamics of the bubble motion affects magnitudes of the liquid turbulence kinetic energy through two parameters: the bubble rise velocity, $\langle u_b \rangle$, and the added mass, m_{am}.

The relative phase velocity certainly strongly influences magnitudes of the liquid turbulence kinetic energy in here considered bubble-array flows since $\langle u_b \rangle$ dramatically decreases with the increase of the liquid viscosity (see Table 3.2). However, a rough estimate shows that the dependance $\langle k_l^P \rangle = f(\mu_l)$ is remarkably steeper than the dependance $\langle u_b \rangle^2 = g(\mu_l)$.

[2]Note that $\langle k_l^P \rangle$ in Figure 4.9b is drawn against the liquid viscosity relative to the viscosity specified in scenario 8BM2

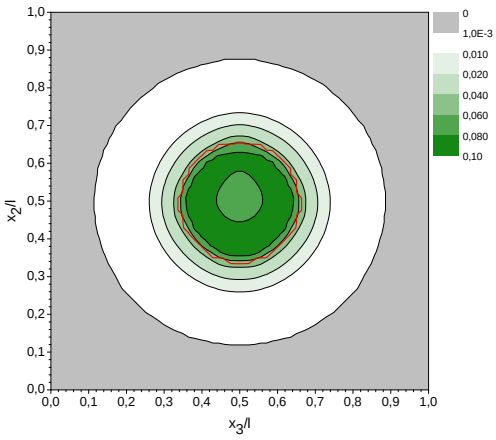

(a) scenario 1BM6

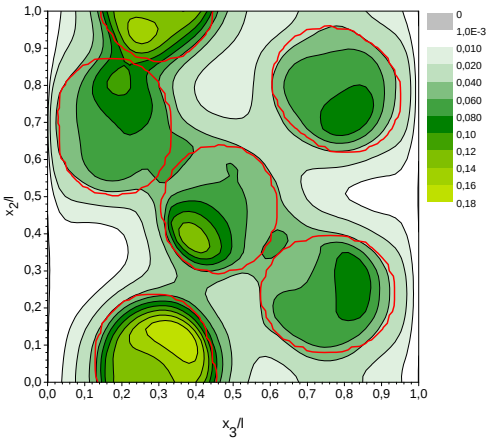

(b) scenario 5BM6

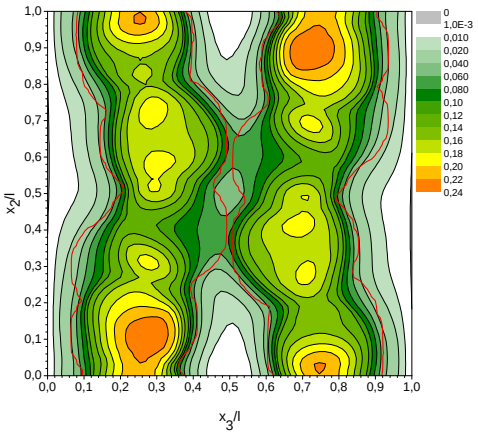

(c) scenario 8BM6

Figure 4.7: Distribution of liquid turbulence kinetic energy in fixed (a) and free (b and c) bubble-array flows evaluated applying line averaging. Red contour lines represent gas volumetric fraction $\alpha_g = 0.1\%$

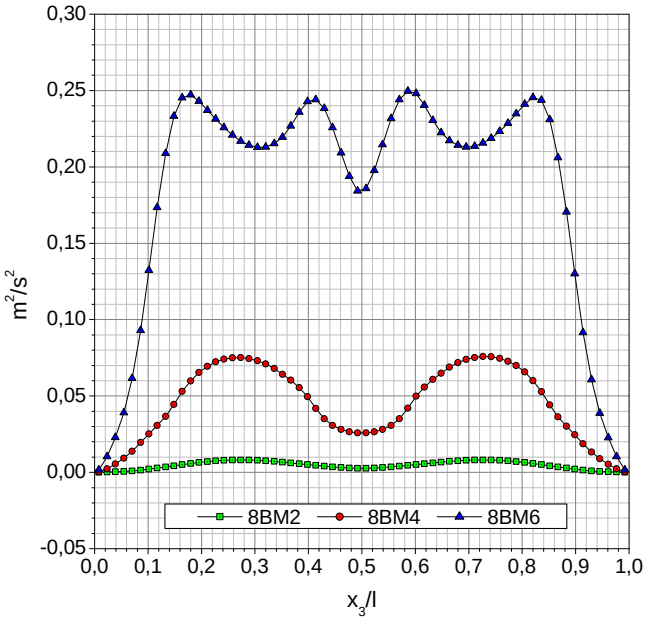

Figure 4.8: Kinetic energy of liquid velocity fluctuations induced by rise of free bubble-arrays through liquids with different viscosity.

This gives rise to the consideration of effects related to the added mass. The added mass for a spherical bubble with the volume V_b is defined as:

$$m_{am}^{s} = 0.5\varrho_l V_b, \tag{4.28}$$

while in the case of an ellipsoidal bubble with the same volume V_b and with the ratio of longer to shorter axis κ by [79]:

$$m_{am}^{e} = Q(\kappa) m_{am}^{s}, \tag{4.29}$$

where:

$$Q(\kappa) = 2\frac{(\kappa^2-1)^{1/2} - \cos^{-1}\kappa^{-1}}{\cos^{-1}\kappa^{-1} - (\kappa^2-1)^{1/2}/\kappa^2}. \tag{4.30}$$

Using the aforementioned relations and the data on bubble axis aspect ratio, κ, from Table 3.2 it can be shown that the shape of bubbles significantly influences the magnitudes of the liquid turbulence kinetic energy. Evaluations of added mass, namely, revealed that comparing to the bubble-array flow case with spherical bubbles (scenario 8BM2) the magnitude of liquid turbulence kinetic energy should be higher 1.159 times in the case 8BM4 and even 1.641 times in the case 8BM6 only due to the ellipsoidal bubble shape in two latter scenarios.

Finally, the formation and mutual interference of bubble wakes are suspected to influence the magnitudes and the distribution of liquid turbulence kinetic energy in bubbly flow

scenarios 8BM2, 8BM4 and 8BM6. The strong liquid viscosity in the bubble-array flow case 8BM2 dissipates the greatest portion of the energy generated by the motion of slow spherical bubbles preventing in that way any formation of bubble wakes. In the medium viscous case 8BM4 a part of the energy generated by the motion of slightly ellipsoidal bubbles is dissipated by viscosity, but a part is released in vortical structures behind the bubbles. Since in this case bubbles move approximatively rectilinearly at significant lateral distances from each other, mutual interactions of their wakes are negligible. In the low viscous case 8BM6, however, bubbles are aggressive oblate ellipsoids moving along non-rectilinear paths and agitating the liquid through the formation of strong wakes and their intensive mutual interactions. The effect of bubble wakes on the distribution of liquid turbulence kinetic energy can be observed analyzing the shapes of corresponding k_l^P profiles given in Figure 4.8. Therefore, while k_l^P profiles in the cases 8BM2 and 8BM4, where the influence of bubble wakes is very weak, are smooth, k_l^P profile in the case 8BM6 has a double saddle-like shape with pronounced peaks in the domains of low gas volumetric fractions. The analysis of the instantaneous liquid velocity field has shown that these peaks are caused by the formation of intensive vortical structures around the bubble equator.

4.3.3 Comparison of computed liquid turbulence kinetic energy in bubble-array flows with predictions based on potential flow theory

The presented DNS based results for the liquid turbulence kinetic energy in bubble-array flows are, further, used to examine the performance of corresponding theoretical approaches. Theoretically, the problem of bubble-induced velocity fluctuations of the liquid phase was firstly addressed by Biesheuvel and van Wijngaarden [5] who applied the potential flow theory on a dilute suspension of spherical identical gas bubbles. Extending considerations to the ellipsoidal bubble shape van Wijngaarden [79] gave the following more general formulation of the turbulence kinetic energy generated in the liquid phase by the relative motion of bubbles:

$$\langle k_l \rangle_{pt} = \frac{1}{2} \frac{n_b m_{am}}{\varrho_l V} \langle u_r \rangle^2, \tag{4.31}$$

where $\langle u_r \rangle$ denotes the volume averaged relative velocity between phases, V represents the volume of flow domain, and n_b stands for the number of bubbles (note that $\langle \alpha_g \rangle = n_b V_b / V$, where V_b is the volume of an individual bubble).

In order to determine whether the description of the liquid phase turbulence by use of the potential flow theory is valid for flow situations at finite Reynolds numbers, Bunner and Tryggvason [10] compared the results obtained by equation 4.31 with the ones evaluated on the basis of their DNS data. DNS based evaluations have shown that turbulence kinetic energy of the liquid phase generated by spherical bubbles rising approximatively rectilinearly at Reynolds number of about 20 is ~ 2.76 times higher than the one evaluated

by equation 4.31. On the basis of this result Bunner and Tryggvason concluded that the fluctuations produced in wakes of bubbles represent a significant portion of the total turbulence kinetic energy in the liquid phase. On the other side, Lance and Bataille [43] found a good agreement between their experimental results and the corresponding potential flow solution for the kinetic energy of liquid phase velocity fluctuations generated by the rise of homogeneous swarm of large ellipsoidal air bubbles through the originally stagnant water (the equivalent bubble diameter $\sim$ 5mm, bubble Reynolds number $\sim$ 1000, helical bubble trajectories). Consequently, they concluded that wakes contribute only a small amount to the total kinetic energy of the fluctuating liquid motion.

The comparison of results obtained by use of the potential flow approach with the ones obtained by use of DNS data in this work is, unfortunately, not straightforward due to the existence of lateral channel walls. Therefore, as the turbulence is in any case not homogeneous in the wall-normal direction, the volume averaging may not be applied and the strict use of the equation 4.31 is not possible. Instead, an engineering approach is adopted. This approach is here presented in detail for the case of plane averaging.

The turbulence kinetic energy of the liquid phase is using the potential flow approach and plane averaging evaluated as:

$$k_{l\gamma}^{P,pt} = \frac{1}{4} Q(\kappa) \alpha_{g\gamma}^{P} |\overline{\overline{\mathbf{u}}}_{r\gamma}^{P}|^2 \tag{4.32}$$

where the subscript γ indicates the wall-normal direction, and $\overline{\overline{\mathbf{u}}}_{r}^{P}$ represents the plane averaged relative velocity between phases. In order to obtain the corresponding overall quantity, profiles of the liquid turbulence kinetic energy evaluated by 4.32 are, further, averaged over the wall-normal distance (replacing k_l^P by $k_l^{P,pt}$ in 4.26 the overall quantity $\langle k_l^{P,pt} \rangle$ is computed). Performing an analogous procedure in cases where line averaging is applied $\langle k_l^{L,pt} \rangle$ is evaluated.

Results for $\langle k_l^{L,pt} \rangle$ and $\langle k_l^{P,pt} \rangle$ are presented in Figure 4.9. It can be seen that the overall turbulence kinetic energy of the liquid phase obtained using the potential flow approach is, comparing to the one evaluated on the basis of DNS data, generally underestimated. Due to higher Reynolds numbers the underestimation is somewhat lower in scenarios with low liquid viscosity than in very viscous bubble-array flow cases: $\sim$ 1.7 times for the case of fixed bubble array flow (scenario 1BM6), $\sim$ 2 times for both free-bubble array flow cases (scenarios 5BM6 and 8BM6) and $\sim$ 2.4 times in scenarios 8BM2 and 8BM4.

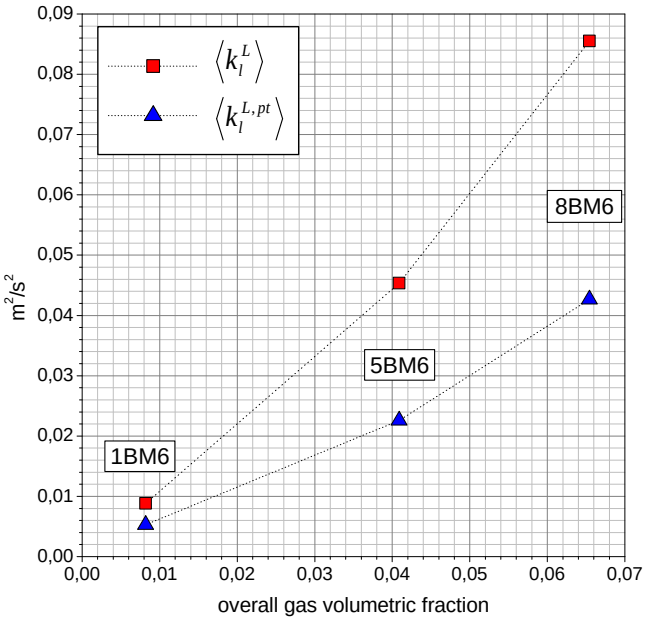

(a) line averaging

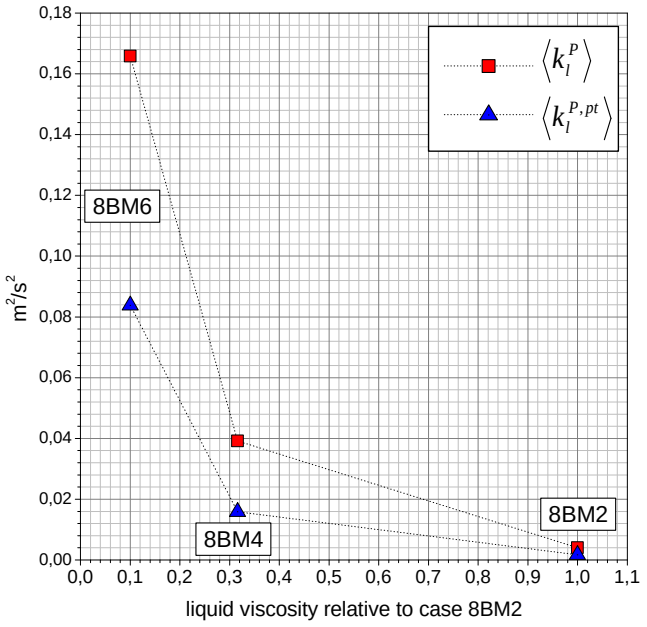

(b) plane averaging

Figure 4.9: Overall turbulence kinetic energy of the liquid phase evaluated on the basis of DNS data ,$\langle k_l^L \rangle$ and $\langle k_l^P \rangle$, and potential flow theory, $\langle k_l^{L,pt} \rangle$ and $\langle k_l^{P,pt} \rangle$.

Chapter 5

Quantitative analysis of mechanisms governing balance of liquid turbulence kinetic energy in bubble-array flows

This chapter focuses on the quantitative analysis of balance terms in the basic equation for liquid turbulence kinetic energy (k_l equation) based on results of presented direct numerical simulations (DNS). The chapter is organized as follows. The first section outlines the software module developed for the numerical evaluation of balance terms in k_l equation. Evaluated results for diffusion transport, viscous dissipation, interfacial generation and transfer of turbulence kinetic energy between the mean and fluctuating liquid flow are presented and discussed in detail in section 2. The relation between different mechanisms governing the liquid turbulence in simulated bubbly flows is analyzed considering the budget of k_l equation in section 3.

5.1 The software module GENERG-TP for evaluation of balance terms in turbulence kinetic energy equation for the liquid phase in bubble-array flows

In order to perform the numerical evaluation of balance terms in the basic equation for the liquid turbulence kinetic energy (equation 2.13), a computer program is developed and as a separate module implemented in the evaluation part of the computer code TURBIT-VoF. This section outlines main features of the developed program structure.

The module is called GENERG-TP. *'GENERG'* is adopted to be the same as the name of the existing module for single-phase turbulence analysis, while *'TP'* indicates that this modul deals with two-phase flows.

The module GENERG-TP consists of two main parts:

- The part called EXACT performs the numerical evaluation of balance terms in the turbulence kinetic energy equation for the liquid phase on the basis of the rigorous mathematical definitions given by equation 2.14. Results are used for the quantitative analysis of mechanisms governing the balance of liquid turbulence kinetic energy in bubble-array flows (presented in this chapter).
- The part called MODELS computes corresponding balance terms on the basis of modelling approaches commonly applied to approximate for practice inappropriate formulations in equation 2.14. Results are used to estimate the assessment of closure assumptions employed in engineering considerations of the liquid phase turbulence in bubbly gas-liquid flows (presented in the next chapter).

Within the part EXACT four subprogram are developed, where the diffusion, dissipation, production and interfacial term are computed on the basis of strict mathematical formulations given by equation 2.14. While the first three routines are independent on the previously existing TURBIT-VoF program structures, the routine for the evaluation of the interfacial term strongly relies on the integration part of TURBIT-VoF.

As presented in the previous chapter, namely, the evaluation of the liquid velocity at the phase interface requires a very precise information about the motion of the interfacial surface. On the other hand, in order to avoid storage of a huge amount of data, results of direct numerical simulations are not saved for each time step of the integration, $\delta\vartheta$, but at significantly larger time distances, $\delta\vartheta_e$ (in the case of fixed bubble-array flow $\delta\vartheta_e = 500\delta\vartheta$ and for free bubble-array flow scenarios $\delta\vartheta_e = 250\delta\vartheta$). Concerning the equation 4.12, this means that the available DNS data provide the information about the unit normal vector, $\mathbf{n}$, at the time instant ϑ_0, but not the information about the distance $\delta\mathbf{x}$ since the position of the phase interface at the time instant $\vartheta_0 + \delta\vartheta$ is not stored. In order to obtain these data the module GENERG-TP is connected with the TURBIT-VoF integration part (see Figure 5.1). In other words, for each time instance considered in the module GENERG-TP, local liquid volumetric fraction is advected by TURBIT-VoF integration job for one time step. After the data on the local liquid volumetric fraction at the time instance $\vartheta_0 + \delta\vartheta$ are known, the interface reconstruction is performed relating once more to corresponding subroutines in the integration part (details on advection and reconstruction algorithms applied in TURBIT-VoF can be found in [62]).

Due to essentially different procedures used to obtain an averaged quantity, most of the subroutines in the module GENERG-TP could not be used for both concepts, line aver-

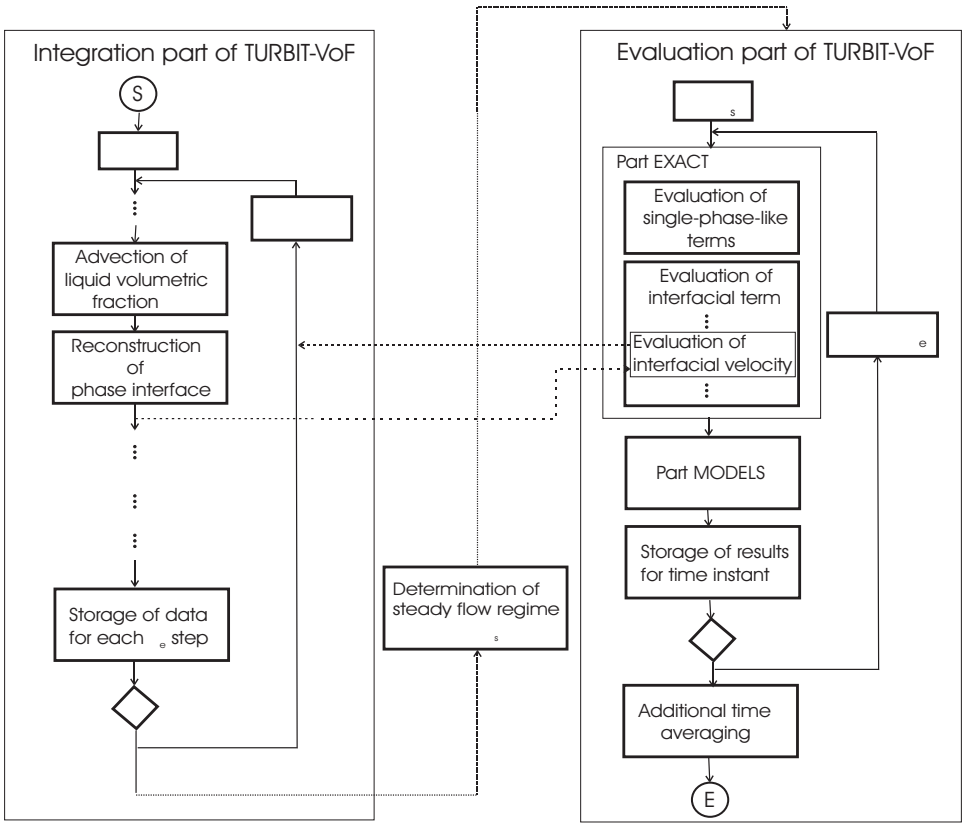

Figure 5.1: Structure of the module GENERG-TP and its connection with the integration part of TURBIT-VoF

aging and plane averaging, but had to be written separately for each averaging case. The additional time averaging of the results obtained using line / plane averaging is performed by subroutines originally implemented in the module GENERG. Time intervals, where the flow is assumed to be steady, as well as the number of data sets used for additional time averaging are presented in Table 4.3 for all the considered bubble-array flows.

All evaluations by the module GENERG-TP are based on the use of dimensionless quantities as defined in TURBIT-VoF methodology (see section 2.3). For consistency reasons, dimensionless formulations of corresponding balance terms from the equation 2.14 are given in the next section together with the results computed by the module GENERG-TP.

5.2 Balance terms in basic equation for liquid turbulence kinetic energy in bubble-array flows: results and discussions

In this section the quantitative analysis of mechanisms governing the balance of liquid turbulence kinetic energy is performed on the basis of DNS data for bubble-array flows. In this context, the diffusion transport, viscous dissipation, interfacial generation and transfer of turbulence kinetic energy between the mean and fluctuating liquid flow evaluated by the module GENERG-TP are presented and discussed in detail.

5.2.1 Diffusion transport of liquid turbulence kinetic energy in bubble-array flows

In the basic balance equation for turbulence kinetic energy of the liquid phase (equation 2.14) the diffusion term is represented by the following sum:

$$\mathrm{Diff}(k_l) = \frac{1}{\varrho_l}\frac{\partial}{\partial x_\beta}(\alpha_l\overline{\overline{\tau_{l\alpha\beta}^{'}u_{l\alpha}^{'}}}) - \frac{\partial}{\partial x_\beta}(\frac{1}{2}\alpha_l\overline{\overline{u_{l\alpha}^{'}u_{l\alpha}^{'}u_{l\beta}^{'}}}) - \frac{1}{\varrho_l}\frac{\partial}{\partial x_\alpha}(\alpha_l\overline{\overline{p_l^{'}u_{l\alpha}^{'}}}), \tag{5.1}$$

where subscripts α and β indicate Cartesian coordinate directions to which Einstein summation rule applies, and the double overbar denotes phase-weighted averaging, while the liquid phase density, pressure fluctuation, velocity fluctuation and mean volumetric fraction are, respectively, represented by ϱ_l, $p_l^{'}$, $u_l^{'}$ and α_l. The fluctuating viscous stress of the liquid phase is defined by:

$$\tau_{l\alpha\beta}^{'} = \mu_l\left(\frac{\partial u_\alpha^{'}}{\partial x_\beta} + \frac{\partial u_\beta^{'}}{\partial x_\alpha}\right), \tag{5.2}$$

where μ_l stands for the liquid viscosity.

Like in single-phase flows the diffusion transport of liquid turbulence kinetic energy in bubbly gas-liquid flows involves three contributions. Thus, the first term in expression 5.1, called molecular diffusion, represents the diffusion of liquid turbulence kinetic energy caused by molecular transport process, the second term, named triple correlation, is regarded as the rate at which liquid turbulence kinetic energy is transported by velocity fluctuations, while the last term represents another form of turbulent transport resulting from the correlation of the liquid pressure and velocity fluctuations and is called pressure correlation. In a general case, each of these terms represents a sum of three contributions in Cartesian coordinate directions, i.e. the total diffusion term, $\mathrm{Diff}(k_l)$, contains nine subterms to be evaluated. However, when the liquid turbulence is homogeneous in certain direction, the diffusion process in this direction does not occur, what significantly simplifies expression 5.1 (partial derivatives in the direction of homogeneous turbulence are zero-valued).

In the context of the aforementioned, the evaluation of the diffusion term by the module GENERG-TP is performed as follows. In cases where the liquid phase turbulence is considered to be homogeneous in the vertical (x_1), direction, i.e. where the line averaging is applied (scenarios 1BM6, 5BM6 and 8BM6) the diffusion of liquid turbulence kinetic energy is computed from:

$$\begin{aligned}\mathrm{Diff}(k_l)^L = &\underbrace{\frac{u_{ref}^3}{l_{ref}}\frac{1}{\rho_l}\frac{1}{\mathrm{Re}_{ref}}\left[\frac{\partial}{\partial X_2}\left(\alpha_l^L\sum_{\beta=1}^{3}\overline{\overline{\mathbf{T}'_{l\beta 2}U'_{l\beta}}}^{L}\right)+\frac{\partial}{\partial X_3}\left(\alpha_l^L\sum_{\beta=1}^{3}\overline{\overline{\mathbf{T}'_{l\beta 3}U'_{l\beta}}}^{L}\right)\right]}_{\text{molecular diffusion}}\\ &\underbrace{-\frac{u_{ref}^3}{l_{ref}}\left[\frac{\partial}{\partial X_2}\left(\alpha_l^L\frac{1}{2}\sum_{\beta=1}^{3}\overline{\overline{U'_{l\beta}U'_{l\beta}U'_{l2}}}^{L}\right)+\frac{\partial}{\partial X_3}\left(\alpha_l^L\frac{1}{2}\sum_{\beta=1}^{3}\overline{\overline{U'_{l\beta}U'_{l\beta}U'_{l3}}}^{L}\right)\right]}_{\text{triple correlation}}\\ &\underbrace{-\frac{u_{ref}^3}{l_{ref}}\frac{1}{\rho_l}\left[\frac{\partial}{\partial X_2}\left(\alpha_l^L\overline{\overline{P'_lU'_{l2}}}^{L}\right)+\frac{\partial}{\partial X_3}\left(\alpha_l^L\overline{\overline{P'_lU'_{l3}}}^{L}\right)\right]}_{\text{pressure correlation}}\end{aligned} \tag{5.3}$$

where the superscript L denotes the line averaging.

In cases where the liquid phase turbulence is assumed to be homogeneous in both directions, vertical (x_1) and span-wise (x_2), i.e. where the plane averaging is applied (scenarios 8BM2, 8BM4 and 8BM6), the expression 5.1 reduces to:

$$\begin{aligned}\mathrm{Diff}(k_l)^P = &\underbrace{\frac{u_{ref}^3}{l_{ref}}\frac{1}{\rho_l}\frac{1}{\mathrm{Re}_{ref}}\frac{\partial}{\partial X_3}\left(\alpha_l^P\sum_{\beta=1}^{3}\overline{\overline{\mathbf{T}'_{l\beta 3}U'_{l\beta}}}^{P}\right)}_{\text{molecular diffusion}}\underbrace{-\frac{u_{ref}^3}{l_{ref}}\frac{\partial}{\partial X_3}\left(\alpha_l^P\frac{1}{2}\sum_{\beta=1}^{3}\overline{\overline{U'_{l\beta}U'_{l\beta}U'_{l3}}}^{P}\right)}_{\text{triple correlation}}\\ &\underbrace{-\frac{u_{ref}^3}{l_{ref}}\frac{1}{\rho_l}\frac{\partial}{\partial X_3}\left(\alpha_l^P\overline{\overline{P'_lU'_{l3}}}^{P}\right)}_{\text{pressure correlation}},\end{aligned} \tag{5.4}$$

where the superscript P stands for the plane averaging.

Since the evaluation of balance terms in the module GENERG-TP is based on use of dimensionless quantities (indicated by capital letters) in expressions 5.3 and 5.4 the reference velocity, u_{ref}, reference length, l_{ref}, and reference Reynolds number, Re_{ref}, appear. It is reminded that the dimensionless liquid density has unit value, $\rho_l = 1$, because the density of the liquid phase is adopted as a reference one.

Contour plots of the diffusion term, $\mathrm{Diff}^L(k_l)$, evaluated by the module GENERG-TP for bubble-array flow scenarios 1BM6, 5BM6 and 8BM6 are presented in Figure 5.2. It can be seen that the turbulence kinetic energy generated in the part of the channel where the bubbles rise is through an intensive diffusion process transported towards the single-phase domains. However, in Figure 5.2 significant differences can be observed when the plot of the diffusion term computed for the fixed bubble-array flow (scenario 1BM6) is compared with the ones evaluated for free bubble-array flows (scenarios 5BM6 and 8BM6). Although something lower values are noticed in the only centre of the channel, the diffusion in the case 1BM6 is over significant part of the two-phase domain negative and almost constant. Therefore, the liquid turbulence kinetic energy is, in this case, almost symmetrically transported from the regions where bubbles rise towards the domains where only the liquid flows. In these domains, however, the diffusion steeply decreases and at a very short distance from the bubble interface may be considered as negligible. Contrary to the fixed bubble-array flow (scenario 1BM6) where the intensity of the diffusion term mainly depends on the position relative to the bubble centre, in scenarios with free bubble-arrays (5BM6 and 8BM6) a strong influence of other bubbles on the diffusion process is evident (see Figure 5.2b and c).

Contributions of corresponding subterms to the total diffusion term are illustrated in Figure 5.3 for the fixed bubble-array flow (scenario 1BM6) at the span-wise position $x_2 = 0.5859l$[1] and for free-bubble array flow (scenario 8BM6) at span-wise position $x_2 = 0.1015l$[2] [3]. In Figure 5.3a it can be seen that the contribution of the pressure correlation to the total diffusion term is, in the case of fixed bubble-array flow, the dominant one, particularly in the single-phase domains, while the contributions of the molecular diffusion and triple correlation are approximatively equal. The dominance of the pressure correlation over the contributions of the molecular diffusion and the triple correlation is also observable in the

[1] Due to symmetrical profiles of liquid turbulence quantities in the fixed bubble-array flow (scenario 1BM6) the central plane $x_2 = 0.5l$ is not convenient to represent the portion of the total diffusion term contributed by an individual subterm.

[2] This position is chosen because the intersection of the corresponding wall-normal plane with the bubble moving on the right-hand side passes through its central part, while the section with the bubble rising on the left-hand side is approximatively in the middle between the bubble centre and the bubble hip. In this way the profiles of the diffusion subterms for two different structures of the liquid flow are put into consideration.

[3] For the sake of consistency corresponding wall-normal profiles in the cases where line averaging applies are presented at mentioned span-wise positions for other balance terms, too.

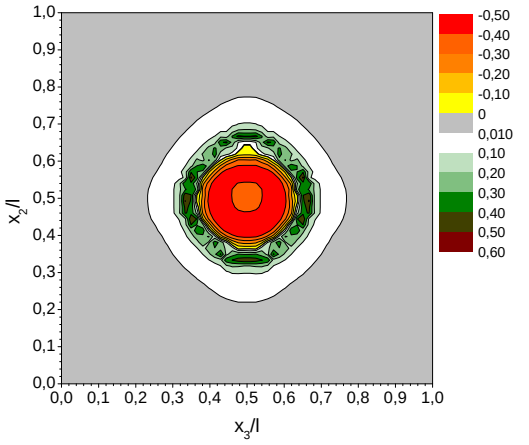

(a) scenario 1BM6

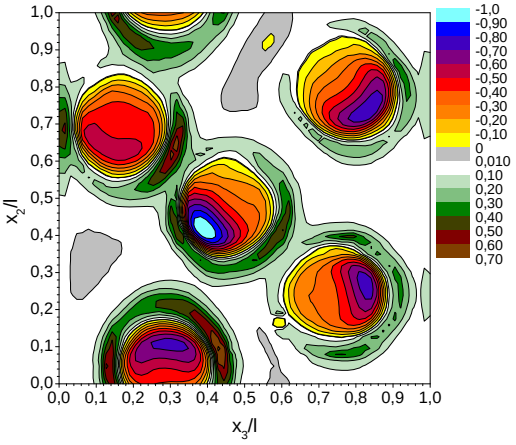

(b) scenario 5BM6

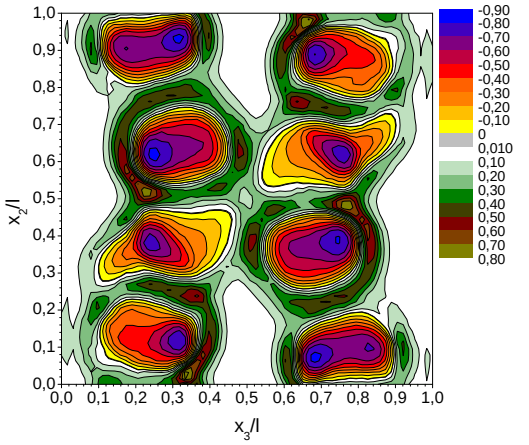

(c) scenario 8BM6

Figure 5.2: Diffusion of liquid turbulence kinetic energy evaluated by module GENERG-TP for fixed (scenario 1BM6) and free (scenarios 5BM6 and 8BM6) bubble-array flows.

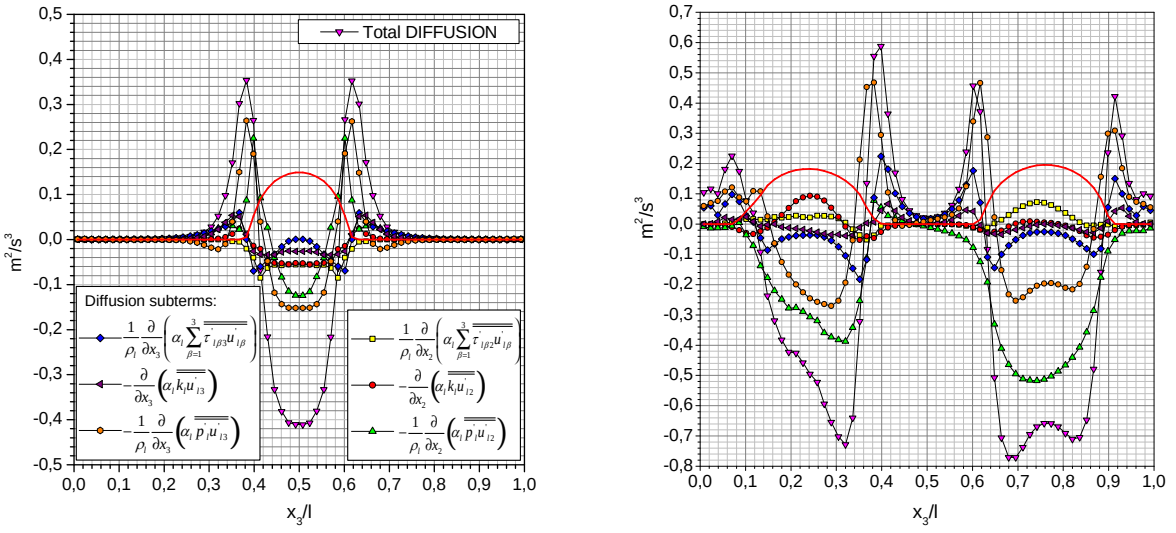

(a) scenario 1BM6 (b) scenario 8BM6

Figure 5.3: Wall-normal profiles of diffusion term and diffusion subterms evaluated by module GENERG-TP for fixed bubble-array flow 1BM6 (at $x_2 = 0.5859l$) and free bubble-array flow 8BM6 (at $x_2 = 0.1015l$). Solid red line represents mean gas volumetric fraction.

free-bubble array flow 8BM6 (see Figure 5.3b).

In Figure 5.4 wall-normal profiles of the total diffusion term and diffusion subterms evaluated applying the plane averaging are compared for free bubble-array flows with different liquid viscosity (scenarios 8BM2, 8BM4 and 8BM6). It can be seen that all the profiles are symmetric with respect to the channel axis, what is to expect since in the case of plane averaging the distribution of bubbles is apparently symmetric with respect to the channel axis. However, the shape of diffusion profiles for different bubble-array flows is significantly different. Therefore, while the diffusion profile for the very viscous case 8BM2 is almost smooth, the profile in the case with the lowest liquid viscosity (scenario 8BM6) is associated with the number of local peaks.

In order to find a proper explanation for observed differences in profiles of the diffusion term the analysis is in the following focused on corresponding diffusion subterms. Wall-normal profiles of diffusion subterms presented in Figure 5.4 show that an increase in the liquid viscosity has a dramatic effect on the role of mechanisms that govern the diffusion transport of the liquid turbulence kinetic energy. Thus, in the case 8BM6 the transport of liquid turbulence kinetic energy from the domains with high gas volumetric fractions is, at a great extent, performed by the work of the fluctuating liquid pressure gradient (expressed by pressure correlation) and, at a lower extent, by the fluctuating velocity (represented by triple correlation). The transport by the fluctuating viscous stress (molecular diffusion)

in this domain is almost negligible. In domains with low gas volumetric fractions and in single-phase regions the role of the different contributions to the total diffusion term is quite different - the molecular diffusion gains importance, while the triple correlation plays a minor role. The pressure correlation, however, represents a significant form of the diffusion transport over almost the whole domain. An increase of the liquid viscosity by the factor of $\sqrt{10}$ (scenario 8BM4), changes the situation appreciably. Therefore, the transport by velocity fluctuations is completely suppressed, while the contributions of the molecular diffusion and the pressure correlation are almost equal. A further increase of the liquid phase viscosity (scenario 8BM2) additionally suppresses the turbulent transport of the liquid turbulence kinetic energy. Although the contribution of the pressure correlation in this case is lower than the one of the molecular diffusion, it is remarkable that even in such a very viscous liquid flow, the diffusion of liquid turbulence kinetic energy resulting from the correlation of pressure and velocity fluctuations is not to neglect.

The observed different intensity of the diffusive transports due to the fluctuating liquid flow is important for the derivation of closure assumptions for the diffusion term. As it will be seen in chapter 6, namely, the approaches for the diffusion modelling are based on closure assumptions derived for single-phase forced flows. In these flows the pressure correlation is of minor importance and is, subsequently, either neglected or grouped with the triple correlation and, further, modelled as a gradient-like process. Since here presented analyses have pointed out the significant role that the pressure correlation plays in the redistribution of the liquid turbulence kinetic energy, the validity of such an assumption for gas-liquid flows may be judged as questionable, at least, for the class of slow bubble-driven liquid flows considered in this work.

5.2.2 Viscous dissipation of liquid turbulence kinetic energy in bubble-array flows

The dissipation term represents the rate at which the turbulence kinetic energy is converted into the thermal internal heat and is equal to the mean rate at which work is done by the fluctuating part of the strain rate against the fluctuating viscous stress. In the basic balance equation for the liquid turbulence kinetic energy 2.14 this term is defined by:

$$\varepsilon_l = -\frac{1}{\varrho_l}\alpha_l \overline{\overline{\tau'_{l\alpha\beta}\frac{\partial u'_{l\alpha}}{\partial x_\beta}}}, \tag{5.5}$$

where the fluctuating viscous stress of the liquid phase, τ'_l, is given by equation 5.2.

The evaluation of the dissipation term by the module GENERG-TP is performed using the following expression:

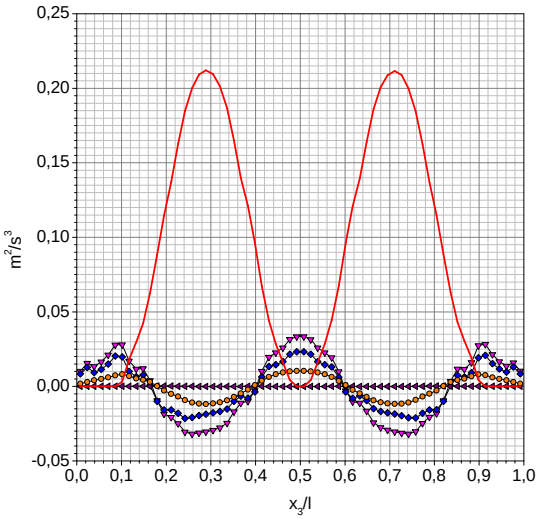

(a) scenario 8BM2

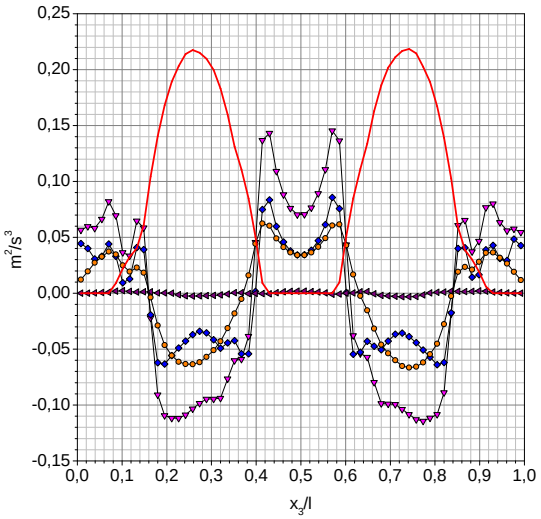

(b) scenario 8BM4

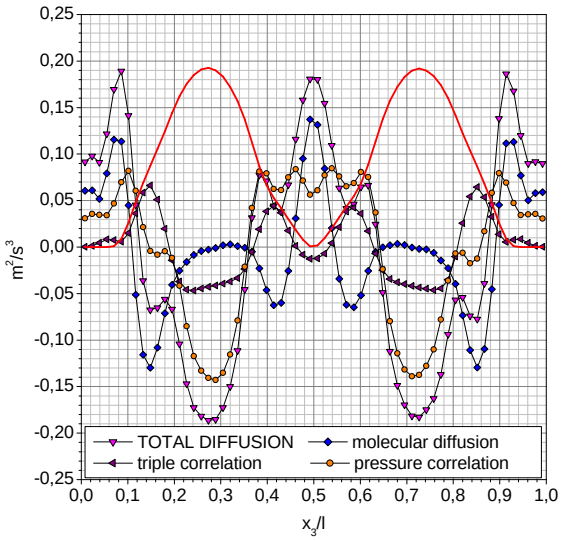

(c) scenario 8BM6

Figure 5.4: Wall-normal profiles of diffusion term and diffusion subterms evaluated by module GENERG-TP for free bubble-array flows with different liquid viscosity. Solid red line represents mean gas volumetric fraction.

$$\varepsilon_l^L = -\frac{u_{ref}^3}{l_{ref}}\frac{\eta_l}{\rho_l}\frac{1}{\mathrm{Re}_{ref}}\alpha_l^L\overline{\overline{\left(\frac{\partial U'_{l\alpha}}{\partial X_\beta}+\frac{\partial U'_{l\beta}}{\partial X_\alpha}\right)\frac{\partial U'_{l\alpha}}{\partial X_\beta}}}^{L}\ , \tag{5.6}$$

for the cases where the line averaging is applied (scenarios 1BM6, 5BM6 and 8BM6), and by:

$$\varepsilon_l^P = -\frac{u_{ref}^3}{l_{ref}}\frac{\eta_l}{\rho_l}\frac{1}{\mathrm{Re}_{ref}}\alpha_l^P\overline{\overline{\left(\frac{\partial U'_{l\alpha}}{\partial X_\beta}+\frac{\partial U'_{l\beta}}{\partial X_\alpha}\right)\frac{\partial U'_{l\alpha}}{\partial X_\beta}}}^{P}\ , \tag{5.7}$$

when the plane averaging is performed (scenarios 8BM2, 8BM4 and 8BM6). Note that in expressions 5.6 and 5.7 η_l represents dimensionless liquid viscosity, $\eta_l = \mu_l/\mu_{l,ref}$.

The dissipation rate ε_l^L evaluated by the module GENERG-TP for bubble-array flows with the low liquid viscosity (scenarios 1BM6, 5BM6 and 8BM6) is displayed in Figure 5.5. The first impression is that the dissipation rate of liquid turbulence kinetic energy increases with the number of bubbles, i.e. with the gas volumetric fraction. In order to make a straightforward estimate of this dependance, the overall magnitudes of the dissipation rate are computed within the whole flow domain, $\langle\varepsilon_l^L\rangle$, within the two-phase domain, $\langle\varepsilon_l^L\rangle_{tp}$, and within the single-phase domain, $\langle\varepsilon_l^L\rangle_{sp}$. The results are presented in Figure 5.7. It can be seen that the magnitude of $\langle\varepsilon_l^L\rangle$ increases non-linearly with $\langle\alpha_g\rangle$: in the range of lower gas volumetric fractions $\langle\varepsilon_l\rangle \propto -3.664\langle\alpha_g\rangle$ (scenario 1BM6 to 5BM6), while for higher gas contents $\langle\varepsilon_l\rangle \propto -5.464\langle\alpha_g\rangle$ (scenario 5BM6 to 8BM6).

The non-linear increase of the dissipation rate with the overall gas volumetric fraction has, already, been observed experimentally by Wang et al. for a pipe bubbly flow and by Lance for a bubbly flow with grid-generated liquid turbulence [81]. Due to essentially different types of considered bubbly flows results obtained in this work cannot be quantitatively compared to the aforementioned ones. It is, however, worth to mention that the dependance of $\langle\varepsilon_l^L\rangle$ on $\langle\alpha_g\rangle$ presented in Figure 5.7 qualitatively agrees with observations of Lance, i.e. in the range of higher gas contents the increase of the dissipation rate with the overall gas volumetric fraction is stronger.

Bunner and Trygvason [11] reported DNS based data for the dissipation rate of liquid turbulence kinetic energy in a bubble-driven liquid flow of the similar type to the one considered in this work. They found that increasing the overall gas volumetric fraction by the factor of 3 (from 2% to 6%) causes an increase of the overall dissipation rate by a factor of 3.056. Hence, the relative increase of the overall dissipation rate with the overall gas volumetric fraction reported by Bunner and Tryggvason ($3.056/3 = 1.018$) is slightly lower comparing to the increase evaluated in this work: $\langle\varepsilon_l^L\rangle^{5\mathrm{BM6}}/\langle\varepsilon_l^L\rangle^{1\mathrm{BM6}} = 1.074\langle\alpha_g\rangle^{5\mathrm{BM6}}/\langle\alpha_g\rangle^{1\mathrm{BM6}}$ and $\langle\varepsilon_l\rangle^{8\mathrm{BM6}}/\langle\varepsilon_l\rangle^{5\mathrm{BM6}} = 1.194\langle\alpha_g\rangle^{8\mathrm{BM6}}/\langle\alpha_g\rangle^{5\mathrm{BM6}}$ (note that superscripts indicate bubble-array flow scenario). The observed differences are only partially caused by the different parameters of bubble-array flow simulations specified in [11] (fully periodic computational domain, $\mathrm{E\ddot{o}}_b = 5$, $\mathrm{Re}_b = 23-25$). What seems to be more important is the way used by Bunner and Tryggvason to set up the simulations with higher gas content. Therefore, the increase of

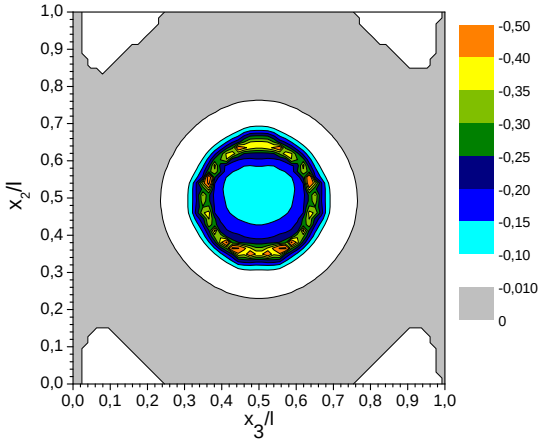

(a) scenario 1BM6

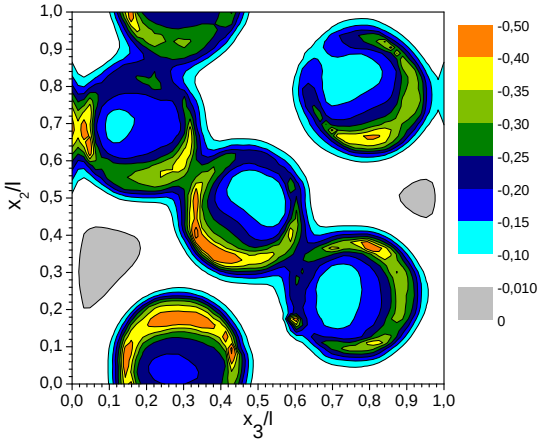

(b) scenario 5BM6

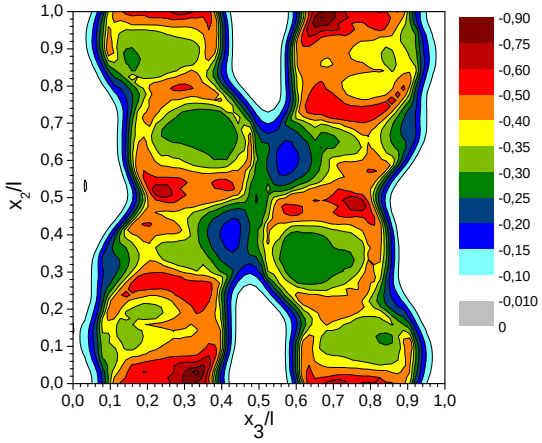

(c) scenario 8BM6

Figure 5.5: Dissipation rate of liquid turbulence kinetic energy evaluated by module GENERG-TP for fixed (scenario 1BM6) and free (scenarios 5BM6 and 8BM6) bubble-array flows.

the gas volumetric fraction in [11] is achieved by specifying the larger diameter of bubbles and not by the addition of new bubbles to the flow domain like it is done in the work presented here. The ratio 1.018, thus, expresses mainly effects of the change in structure and size of bubble wakes due to larger bubbles, and not the effects of increased number of agitators on the dissipation of liquid turbulence kinetic energy.

Figure 5.5 shows that the maximal values of the dissipation rate in bubbly flows with low liquid viscosity are, generally, reached at the peripheral parts of bubbles. This effect associated to the large gradients of the fluctuating liquid flow in the vicinity of gas-liquid interface is, especially, pronounced in the case of fixed bubble-array flow. In Figure 5.5a it can, namely, be seen that in the narrow annular-like region containing bubble interface the magnitude of the dissipation rate is locally more than double higher comparing to the neighbouring central domain. This is even more evident in Figure 5.6a, where corresponding wall-normal profiles of the dissipation term and dissipation subterms are depicted. There it can be seen that all the profiles change steeply in the vicinity of the bubble border and reach a local minimum in interfacial cells (positions where the mean gas volumetric fraction changes from zero).

In scenarios with free bubble-array flows the situation is, however, more complex. For instance, the wall-normal profile of the dissipation term for the free bubble-array flow scenario 8BM6 (Figure 5.6b) shows that the mentioned peaks at the positions of bubble interfaces are also observable, but are significantly less pronounced with respect to the magnitudes of the dissipation in the domains where bubbles rise. On the other hand, the profile of the dissipation term in the single-phase region seems to be even steeper than the one in the fixed bubble-array flow scenario 1BM6. This fact implies that the portion of the dissipation rate within two-phase domains increases in scenarios with multiple bubbles. Figure 5.7 shows that such a situation is also valid on the level of overall dissipation quantities. Moreover, it can be seen that the overall dissipation rate within the two-phase domain is drastically increased in the case with the densest bubble population: comparing to the case 1BM6 $\langle \varepsilon_l^L \rangle_{tp}$ is only $\sim 7\%$ higher in the case 5BM6, but even $\sim 70\%$ in the case 8BM6. This effect hardly can be related to the increased gradients of liquid turbulence quantities due to lateral movements of bubbles because in both scenarios with free bubble-arrays, 5BM6 and 8BM6, bubbles rise along non-rectilinear paths (see Figure A.1 and Figure A.2).

The observed phenomenon indicates that the mechanism governing the dissipation of liquid turbulence kinetic energy is closely related to the mutual bubble-bubble distances. Therefore, since the bubbles in scenarios 1BM6 and 5BM6 are at significant distances from each other, the turbulence structures formed in bubble wakes are, mainly, controlled by the flow induced by individual bubbles. This means that small eddies produced in the two-phase domain can freely penetrate in the single-phase regions. In the scenario 8BM6, however, the bubble packing is sufficiently dense to prevent a free release of turbulent eddies in domains permanently occupied by the liquid phase. Consequently, the eddies generated

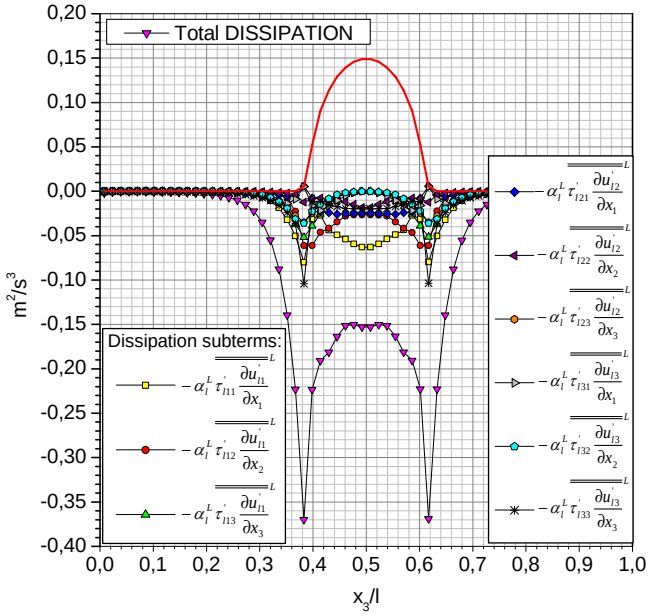

(a) fixed bubble-array flow (scenario 1BM6)

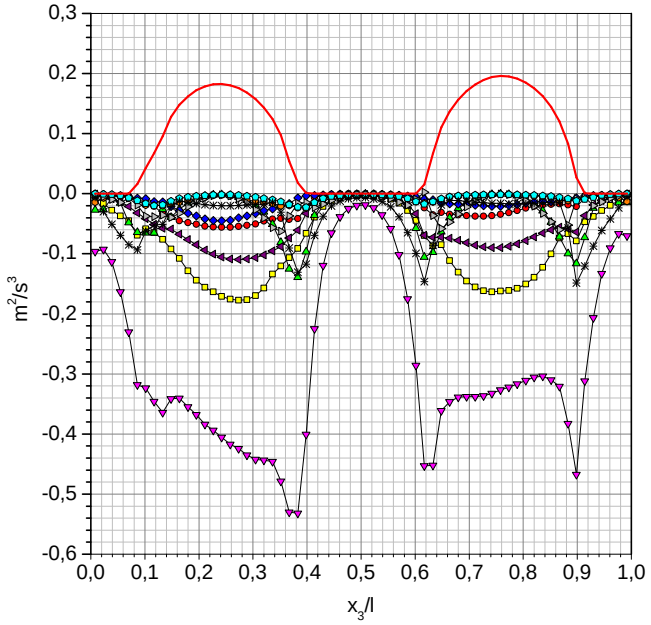

(b) free bubble-array flow (scenario 8BM6)

Figure 5.6: Wall-normal profiles of dissipation term and dissipation subterms evaluated by module GENERG-TP for fixed bubble-array flow 1BM6 (at $x_2 = 0.5859l$) and free bubble-array flow 8BM6 (at $x_2 = 0.1015l$). Solid red line represents mean gas volumetric fraction.

in wakes of individual bubbles decay faster owing to the shear stress associated with the motion of other bubbles.

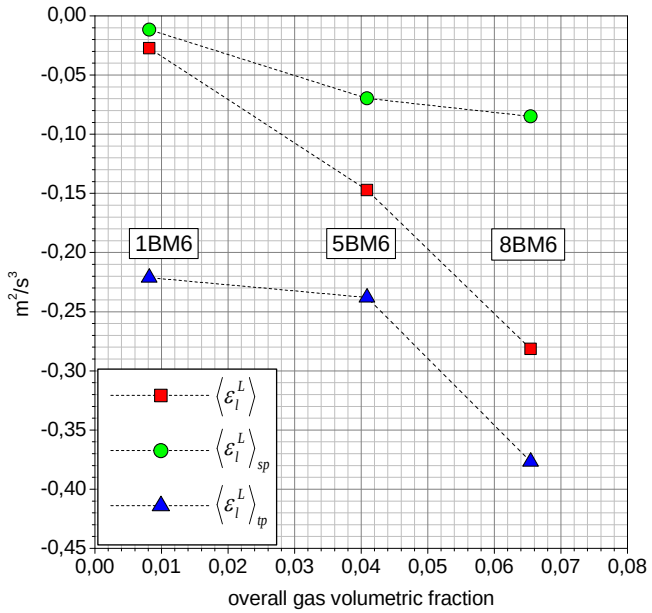

Figure 5.7: Overall dissipation rate of liquid turbulence kinetic energy within the whole flow domain, $\langle \varepsilon_l^L \rangle$, within the single-phase domain, $\langle \varepsilon_l^L \rangle_{sp}$, and within the two-phase domain, $\langle \varepsilon_l^L \rangle_{tp}$, in dependance on overall gas volumetric fraction for bubble-array flows with low liquid viscosity.

It is, further, suspected that the very intensive dissipation of the liquid turbulence kinetic energy in the two-phase domain observed in the simulation scenario 8BM6 is related to the mutual interaction of turbulence structures with interfacial structures. That such an interaction can be an important energy exchange mechanism in bubbly flows and can even reduce the intensity of the liquid turbulence was firstly postulated by Serizawa and Kataoka [68]. The currently accepted explanation of the phenomenon is as follows. On their way towards the single-phase regions turbulence eddies generated in the two-phase domains come into collisions with bubble interfaces. As a result of these interactions an eddy fragmentation process occurs intensifying the generation rate of small turbulence scales that can be dissipated by the viscosity.

Wall-normal profiles of the dissipation term computed for free bubble-array flows with different liquid viscosity (scenarios 8BM2, 8BM4 and 8BM6) are compared in Figure 5.8, while corresponding overall magnitudes of the dissipation rate evaluated within the whole domain, $\langle \varepsilon_l^P \rangle$, within the single-phase domain, $\langle \varepsilon_l^P \rangle_{sp}$, and within the two-phase domain, $\langle \varepsilon_l^P \rangle_{tp}$ are presented in Figure 5.9. It can be seen that the shape of the dissipation profiles significantly changes with change of the liquid viscosity: contrary to the smooth ε_l^P profile in the very viscous case 8BM2, the dissipation profile in the low viscous case 8BM6 is

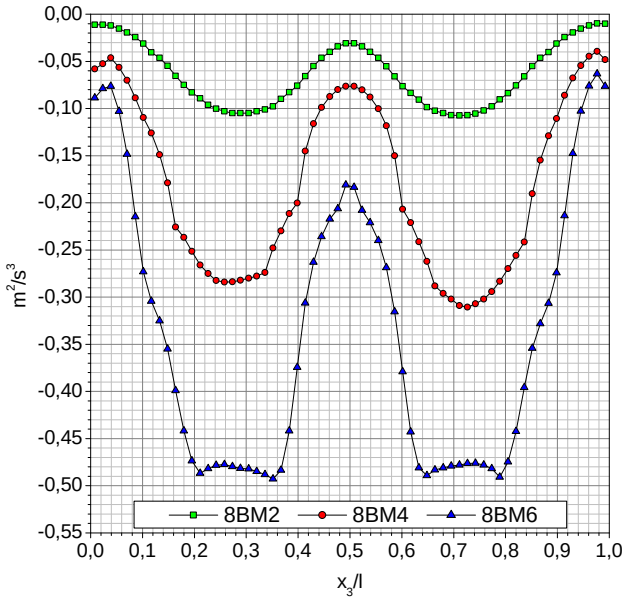

Figure 5.8: Dissipation rate of liquid turbulence kinetic energy evaluated by module GENERG-TP for free bubble-array flows with different liquid viscosity.

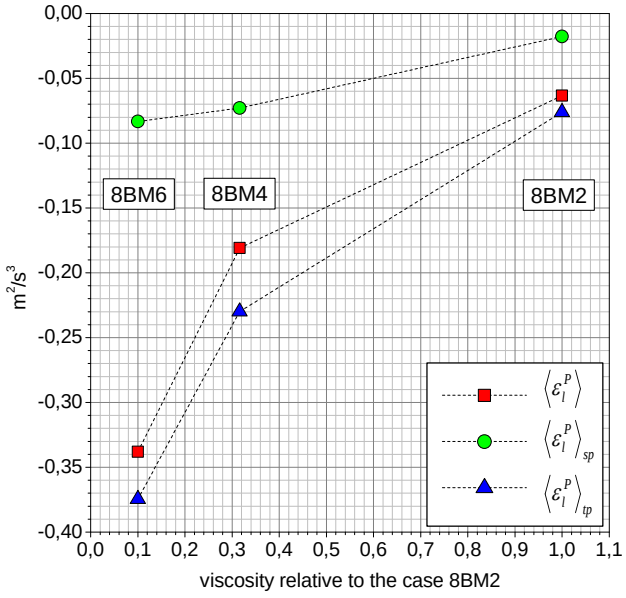

Figure 5.9: Overall dissipation rate of liquid turbulence kinetic energy within the whole flow domain, $\langle \varepsilon_l^P \rangle$, within the single-phase domain, $\langle \varepsilon_l^P \rangle_{sp}$, and within the two-phase domain, $\langle \varepsilon_l^P \rangle_{tp}$ for bubble-array flows with different liquid viscosity.

accompanied with almost flat parts in domains where bubbles rise and very steep gradients in regions where the gas volumetric fraction changes to zero. The differences between the considered bubble-array flows are, further, illustrated comparing the size of turbulence structures at which the dissipation of the liquid turbulence kinetic energy occurs. An average size of turbulence eddies that are dissipated by viscosity is defined by Kolmogorov length scale [75]:

$$\eta_l^K = \left(\frac{\nu_l^3}{|\varepsilon_l|} \right)^{1/4}, \tag{5.8}$$

where ν_l^K stands for the kinematic viscosity of the liquid phase and ε_l is the total dissipation rate. Here Kolmogorov length scale is evaluated by replacing ε_l in expression 5.8 by $\langle \varepsilon_l^L \rangle$ in the case of line averaging, i.e. by $\langle \varepsilon_l^P \rangle$ when the plane averaging is applied. In order to obtain dimensionless quantities scaling with equivalent bubble diameter, d_b, is performed. The results are presented in Table 5.1. It can be seen that Kolmogorov length scale is, except for the case 8BM2, always smaller than the bubble diameter, but significantly larger than the mesh cell size[4]. This means that the numerical grid imposed on the flow domain in all the bubble-array flow scenarios is sufficiently fine to resolve the smallest flow scales. Magnitudes of Kolmogorov length scale relative to the bubble diameter further indicate crucial differences in approaches used in numerical simulations of two-phase particulate and two-phase bubbly flows. In numerical simulations of flows with particles, namely, the Kolmogorov length scale is assumed to be larger than the particle size, what implies that the particles may be modelled as points. The values of η_l^K/d_b presented in Table 5.1 indicate that such an assumption is impossible even for very slow bubbly flows.

Table 5.1: Kolmogorov length, η_l^K, scaled with equivalent bubble diameter, $d_b = 0.25l$, for simulated bubble-array flows.

averaging type	line			plane		
scenario	1BM6	5BM6	8BM6	8BM6	8BM4	8BM2
η_l^K/d_b	0.3108	0.2042	0.1736	0.1659	0.4602	1.4179

The aforementioned results indicate a complex influence of the flow parameters on the dissipation of liquid turbulence kinetic energy. An attempt to shed some light on the dependance of the overall dissipation rate on overall flow conditions is presented in the following. In a rough estimate the dissipation rate of the liquid turbulence kinetic energy in slow bubble-driven liquid flows can be related to the work of interfacial forces. Considering the drag force to be the dominant one the following relation can be established [43]:

$$\varepsilon_l \propto \frac{\alpha_g}{d_b} C_d u_r^3, \tag{5.9}$$

[4]It is reminded that in all the simulations cubic cells of the size $0.0625d_b$ are specified

where C_d represents the drag coefficient. The performance of the expression 5.9 cannot be tested because the proportionality coefficient is not given. However, using the DNS based data the nature of the dependance of the dissipation rate on flow parameters as proposed by expression 5.9 can be examined.

Adopting the commonly used formulation of the drag coefficient as function of Morton (M), bubble Eötvös ($\mathrm{E\ddot{o}}_b$) and bubble Reynolds (Re_b) number [4]:

$$C_d = \frac{4}{3}\frac{\mathrm{E\ddot{o}}_b^{3/2}}{\mathrm{M}^{1/2}\mathrm{Re}_b^2}, \tag{5.10}$$

it can be shown that the behaviour of the overall dissipation rate in flow configurations where only number of bubbles changes (scenarios 1BM6, 5BM6 and 8BM6) should obey to:

$$\langle \varepsilon_l^L \rangle = C^L \langle \alpha_g \rangle \langle u_r \rangle, \tag{5.11}$$

while in systems where only the viscosity of liquid phase is different (scenarios 8BM2, 8BM4 and 8BM6) to:

$$\langle \varepsilon_l^P \rangle = C^P \langle u_r \rangle, \tag{5.12}$$

where C^L and C^P represent proportionality coefficients.

Evaluations performed here have revealed an optimistic result concerning the expression 5.12. Therefore, despite dramatically different magnitudes of the mean relative velocity in simulation scenarios 8BM2, 8BM4 and 8BM6 (see Table 3.2), the coefficient, C^P turned out to be approximatively constant, $C^P \sim -0.4$. On the other side, no rule for the behaviour of the coefficient C^L from the expression 5.11 could be found.

Finally, the reliability of an experimental determination of the dissipation rate in bubble-driven liquid flows is tested. In an experimental approach, namely, the expression 5.5 cannot be used because nine components of the fluctuating strain rate cannot be measured with currently available experimental techniques. In the isotropic single-phase turbulence, however, the dissipation rate can be expressed as [27] [75]:

$$\varepsilon = -15\nu \overline{\left(\frac{\partial u_1^{'}}{\partial x_1}\right)^2}, \tag{5.13}$$

where the single overbar indicates averaging. When the liquid phase within a bubbly flow is concerned, the expression 5.13 takes the following form:

$$\varepsilon_l = -15\alpha_l \nu_l \overline{\overline{\left(\frac{\partial u_{l1}^{'}}{\partial x_1}\right)^2}}. \tag{5.14}$$

From experimental point of view it would be extremely gratifying to use this simple expression for ε_l since only the component of the fluctuating liquid velocity in the rise direction, $u_{l1}^{'}$, should be measured.

Evaluations based on DNS data have, unfortunately, shown that magnitudes of ε_l determined by expression 5.14 differ significantly from the ones computed using the fundamental definition of the dissipation rate 5.5 for all the cases of bubble-array flows. Here, the poor performance of the expression 5.14 is illustrated in Figure 5.10 for the case of free bubble-array flow 8BM6, where a systematic overestimation of the magnitudes of the dissipation rate can be seen. However, while in the single-phase domains expression 5.14 predicts the correct trend of the dissipation curve with an overestimation of below 20%, in the regions where bubbles rise it totally fails. It is, therefore, stressed that an experimental determination of the dissipation rate based on its simplified formulation 5.14 cannot be accepted as a reliable one, at least, for the class of slow bubble-driven liquid flows considered in this work.

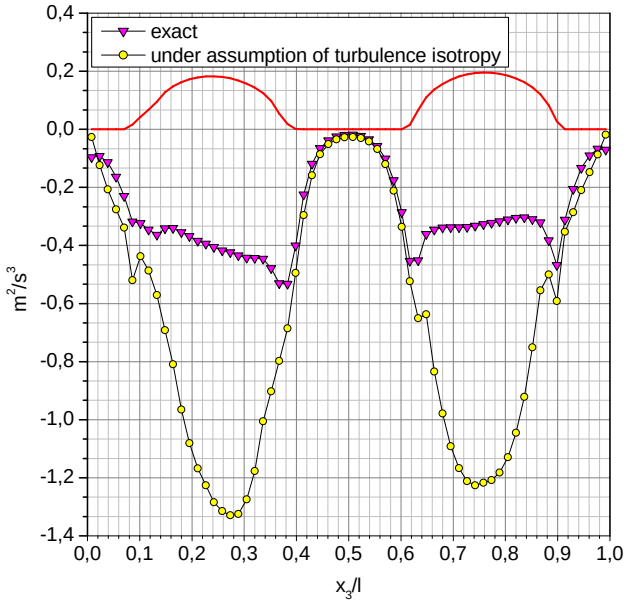

Figure 5.10: Dissipation term evaluated under the assumption of isotropic liquid phase turbulence (expression 5.13) versus the exact one (expression 5.5) for free bubble-array flow 8BM6. Evaluations are done applying line averaging. Results are presented for span-wise position $x_2 = 0.1015l$.

5.2.3 Transfer of turbulence kinetic energy between the mean and fluctuating flow of the liquid phase in bubble-array flows

The production term represents the rate at which the turbulence kinetic energy is transferred between the mean and the fluctuating flow field. This term is seen to be the rate at

which work is done by the mean strain against the turbulent stresses and is given as:

$$\Pi_l = -\alpha_l \overline{\overline{\rho}} \overline{\overline{u'_{l\alpha} u'_{l\beta}}} \frac{\partial \overline{\overline{u}}_{l\alpha}}{\partial x_\beta}. \tag{5.15}$$

In the module GENERG-TP the production term is evaluated as:

$$\Pi_l^L = -\alpha_l^L \frac{u_{ref}^3}{l_{ref}} \left[\sum_{\beta=1}^{3} \overline{\overline{\rho}}^L \overline{\overline{U'_{l\beta} U'_{l2}}}^L \frac{\partial \overline{\overline{U}}_{l\beta}^L}{\partial X_2} + \sum_{\beta=1}^{3} \overline{\overline{\rho}}^L \overline{\overline{U'_{l\beta} U'_{l3}}}^L \frac{\partial \overline{\overline{U}}_{l\beta}^L}{\partial X_3} \right] \tag{5.16}$$

in cases where the line averaging is applied (scenarios 1BM6, 5BM6 and 8BM6), and as:

$$\Pi_l^P = -\alpha_l^P \frac{u_{ref}^3}{l_{ref}} \left[\sum_{\beta=1}^{3} \overline{\overline{\rho}}^P \overline{\overline{U'_{l\beta} U'_{l3}}}^P \frac{\partial \overline{\overline{U}}_{l\beta}^P}{\partial X_3} \right] \tag{5.17}$$

for scenarios where the plane averaging is performed (8BM2, 8BM4 and 8BM6).

This term is called production, because in shear flows it is always positive. Figure 5.11, however, shows that in the major part of the channel negative values of the production term are evaluated by the module GENERG-TP. This is, especially, pronounced in the case of fixed bubble-array flow (scenario 1BM6), where no positive magnitude of the production term is found. Although, this result may seem surprising and bring into discussion the name of this term, the physics lying behind it is easy to understand taking into account that the motion of the liquid phase is driven by rising bubbles, i.e. that the energy in the liquid flow is transferred from the fluctuating liquid flow caused by moving bubbles to the mean liquid flow.

Since the considered bubble-driven liquid flows are slow, the mean strain rate of the liquid phase is weak, what results in low absolute magnitudes of the production term (in the next section it will be seen that the magnitude of the production term is significantly lower comparing to the magnitudes of other balance terms). This is, particularly, true for bubble-array flow scenarios where the plane averaging is applied (scenarios 8BM2, 8BM4 and 8BM6). As in these cases the mean liquid strain includes only derivatives in the wall-normal direction negligible values of the production term (order of magnitude $10^{-3} m^2/s^3$) are evaluated by the module GENERG-TP.

5.2.4 Interfacial generation of liquid turbulence kinetic energy in bubble-array flows

The interfacial effects in the basic balance equation for the liquid turbulence kinetic energy 2.14 are expressed as:

$$\Upsilon_l = -\frac{1}{\varrho_l} \overline{p'_{li} u'_{li\alpha} n_{l\alpha} a_i} + \frac{1}{\varrho_l} \overline{\tau'_{li\alpha\beta} u'_{li\alpha} n_{l\beta} a_i}, \tag{5.18}$$

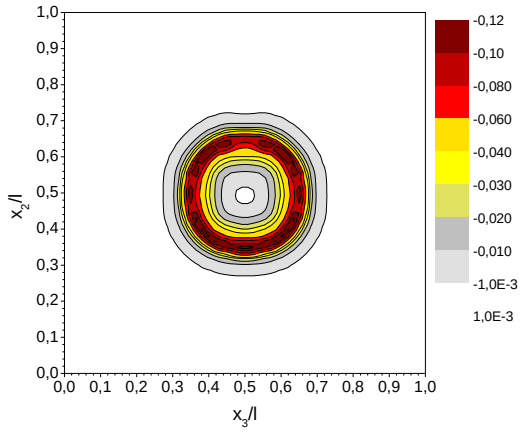

(a) scenario 1BM6

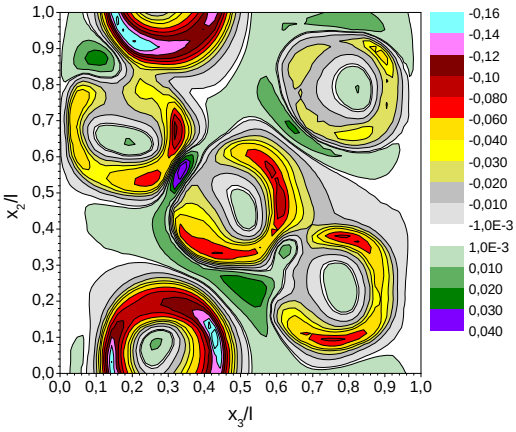

(b) scenario 5BM6

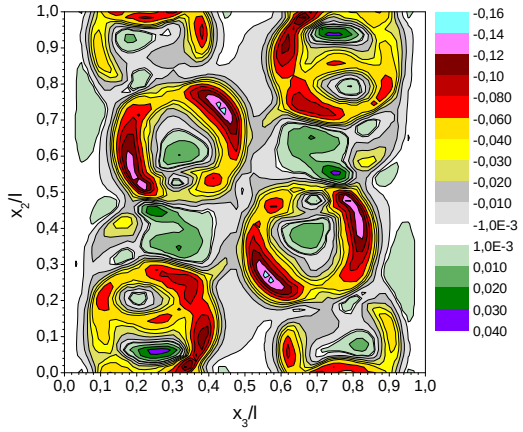

(c) scenario 8BM6

Figure 5.11: Production term in equation 2.14 evaluated by module GENERG-TP for fixed (scenario 1BM6) and free (scenarios 5BM6 and 8BM6) bubble-array flows.

where $p_{li}^{'}$ and $u_{li}^{'}$ stand for fluctuating interfacial liquid pressure and velocity, respectively, $n_{l\alpha}$ represents the unit normal vector at the interface pointing outward the liquid and a_i denotes the interfacial area concentration. The fluctuating interfacial viscous stress of the liquid phase, $\tau_{li}^{'}$, is defined replacing $u_l^{'}$ by $u_{li}^{'}$ in 5.2.

In the module GENERG-TP the interfacial term is evaluated using the following expression:

$$\Upsilon_l^L = \frac{1}{\rho_l}\frac{u_{ref}^3}{l_{ref}}\left[- \overline{P_{li}^{'}U_{li\alpha}^{'}n_{l\alpha}A_i}^L + \frac{1}{\mathrm{Re}_{ref}}\overline{\mathbf{T}_{li\alpha\beta}^{'}U_{li\alpha}^{'}n_{l\beta}A_i}^L\right], \tag{5.19}$$

when the line averaging is applied, and as:

$$\Upsilon_l^P = \frac{1}{\rho_l}\frac{u_{ref}^3}{l_{ref}}\left[- \overline{P_{li}^{'}U_{li\alpha}^{'}n_{l\alpha}A_i}^P + \frac{1}{\mathrm{Re}_{ref}}\overline{\mathbf{T}_{l\alpha\beta}^{'}U_{li\alpha}^{'}n_{li\beta}A_i}^P\right], \tag{5.20}$$

when the plane averaging is performed.

The evaluation of the interfacial term comparing to the evaluations of other balance terms in the equation 2.14 is the most complex one. The interfacial term, namely, involves 12 subterms all of them requiring the detailed information about the interfacial structure (unit normal vector and interfacial area concentration) as well as about the fluctuating velocity and pressure at the liquid side of the phase interface. In this context, an experimental determination of the interfacial term with the current status of measuring technique cannot be expected. Further, as the interfacial term is peculiar to gas-liquid flows, the knowledge collected in the domain of single-phase turbulence cannot be used as a basis for the investigation of this term. Direct numerical simulations of bubbly flows, therefore, represent the only alternative to elucidate the effects of bubble interfaces on the liquid phase turbulence. However, in spite of the significant progress in this domain, to the best knowledge of the author, no evaluation of the interfacial term by the use of its basic definition 5.18 is reported so far. On the other hand, in the number of references, where an engineering approach[5] is adopted or where pure theoretical considerations are performed (see for example [32] [68]), it is postulated that this term plays an important role in the conservation of liquid turbulence kinetic energy.

The evaluations performed by the module GENERG-TP prove that this postulation is correct. The effects of phase interfaces on the transfer of liquid turbulence kinetic energy are, namely, more than evident in Figure 5.12, where contour plots of the interfacial term are presented for bubble-array flows with low liquid viscosity (scenarios 1BM6, 5BM6 and 8BM6), as well as in Figure 5.14, where wall-normal profiles of the interfacial term for bubble-array flows with different liquid viscosity (scenarios 8BM2, 8BM4 and 8BM6) are given.

[5] An overview of liquid turbulence models is given in chapter 2, while details about modelling of interfacial turbulence transfer are presented in chapter 6

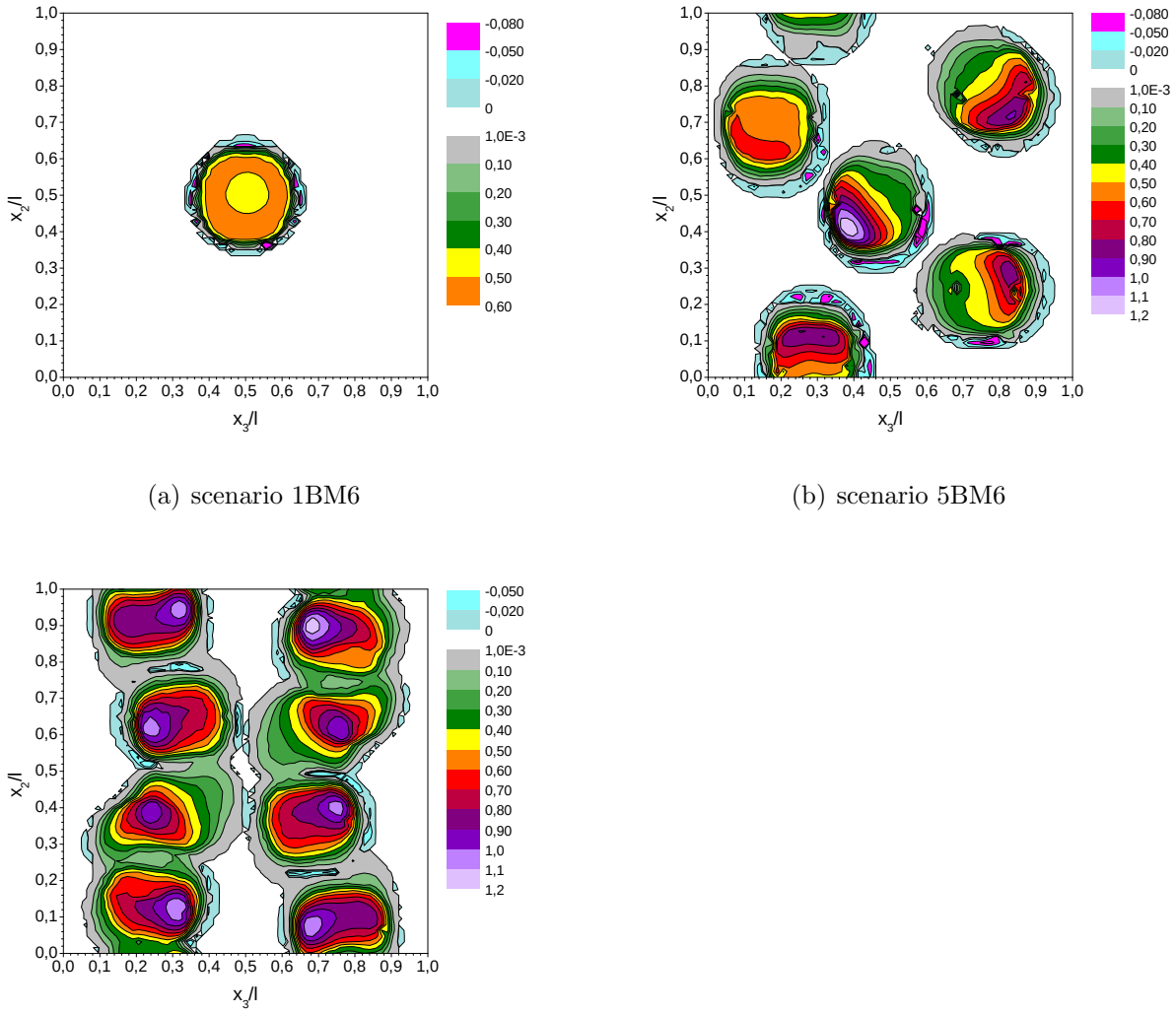

(a) scenario 1BM6

(b) scenario 5BM6

(c) scenario 8BM6

Figure 5.12: Interfacial generation of liquid turbulence kinetic energy evaluated by module GENERG-TP for fixed (scenario 1BM6) and free (scenarios 5BM6 and 8BM6) bubble-array flows.

Because the interfacial term is directly related to the presence of bubble interfaces, non-zero values are evaluated only in domains of the channel where bubbles rise. In both figures, 5.12 and 5.14, it is clearly seen that the interfacial term represents a source of liquid turbulence kinetic energy [6]. Moreover, since the so-called production term turned out to be negative and the diffusion term has no net contribution, the interfacial term is the only one that supplies the fluctuating liquid flow with energy.

Figure 5.12 shows that an increase of the number of suspended bubbles has significant effect on the magnitude and distribution of the interfacial term. A non-linear intensification of the interfacial liquid turbulence generation with the increase of the gas phase content is illustrated in Figure 5.13 where overall magnitudes of interfacial term, $\langle \Upsilon_l^L \rangle$, are presented versus the overall gas volumetric fraction, $\langle \alpha_g \rangle$. Therefore, in the range of lower gas volumetric fractions (scenario 1BM6 to scenario 5BM6) the following relation is found $\langle \Upsilon_l^L \rangle \propto 3.4771 \langle \alpha_g \rangle$, while for higher gas contents (scenario 5BM6 to 8BM6) the dependance of $\langle \Upsilon_l^L \rangle$ on $\langle \alpha_g \rangle$ is stronger, $\langle \Upsilon_l^L \rangle \propto 5.128 \langle \alpha_g \rangle$. Since the interfacial area concentration linearly changes with the number of bubbles, $\langle a_i \rangle \propto 6.195 \langle \alpha_g \rangle$, such an increase in magnitudes of the interfacial term is, certainly, associated with the intensification of liquid phase fluctuations in the vicinity of phase interfaces. This can be even better observed when the interfacial production of the liquid turbulence kinetic energy in free bubble-array flows with different liquid viscosity is compared (see Figure 5.14). Therefore, despite the identical magnitudes of the interfacial area concentration, computed values of the interfacial term differ remarkably.

The expression 5.18 does not look attractive for an analysis of effects that bubble interfaces make on the liquid phase turbulence. Moreover, it looks frightening. An attempt to draw conclusions about the physical meaning and behaviour of interfacial term on the basis of its 12 different contributions does not seem reasonable. In this context, the analyses of the interfacial term are performed as follows.

After some simple mathematical manipulations the definition of the interfacial term 5.18 can be expressed in the following form [78]:

$$\Upsilon_l = \frac{1}{\varrho_l} \overline{\mathbf{u}'_{li} \left[-\left(p_{li} - \overline{\overline{p}}_{li}\right)\mathbf{I} + \tau_{li} \right] \nabla \Phi_l} - \frac{1}{\varrho_l} \left[\left(\overline{\overline{p}}_{li} - \overline{\overline{p}}_l\right)\mathbf{I} + \overline{\overline{\tau}}_l \right] : \overline{\mathbf{u}'_{li} \nabla \Phi_l}, \tag{5.21}$$

where the unit tensor is denoted by $\mathbf{I}$, the gradient of the liquid phase indicator function is given by:

$$\nabla \Phi_l = \mathbf{n}_l a_i, \tag{5.22}$$

and the average interfacial pressure of the liquid phase is defined as [32]:

$$\overline{\overline{p}}_{li} = \frac{\overline{p_{li} a_i}}{\overline{a}_i}. \tag{5.23}$$

[6] It is noted that small patches with negative values of interfacial term in Figure 5.12 are suspected to be caused by numerical inaccuracy in the evaluation of characteristics of the interfacial structure and / or the interfacial velocity of the liquid phase and, should, therefore, not be taken into consideration.

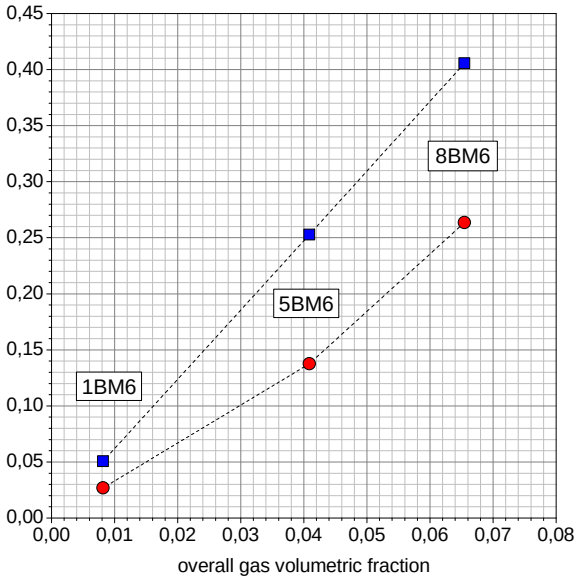

Figure 5.13: Overall magnitudes of interfacial term, $\langle \Upsilon_l^L \rangle (m^2/s^3)$, (red circles) and interfacial area concentration, $\langle a_i \rangle (m^{-1})$ (blue squares) in dependance on overall gas volumetric fraction for bubble-array flow scenarios with low liquid viscosity.

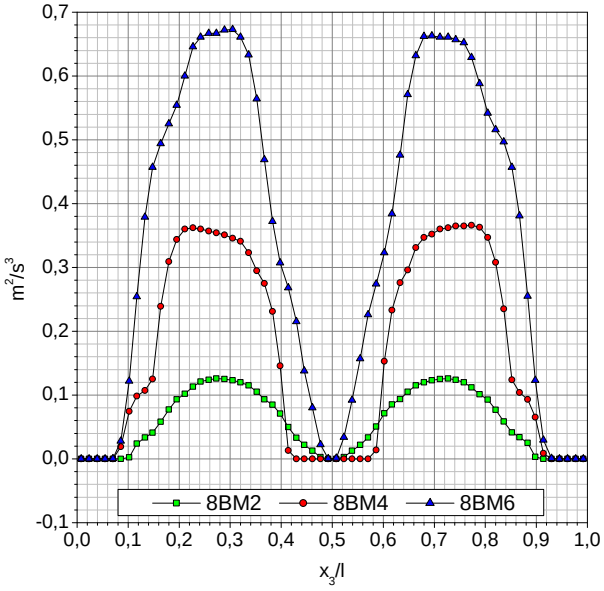

Figure 5.14: Interfacial generation of liquid turbulence kinetic energy evaluated by module GENERG-TP for free bubble-array flows with different liquid viscosity.

Reminding, further, that the instantaneous interfacial force density is formulated by [19]:

$$\mathbf{M}_l = \left[-\left(p_{li} - \overline{\overline{p}}_{li}\right)\mathbf{I} + \tau_{li} \right] \nabla \Phi_l, \tag{5.24}$$

two mechanisms that govern the interfacial generation of the liquid turbulence kinetic energy can be identified in expression 5.21: the one defined by the correlation between the instantaneous interfacial force density, $\mathbf{M}_l$, and the liquid velocity fluctuation, $\mathbf{u}_{li}^{'}$, and the other one involving the correlation between the liquid velocity fluctuation, $\mathbf{u}_{li}^{'}$, and the dynamics of the interface (expressed through the gradient of the liquid phase indicator function, $\nabla \Phi_l$).

Evaluations performed by the module GENERG-TP have revealed an optimistic result: the contribution of the first term in expression 5.21 to the total interfacial generation of liquid turbulence kinetic energy is absolutely dominant comparing to the contribution of the second term (for an illustration see Figure 5.15). In order to demonstrate the benefit of this result for the derivation of corresponding closure assumption for the interfacial term, Υ_l, considerations are extended to the whole two-phase mixture.

Therefore, assuming that the aforementioned conclusion about the negligible contribution of the correlation between the velocity fluctuations and the interface dynamics may be extended to the gas phase ($\overline{\mathbf{u}_g^{'} \nabla \Phi_g} \sim 0$), the interfacial generation of the turbulence kinetic energy in the gas phase can be expressed by:

$$\Upsilon_g = \frac{1}{\varrho_g} \overline{\mathbf{u}_{gi}^{'} \mathbf{M}_g}, \tag{5.25}$$

where the subscript g indicates the gas. The interfacial generation of the turbulence kinetic energy in two-phase mixture, Υ_{tp}, is, subsequently, given as:

$$\varrho_{tp} \Upsilon_{tp} = \varrho_l \Upsilon_l + \varrho_g \Upsilon_g = \sum_{k=l,g} \overline{\mathbf{u}_{ki}^{'} \mathbf{M}_k}, \tag{5.26}$$

where, the subscripts k and tp indicate the phase (liquid or gas) and the two-phase mixture, respectively. From the expression above the following formulation of the interfacial term in the balance equation for the liquid turbulence kinetic energy can be established:

$$\Upsilon_l = \frac{1}{\varrho_l} \sum_{k=l,g} \overline{\mathbf{u}_{ki}^{'} \mathbf{M}_k} - \frac{\varrho_g}{\varrho_l} \Upsilon_g. \tag{5.27}$$

Having in mind the definition of interfacial velocity fluctuation, $\mathbf{u}_{ki}^{'} = \mathbf{u}_{ki} - \overline{\overline{\mathbf{u}}}_k$, the equality of phase interface velocities in the absence of phase change, $\mathbf{u}_{li} = \mathbf{u}_{gi}$, and validity of the principle of action and reaction on the phase interface, $\mathbf{M}_l = -\mathbf{M}_g$, the expression 5.27 can be given in the following form:

$$\Upsilon_l = \frac{1}{\varrho_l} \overline{\mathbf{M}}_l (\overline{\overline{\mathbf{u}}}_l - \overline{\overline{\mathbf{u}}}_g) - \frac{\varrho_g}{\varrho_l} \Upsilon_g. \tag{5.28}$$

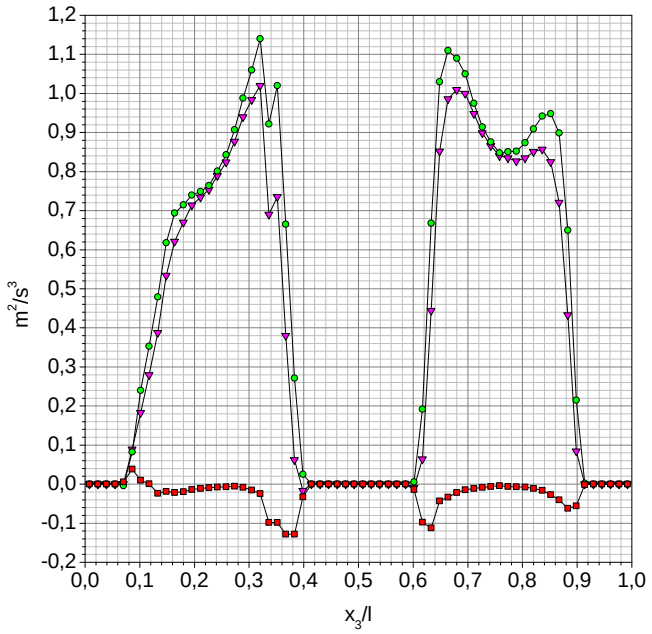

Figure 5.15: Total interfacial term evaluated by 5.18 (pink triangles) and interfacial subterms in expression 5.21, $\overline{\mathbf{u}'_{li}\mathbf{M}_l}/\varrho_l$ (green circles) and $\left[(\overline{\overline{p}}_{li} - \overline{\overline{p}}_l)\mathbf{I} + \overline{\overline{\tau}}_l\right] : \overline{\mathbf{u}'_{li}\nabla\Phi_l}/\varrho_l$ (red squares), for free bubble-array flow 8BM6. Results are presented for span-wise position $x_2 = 0.1015l$.

The benefit of the relation 5.28 is indispensable for engineering considerations of the liquid turbulence in bubbly flows. Since in typical bubbly gas-liquid flows, namely, the ratio of phase densities, ϱ_g/ϱ_l, is very low, it is reasonable to neglect the second term in 5.28 and express the interfacial generation of liquid turbulence kinetic energy as the rate at which the work of interfacial forces in the relative motion of bubbles is performed. In this way the problem of proper modelling of interfacial effects on the liquid phase turbulence is shifted to the determination of proper closure assumptions for interfacial forces. Although the accuracy of closure laws for the interfacial force density is still an open question, it is noted that in that field much more knowledge is collected comparing to the domain of the liquid turbulence modelling in bubbly flows.

5.3 Budget of basic equation for turbulence kinetic energy of the liquid phase in bubble-array flows

In order to examine the relation between different mechanisms governing the liquid turbulence in bubble-array flows, the results presented in the previous section are here summa-

rized and the budget of the basic balance equation for the turbulence kinetic energy of the liquid phase (further called k_l equation) is established.

The budget of the k_l equation is presented in Figures 5.16 through 5.18 for bubble-array flows with the low liquid viscosity (scenarios 1BM6, 5BM6 and 8BM6) and in Figure 5.19 for bubble-array flows with different liquid viscosity (scenarios 8BM2, 8BM4 and 8BM6). It is noted that for simulation scenarios 1BM6, 5BM6 and 8BM6, where the line averaging is applied due to two-dimensional profiles of balance terms it was not possible to present a detailed budget of the exact k_l equation for the whole flow domain. Instead, the relation between the balance terms in k_l equation is given locally at the representative wall-normal, i.e. span-wise positions.

In the case of fixed bubble-array flow (scenario 1BM6) wall-normal profiles of all the balance terms on the right-hand-side of the equation 2.14 are given for two span-wise positions: the one intersecting the bubble through its central part (Figure 5.16a) and the other one intersecting bubble in the middle between its centre and its hip (Figure 5.16b). Note that, due to the symmetry of the fluctuating liquid flow in this scenario, span-wise profiles show the same behaviour of balance terms as corresponding wall-normal profiles.

Figure 5.16 shows that in the fixed bubble-array flow scenario profiles of all the balance terms are symmetric with respect to the channel axis. Non-zero values are noticed only in the central part of the channel where bubbles rise. Strong gradients of the liquid phase quantities in the region between the part of the channel through which bubbles move and the one permanently occupied with the liquid phase cause sharp peaks in profiles of all the balance terms at these locations. In Figure 5.16a it can, further, be observed that the diffusion from the two-phase domain towards the single-phase regions represents an important mechanism of the liquid turbulence energy transfer. A rough estimate of the mean magnitudes in the core region of the two-phase domain, where profiles of balance terms do not change steeply ($x_3 = (0.4 \div 0.6)l$) reveals, namely, that approximatively one fourth of the turbulence kinetic energy generated by bubble interfaces is dissipated, while the rest is through an intensive diffusion process transported towards domains occupied only with the liquid phase. In regions containing peripheral parts of bubbles and in the single-phase domain close to bubble interfaces this portion of energy is intensively dissipated, not only through the work performed by the fluctuating strain against the fluctuating viscous stress (dissipation term), but also through the work of the mean strain against the turbulent stresses (production term). The comparison of Figure 5.16a with Figure 5.16b shows that the relative position with respect to the bubble centre influences the magnitude of the balance terms, but not the mechanisms of turbulence energy transport (ratio between individual balance terms in Figure 5.16b is approximatively the same as in Figure 5.16a). Wall-normal profiles of balance terms in k_l equation for bubble-array flow scenario 5BM6 are presented for span-wise position $x_2 = 0.1015l$, where the corresponding wall-normal plane on the left-hand-side passes through the middle between the center and the hip of the bubble rising in this domain, while on the right-hand-side intersects the single-phase

region very close to the interface of the bubble rising in that part of the channel.

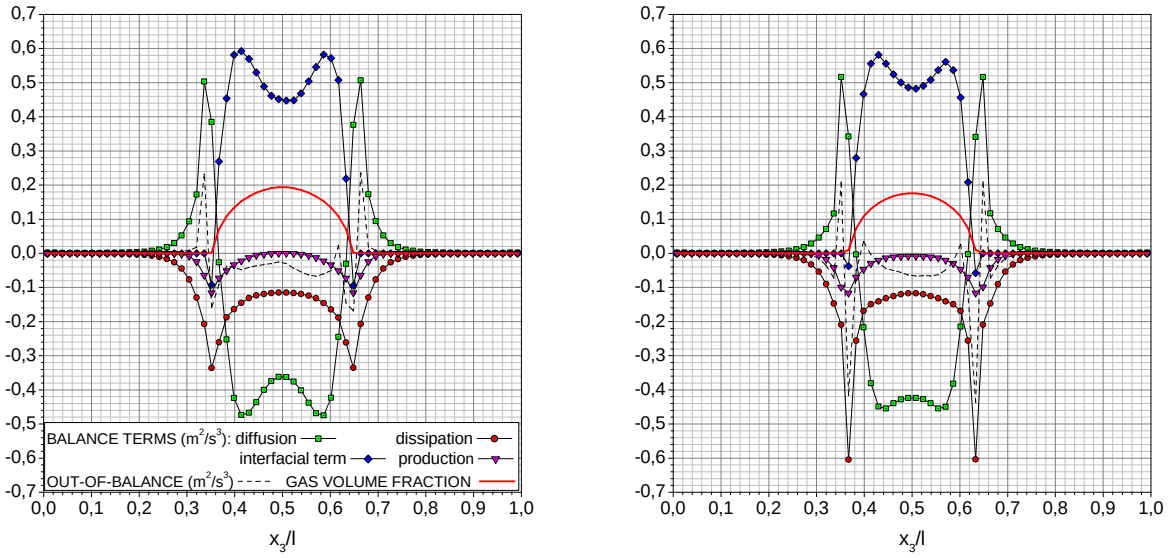

(a) $x_2 = 0.4922l$ (b) $x_2 = 0.5547l$

Figure 5.16: Wall-normal profiles of balance terms in basic equation for liquid turbulence kinetic energy 2.14 evaluated by module GENERG-TP for fixed bubble-array flow 1BM6.

This span-wise position is chosen on purpose because it provides the analysis of the effects of other bubbles on the turbulence kinetic energy transfer. Concerning the relative position to the bubble centre, namely, profiles on the left-hand-side of Figure 5.17a are comparable with the ones given in Figure 5.16b. Therefore, since the liquid flow in the system with multiple bubbles is more uniformly agitated than in the rigid case of the fixed bubble-array flow, peaks of balance terms in Figure 5.17a are significantly less pronounced than the ones in Figure 5.16b. Since the bubble-induced liquid perturbations in the scenario 5BM6 are also stronger than in the case 1BM6, higher magnitudes of all balance terms noticed in Figure 5.17a than in Figure 5.16b are to expect. It is, however, surprising that the presence of other bubbles almost does not affect the mentioned quantitative relationship between different mechanisms of the liquid turbulence energy transfer. Profiles of balance terms on the left-hand-side of Figure 5.17a show, namely, that in the core of the flow domain, where bubble rises, approximatively one fourth of the liquid turbulence kinetic energy generated by moving bubble interfaces is dissipated, while the rest diffuses. Moreover, Figure 5.17b indicates that, like in the fixed bubble-array flow case, this ratio is independent on the relative position to the bubble centre (profiles of balance terms in Figure 5.17b are presented for the span-wise plane $x_3 = 0.8047l$ that intersects both bubbles approximatively through the middle between the bubble centre and the bubble hip). Finally, on the right-hand-side

of Figure 5.17a it can be seen that the portion of turbulence kinetic energy transported to the single-phase domain is, in the only vicinity of the bubble interface, intensively dissipated into the thermal internal heat.

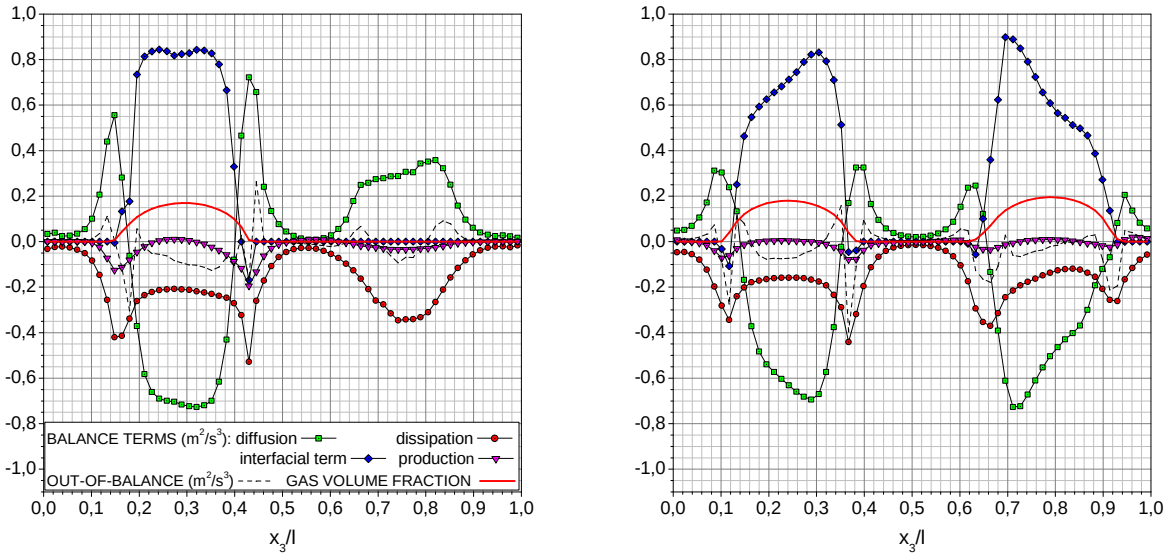

(a) $x_2 = 0.1015l$ (b) $x_3 = 0.8047l$

Figure 5.17: Wall-normal (a) and span-wise (b) profiles of balance terms in basic equation for liquid turbulence kinetic energy 2.14 evaluated by module GENERG-TP for the free bubble-array flow 5BM6.

The budget of k_l equation for the free bubble-array flow scenario 8BM6 is illustrated in Figure 5.18a for the span-wise position $x_2 = 0.1015l$ and in Figure 5.18b for the wall-normal distance $x_3 = 0.2734l$. Concerning the relative position to the bubble centre, Figure 5.18a provides the comparison of the evaluated balance terms for the scenario 8BM6 with the ones for the scenario 5BM6 (the left part of the Figure 5.18a is comparable with the left part of Figure 5.17a), and with the ones in the case of fixed bubble-array flow (the right part of Figure 5.18a is comparable with Figure 5.16a). The comparison reveals significant differences between the liquid turbulence energy budget for the case 8BM6 and the ones for the scenario 5BM6 and for the scenario 1BM6. In Figure 5.18a, namely, any sharp peaks are not seen in the dissipation profile, while the peaks in the diffusion profile are significantly suppressed comparing to the case 5BM6 and, particularly, to the case 1BM6.

The relationship between the mechanisms governing the balance of liquid turbulence kinetic energy is also different than in two other cases of bubble-array flows with the low liquid viscosity. Thus, compared to the bubble-array flow scenarios 1BM6 and 5BM6 the dissipated portion of the liquid turbulence kinetic energy in two-phase domains is increased

in the bubbly flow scenario 8BM6. Subsequently, the diffusion towards single-phase domains is suppressed. The relationship between these balance terms, further, depends of the relative position to the bubble centre so that an estimate equivalent to the one in cases 1BM6 and 5BM6 could not be made.

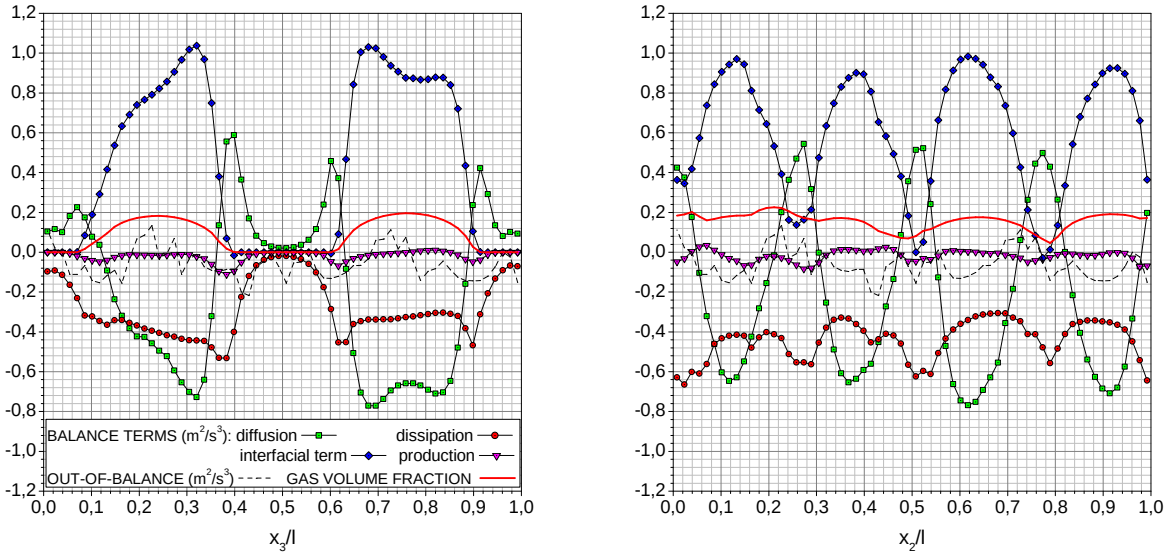

(a) $x_2 = 0.1015l$ (b) $x_3 = 0.2734l$

Figure 5.18: Wall-normal (a) and span-wise (b) profiles of balance terms in basic equation for liquid turbulence kinetic energy 2.14 evaluated by module GENERG-TP for free bubble-array flow 8BM6.

It has, already, been mentioned that the peculiar behaviour of balance terms in the k_l equation for the case with the densest bubble population (scenario 8BM6) is suspected to relate to the short bubble-bubble distances. An attempt to illustrate this effect is made in Figure 5.18b, where the span-wise profiles of balance terms in k_l equation are given for such a dense bubble packing that the gas volumetric fraction is non-zero valued over the whole distance. Therefore, due to the high agitation of liquid flow by bubble displacements as well as by mutual hydrodynamic interactions of bubble wakes, the curve representing the dissipation term lies in the range $|\varepsilon_l^L| \sim 0.4 \div 0.6 m^2/s^3$ with no peaks, but rather with moderate hesitations. On the other hand, since the interfacial generation of the liquid turbulence kinetic energy is strictly related to the bubble presence, the profile of the interfacial term consists of parabolic-like pieces with magnitudes spanning from $\sim 1.0 m^2/s^3$ in the domains containing central parts of the bubbles to zero in the domains where the liquid phase mainly flows. The magnitude of the production term is, further, so low that it may be neglected. Therefore, in order to establish a local balance, some energy from the two-phase domains must be transported towards the single-phase regions,

what should be performed by the diffusion term. Indeed, Figure 5.18b shows that, in spite of the very intensive dissipation, a significant part of the liquid turbulence kinetic energy produced by the interfacial term diffuses towards the bubble interspaces occupied by the liquid phase. It can, therefore, be concluded that even in a flow with such a dense bubble population, the diffusion process is an important mechanism that affects the balance of the liquid turbulence kinetic energy.

Figure 5.19 presents the budget of k_l equation for free bubble-array flows with different liquid viscosity. It is reminded that the balance terms given in Figure 5.19 are obtained by applying the plane averaging, i.e. assuming the homogeneous liquid turbulence in both directions, vertical and span-wise. Such an assumption results in something lower portion of the liquid turbulence energy that is through the diffusion process transported from the two-phase domains towards the single-phase regions. Nevertheless, Figure 5.19 shows that, due to the local nature of the interfacial term, the diffusion term acts to redistribute the turbulence kinetic energy of the liquid phase. Thus, for scenario 8BM6 and scenario 8BM2 approximatively the same portion of liquid turbulence kinetic energy generated by bubble interfaces diffuses into single-phase domain ($\sim 16\%$), while in the scenario 8BM4 the portion is something higher ($\sim 23\%$).

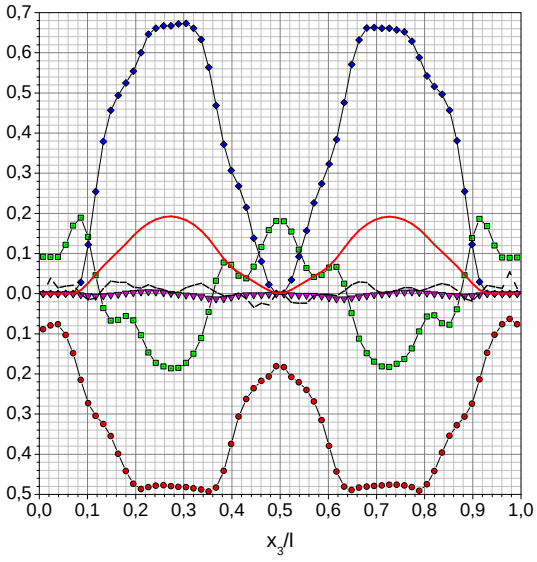

(a) scenario 8BM6

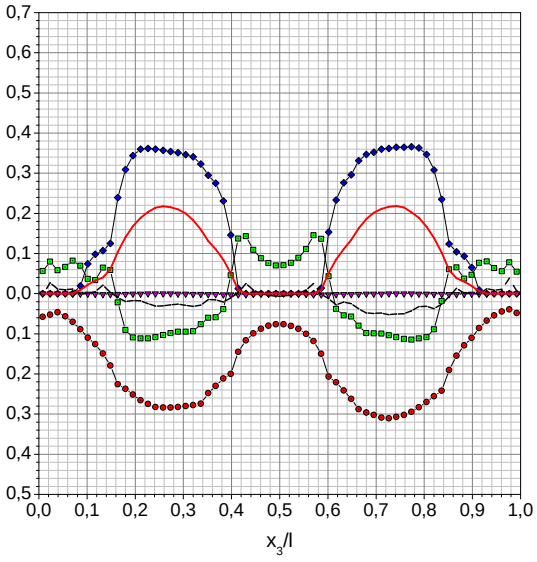

(b) scenario 8BM4

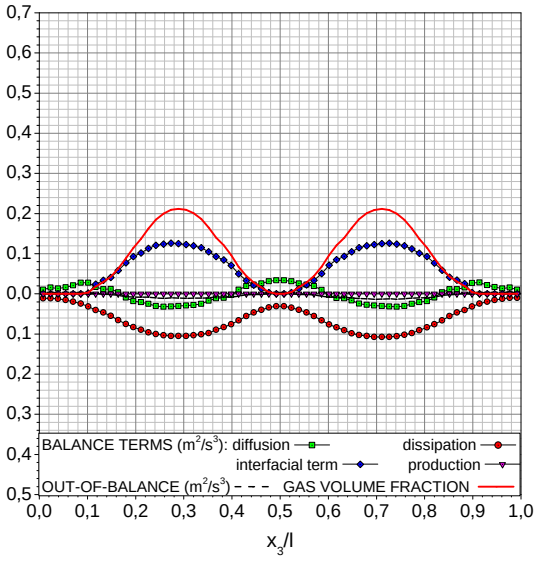

(c) scenario 8BM2

Figure 5.19: Budget of the basic equation for liquid turbulence kinetic energy 2.14 evaluated by module GENERG-TP for free bubble-array flows with different liquid viscosity.

Chapter 6

Assessment of closure assumptions for balance terms in turbulence kinetic energy equation for the liquid phase in bubble-array flows

The objective of this chapter is to test the assessment of closure assumptions for balance terms in turbulence kinetic energy equation for the liquid phase in bubbly gas-liquid flows (k_l equation). In this context, engineering formulations for both single-phase-like and interfacial terms applied in k_l equation of currently used $k-l$, $k-\varepsilon$ and algebraic stress models are put into consideration. Performance of these closure assumptions for here considered bubble-array flows is tested against the corresponding balance terms evaluated according to their basic definitions. Possibilities for the development of improved closure relations are discussed.

6.1 Use of direct numerical simulations for improvement of liquid turbulence models: advantages and limitations

The accurate modelling of bubbly gas-liquid flows crucially depends on the realistic description of the liquid phase turbulence. Current generation of computational fluid dynamic codes for bubbly flows employs several different concepts for modelling of the liquid phase turbulence - starting from a trivial case where turbulence effects are completely neglected to the very complicated differential Reynolds stress models (the review of engineering liquid

turbulence models is given in section 2.2). Among these, far the most popular approach is the two-phase $k-\varepsilon$ model, not only because it is most often used, but also because the range of its application spans from very slow flows in bubble columns and air-lift reactors to the high Reynolds number flows in pipes and ducts. Further, when one takes into account that:

1. laminar models are proven to be inappropriate,
2. algebraic models used in early phase of liquid turbulence modelling are today considered as outdated and
3. differential Reynolds stress models are, due to their complexity, not expected to find a wide application,

it turns out that all the promising approaches, $k-l$, $k-\varepsilon$ and algebraic stress models, are based on the balance equation for the liquid turbulence kinetic energy (k_l equation). It is, therefore, not an exaggeration to state that k_l equation represents a corner stone of turbulence modelling in the domain of bubbly flows.

The current status of closure assumptions employed in k_l equation against the rigorous mathematical formulations given by equation 2.14 can be summarized as follows.

- Single-phase-like terms involve production, diffusion and dissipation of liquid turbulence kinetic energy. Except for being multiplied with the mean liquid volumetric fraction, these terms are, principally, of the same form as the ones involved in the turbulence kinetic energy equation for single-phase flows. Subsequently, the derivation of closure assumptions for single-phase-like terms in k_l equation for bubbly flows is based on an adjustment of the respective single-phase approximations. As it is not clear whether / how far the closure assumptions originally developed for single-phase flows can retain their validity when the dispersed phase is present, such an approach might be argued as highly uncertain.
- Interfacial transfer of the liquid turbulence kinetic energy is in basic k_l equation 2.14 expressed through an additional term that represents the peculiarity of gas-liquid flows and is called interfacial term. On the other hand, effects of suspended bubbles are in modelling approaches either totaly neglected or included through more or less empirically established relations. However, although having a similar starting point, proposed closure assumptions differ from author to author conspicuously. It may, therefore, be stated that a generally accepted closure for the interfacial term is not available.

In relation to the aforementioned, it can be concluded that the formulation of closure assumptions for balance terms in k_l equation needs to be rigorously examined with the

particular attention focused on the effects of moving interfaces. The main goal of this chapter is to test how the corresponding closure assumptions perform for here considered bubble-array flows. In this context, balance terms evaluated by currently available engineering formulations are compared with the ones presented in the previous chapter where rigorous mathematical formulations given by equation 2.14 are used. For the sake of clarity, in the text hereafter the former is called *modelled*, while the latter is named *exact*.

The analyses to be presented do not cover the whole family of liquid turbulence models based on k_l equation. As it could be seen in section 2.2, namely, the complexity of the problem resulted in different ways followed by engineers, not only to specify closure assumptions for balance terms, but also to establish the modelled structure of k_l equation. Therefore, in number of references two-equation models ($k-\varepsilon$ and algebraic stress models) are reported, where the total turbulence kinetic energy is decomposed into two statistically independent contributions: the one resulting from the liquid displacement by moving bubbles and the other one shear-induced that also contains the liquid turbulence kinetic energy in bubble wakes. These models, further, consider the dissipation rate of liquid turbulence kinetic energy as a linear superposition of the dissipation in bubble wakes and the dissipation due to cascading. However, since here applied averaging method provides only the information about the total liquid velocity fluctuations, i.e. the total turbulence kinetic energy and the total dissipation rate, the assessment of closure assumptions applied in such an approach could not be examined. In order to isolate each effect that contributes to the liquid velocity fluctuations, one should introduce two different averaging operators: the first one would be an average over all configurations of the bubble swarm for a given realization of the liquid turbulent field; the second an average over all realizations of the turbulent field, but for a given configuration of the swarm. Such a method is, however, unrealistic, because it is impossible to control each random process separately - the motion of the bubbles is affected by large-scale liquid fluctuations and turbulent eddies in the liquid phase are distorted by velocity gradients induced by bubble displacements [43].

The use of direct numerical simulations (DNS) for the verification and further improvement of closure assumptions employed in liquid turbulence models is associated with significant restrictions. The reported engineering approximations are, namely, developed for the two-fluid formulation of bubbly flows where the strongly heterogeneous gas-liquid flow is replaced by a mixture of two coexisting equivalent fluids with averaged physical properties. The profiles of exact balance terms through the bubble centre, through the bubble hip, in the vicinity of the bubble interface, etc. are useful to elucidate mechanisms governing the liquid turbulence kinetic energy, but are too academic to test semi-empirical engineering descriptions of these mechanisms. When a slow bubble-driven liquid flow between two infinite rigid walls is considered, an engineer focuses only on the wall-normal profiles of corresponding flow parameters. For this reason, considerations in this chapter concern only bubble-array flows with the densest bubble population where the plane averaging[1] is

[1]Since only the plane averaging is considered its indicating with the superscript P is omitted in this chapter.

applied (simulation scenarios 8BM2, 8BM4 and 8BM6).

6.2 Assessment of closure assumptions for single-phase-like terms

This section deals with the assessment of closure assumptions for single-phase-like terms in balance equation for liquid turbulence kinetic energy. In this context, performance of commonly used engineering formulations for production, diffusion and dissipation term is tested for bubble-array flows considered in this work.

6.2.1 Production term

Commonly used model for the production term is based on the assumption that turbulent stresses are proportional to the mean strain rate in the liquid phase:

$$\Pi_l = \alpha_l \nu_l^{\text{eff}} [\nabla \overline{\overline{\mathbf{u}}}_l + \nabla \overline{\overline{\mathbf{u}}}_l^T] : \nabla \overline{\overline{\mathbf{u}}}_l \tag{6.1}$$

where α_l indicates the mean liquid volumetric fraction, $\overline{\overline{\mathbf{u}}}_l$ denotes the mean liquid velocity and ν_l^{eff} represents the so-called effective viscosity of the liquid phase.

In two-phase $k-l$ models the liquid effective viscosity, ν_l^{eff}, is given by [34] [33] [35]:

$$\nu_l^{\text{eff}} = \beta_1 l_{tp} \sqrt{k_l}, \tag{6.2}$$

where l_{tp} denotes the two-phase mixing length, k_l represents the turbulence kinetic energy of the liquid phase and the coefficient $\beta_1 = 0.56$. It is noted that the method proposed for the determination of l_{tp} is not strictly followed when the assessment of closure assumptions applied in $k-l$ model is estimated for bubble-array flows. The definition of l_{tp} as the sum of shear-induced mixing length, l_{si}, and bubble-induced mixing length, l_b, used in [34] [33] [35] for analysis of bubbly flows with high Reynolds numbers is found to be inappropriate for here considered very slow bubble-driven liquid flows. In this context, it was reasonable to neglect l_{si} and assume $l_{tp} = l_b$ (further details about l_b can be seen in section 2.2).

When the two-equation models are concerned, approaches used to evaluate ν_l^{eff} can be classified into the following three groups:

- Only the eddy viscosity evaluated by two-phase $k-\varepsilon$ model, $\nu_l^{k\varepsilon}$, is considered [6] [22] [74] [78] [58] [50] [80] [86] [70] [73] [28] [59] [26] [52] [53] [66]:

$$\nu_l^{\text{eff}} = \underbrace{C_\mu k_l^2 / |\varepsilon_l|}_{\nu_l^{k\varepsilon}}. \tag{6.3}$$

- Beside $\nu_l^{k\varepsilon}$ the molecular viscosity of the liquid phase, ν_l is taken into account [54] [57] [56] [87]:

$$\nu_l^{\text{eff}} = \underbrace{C_\mu k_l^2/|\varepsilon_l|}_{\nu_l^{k\varepsilon}} + \nu_l. \tag{6.4}$$

- In addition to $\nu_l^{k\varepsilon}$ the bubble-induced eddy viscosity, ν_l^b, evaluated by model of Sato et al. [65] is taken into consideration [38]:

$$\nu_l^{\text{eff}} = \underbrace{C_\mu k_l^2/|\varepsilon_l|}_{\nu_l^{k\varepsilon}} + \underbrace{0.6\alpha_g d_b|\overline{\overline{\mathbf{u}}}_r|}_{\nu_l^b}. \tag{6.5}$$

The following notation is used in the aforementioned relations: ε_l represents the dissipation rate of the liquid turbulence kinetic energy, ν_l denotes the kinematic liquid viscosity, α_g is the mean gas volumetric fraction, $\overline{\overline{\mathbf{u}}}_r$ stands for the mean relative velocity between the phases and d_b indicates the equivalent bubble diameter. It is noted that the coefficient $C_\mu = 0.09$ is adopted by all the authors.

Using presented closure assumptions the production term is evaluated for bubble-array flow scenarios 8BM6, 8BM4 and 8BM2. The comparison of obtained results with the exact production term is presented in Figure 6.1 for the bubble-array flow scenario 8BM6. It is noted that analogous evaluations for two other bubble-array flow scenarios (8BM4 and 8BM2) revealed approximatively the same relationship between the exact and modelled production term as observed in the case 8BM6. In this context, the results for these two scenarios are here not presented.

Results presented in Figure 6.1 indicate an extremely poor modelling of the production term. First, none of the applied closure assumptions was able to predict negative values of the production term evaluated by its basic mathematical formulation. Second, absolute magnitudes of the production term are overestimated. However, while this overestimation is in the case of $k-l$ model and $k-\varepsilon$ with $\nu_l^{\text{eff}} = \nu_l^{k\varepsilon}$ moderate, it is strong for the case where $\nu_l^{\text{eff}} = \nu_l^{k\varepsilon} + \nu_l$ and drastic when bubble-induced eddy viscosity is accounted for ($\nu_l^{\text{eff}} = \nu_l^{k\varepsilon} + \nu_l^b$). For the type of bubbly flows considered here this fact is very important. Therefore, since the magnitudes of the exact production term are very low, this term does not influence the balance of the liquid turbulence kinetic energy significantly. In this context, having positive or negative, but very low magnitudes of the production term, will not dramatically change predicted values for the liquid turbulence kinetic energy. However, having the production term evaluated by a $k-\varepsilon$ model where the effective liquid viscosity is modelled as $\nu_l^{\text{eff}} = \nu_l^{k\varepsilon} + \nu_l^b$ will certainly result in unacceptable discrepancies.

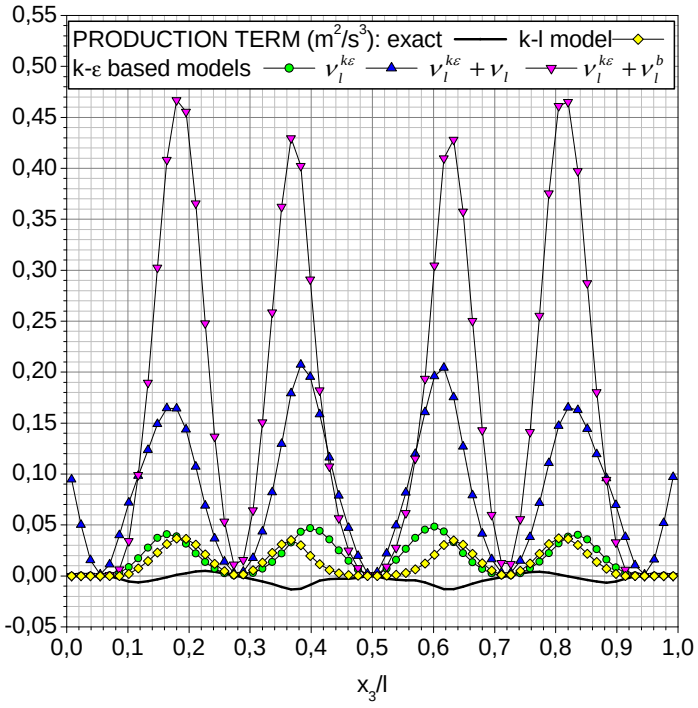

Figure 6.1: Performance of closure assumptions for the production term in k_l equation for bubble-array flow scenario 8BM6.

6.2.2 Diffusion term

The common closure relation for the diffusion term is, like in single phase flows, based on the assumption that the diffusion flux of k_l is proportional to the gradient of k_l:

$$\mathrm{Diff}(k_l) = \nabla \cdot [\alpha_l \nu_l^{\mathrm{Diff}} \nabla k_l], \tag{6.6}$$

where α_l denotes the mean liquid volumetric fraction and ν_l^{Diff} represents coefficient of the diffusion.

In $k-l$ models the diffusion coefficient is evaluated employing the following relation [34] [33] [35]:

$$\nu_l^{\mathrm{Diff}} = \underbrace{0.5\nu_l + \beta_2 l_{tp}\sqrt{k_l}}_{\nu_l^{kl}}, \tag{6.7}$$

where the coefficient $\beta_2 = 0.38$.

When two-equation models are concerned, ν_l^{Diff} is evaluated in an analogous way as the effective eddy viscosity, ν_l^{eff}. Therefore, the different approaches can be selected as follows:

- $\nu_l^{\text{Diff}} = \nu_l^{k\varepsilon}$ (see 6.3) [78] [58] [50] [70] [66]

- $\nu_l^{\text{Diff}} = \nu_l^{k\varepsilon} + \nu_l$ (see 6.4) [6] [22] [74] [80] [86] [73] [54] [28] [59] [26] [52] [53] [57] [56] [87]

- $\nu_l^{\text{Diff}} = \nu_l^{k\varepsilon} + \nu_l^b$ (see 6.5) [38].

Profiles of the diffusion term evaluated on the basis of presented closure assumptions are compared with the exact one in Figure 6.2 for all three considered bubble-array flows. Contrary to the production term where similar relationship between the modelled and exact results is observed for all the considered bubble-array flows, significantly different behaviour of the predicted diffusion term is noticed when scenarios 8BM2, 8BM4 and 8BM6 are compared.

In the case 8BM2 it can be seen that closure assumptions used in $k-l$ and $k-\varepsilon$ models with $\nu_l^{\text{Diff}} = \nu_l^{k\varepsilon} + \nu_l$ underestimate the magnitudes of the diffusion term, but correctly predict the shape of the diffusion profile over the whole channel width. Such a situation is to expect when one reminds that in this the most viscous case significant contribution to the exact diffusion term is made by the molecular diffusion that is in these two modelling approaches included through ν_l. On the other side, closures where the liquid viscosity is not taken into account totally failed predicting approximatively zero values of the diffusion term. Since the analysis of the exact diffusion term has shown that the contribution of the triple correlation in this case of bubble-array flow is negligible, this implies that the modelling of the pressure correlation term is not appropriate.

However, while the results for the scenario 8BM2 give a hope that acceptable modelling of the diffusion term could be achieved establishing a proper closure for the diffusion coefficient, ν_l^{Diff}, the evaluations for the bubble-array flow with the lowest liquid viscosity (scenario 8BM6) clearly indicate that the whole concept of currently used engineering formulations for the diffusion transport of liquid turbulence kinetic energy in bubbly flows is inappropriate. There, it can be seen that dramatic disagreement between the modelled and exact diffusion terms occurs in the two-phase regions of the channel - not only the magnitudes of the diffusion term are incorrectly predicted, but also its sign. The attempt to include the two-phase effects in the diffusion coefficient through the bubble-induced eddy viscosity, ν_l^b, resulted in even higher discrepancies.

Therefore, it may be stated that the modelling approaches where the diffusion flux is related to the gradient of the liquid turbulence kinetic energy cannot provide a realistic description of the transport processes in fluctuating bubble-driven liquid flows.

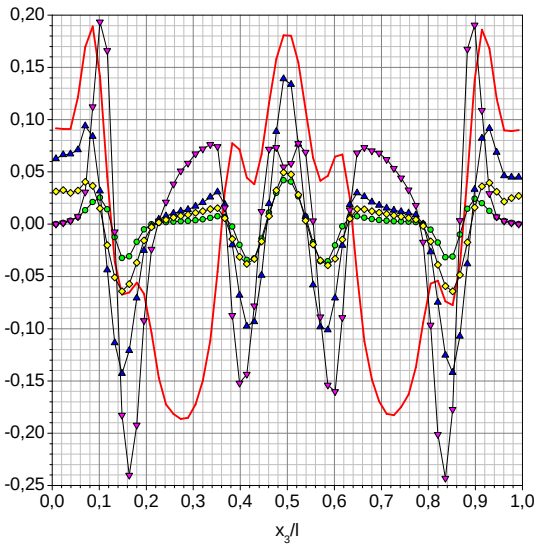

(a) scenario 8BM6

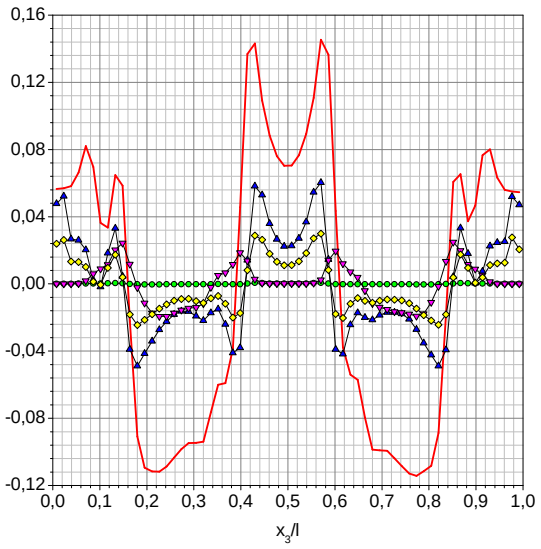

(b) scenario 8BM4

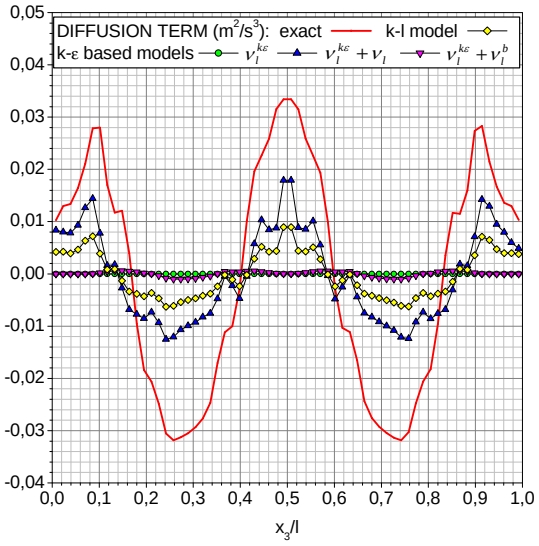

(c) scenario 8BM2

Figure 6.2: Performance of closure assumptions for the diffusion term in k_l equation for bubble-array flows with different liquid viscosity. Notations given in c) apply to the whole Figure.

6.2.3 Dissipation term

While the production and diffusion of liquid turbulence kinetic energy are in all the considered models expressed in the form of closure assumptions, the dissipation term in $k-\varepsilon$ and algebraic stress models is evaluated by a separate transport equation. An analysis of closure assumptions employed in the transport ε_l equation requires corresponding evaluations of involved balance terms on the basis of their strict mathematical formulations. However, such an analysis is not straightforward because the structures of the basic ε_l equation and the transport ε_l equation used in turbulence models are not identical. The basic ε_l equation is derived applying rigorous mathematical formulations of gas-liquid two-phase flows and contains, therefore, number of terms that include higher order correlations of velocity, pressure, viscous stress and interface dynamics [32]. On the other side, the transport ε_l equation is merely a model itself since it is established by introducing dimensionally appropriate terms corresponding to each term in k_l equation. Therefore, testing modelling approaches for the dissipation rate employed in two-equation models requires very complex analysis and is beyond the scope of this work. In this context, when the dissipation term is concerned, considerations are restricted on closure assumptions used in the one-equation $k-l$ model.

Therefore, in [34], [33] and [35] the following closure assumption for the dissipation rate has been proposed:

$$\varepsilon_l = \gamma_1 \alpha_l k_l^{3/2} / l_{tp}, \tag{6.8}$$

where the coefficient $\gamma_1 = 0.18$.

Results obtained using the above definition of the dissipation term are presented in Figure 6.3. Since two-phase mixing length, l_{tp}, as defined in this work involves only the bubble-induced contribution, the dissipation rate in channel regions permanently occupied by the liquid phase could not be computed by 6.8. The comparison of the dissipation term evaluated by expression 6.8 with the exact one shows poor performance of 6.8 for all the considered bubble-array flows.

6.3 Assessment of closure assumptions for interfacial turbulence energy transfer

Contrary to the modelling of single-phase-like terms, where no specific two-phase closure assumptions have been developed, various models for the interfacial term are proposed in the bubbly flow literature. Despite the variety of the modelling approaches, a generally followed concept relates the interfacial term to the work of interfacial forces.

The validity of such an approach has, already, been confirmed in chapter 5. It has, namely,

been shown that for commonly used gas-liquid mixtures with high density ratios the rigorous mathematical formulation of the interfacial term in k_l equation can with, an acceptable accuracy, be approximated by the first term on the right-hand-side of equation 5.28 that represents the work of interfacial forces in the relative motion of bubbles. However, since bubble-array flows considered in this work are associated with the low density ratio ($\varrho_g/\varrho_l = 0.5$), the second term on the right-hand-side of equation 5.28 has to be taken into account. In this context, the performance of closure assumptions for the interfacial turbulence energy transfer is tested against the following sum:

$$\Upsilon = \Upsilon_l + \frac{\varrho_g}{\varrho_l}\Upsilon_g, \tag{6.9}$$

where Υ_l denotes the exact interfacial term for the liquid phase evaluated in chapter 5 and Υ_g represents the exact interfacial term for the gas phase to be evaluated here.

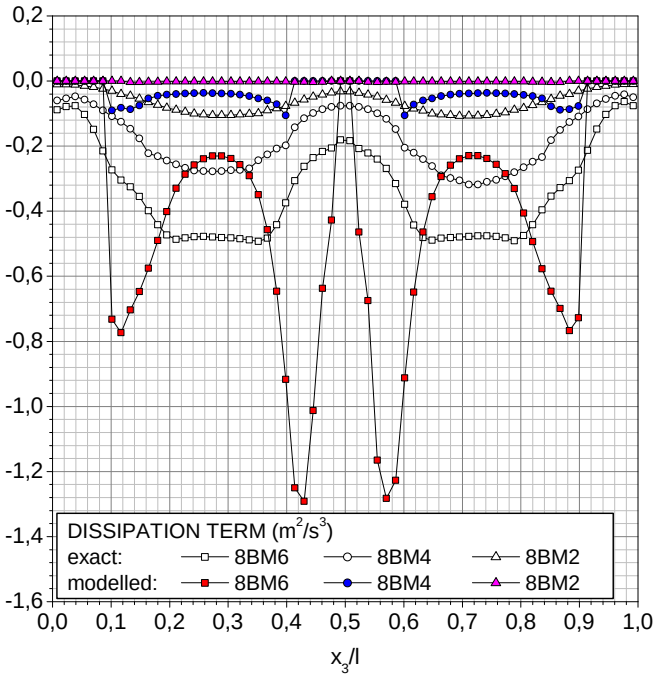

Figure 6.3: Performance of closure assumption for the dissipation term in $k-l$ models for bubble-array flows with different liquid viscosity.

The interfacial generation of the turbulence kinetic energy in the gas phase is defined by [32]:

$$\Upsilon_g = -\frac{1}{\varrho_g}\overline{p'_{gi}u'_{gi\alpha}n_{g\alpha}a_i} + \frac{1}{\varrho_g}\overline{\tau'_{gi\alpha\beta}u'_{gi\alpha}n_{g\beta}a_i}, \tag{6.10}$$

Table 6.1: List of currently used engineering formulations of interfacial turbulence transfer

Reference	Model	Υ^d model	Υ^{nd} model
Morel [50]	M1	D1	ND1
Troshko and Hassan [78]	M2	D1	-
Boisson and Malin [6]	M3	D2	-
Olmos et al. [54]	M4	D3	-
Pfleger and Becker [56]	M5	D4	-
Kataoka and Serizawa [33] [34]	M6	D5	ND2
Lahey and Drew [41]	M7	D6	-
Sheng and Irons [70]	M8	D7	ND3
Hill et al. [26]	M9	D8	-
Oey et al. [53]	M10	D9	-

where $p_{gi}^{'}$, $u_{gi}^{'}$ and $\tau_{gi}^{'}$ respectively represent fluctuating pressure, velocity and viscous stress at the gas side of the phase interface, $n_{g\alpha}$ denotes the unit normal vector at the phase interface pointing outward the gas and a_i stands for the interfacial area concentration.

It is noted that the evaluation of interfacial turbulence effects in the gas phase required the development of numerous procedures concerning the averaging of the instantaneous gas flow, the determination of the interfacial gas quantities and the computation of Υ_g itself. The applied methods are analogous to the ones used when the liquid phase is considered and are, from this reason, here not presented. Instead, the attention is focused to the obtained results.

Figure 6.4 shows that the interfacial generation of turbulence kinetic energy in the liquid phase is higher than in the gas one for all considered bubble-array flows. The observed differences are, however, not dramatic: the ratio Υ_l/Υ_g is ~ 2.441 for scenario 8BM2, ~ 5.181 for scenario 8BM4 and ~ 5.655 for scenario 8BM6. Therefore, accounting for the second term in 6.9 is reasonable for here analyzed gas-liquid flows with the low density ratio. In this context, the performance of closure assumptions applied in engineering turbulence models for bubbly flows is in the text hereafter examined with respect to Υ as defined by 6.9.

An inspection of reported formulations reveals that closure assumptions for the interfacial term can be decomposed into two parts: the one including the drag, Υ^d, and the other one where all other non-drag effects are involved, Υ^{nd}. Table 6.1 shows that Υ^d is not only included in all the models, but is also considered as the only contribution to the interfacial term by most of the authors. In this context, closure approximations for the interfacial term are, here, considered from this point of view.

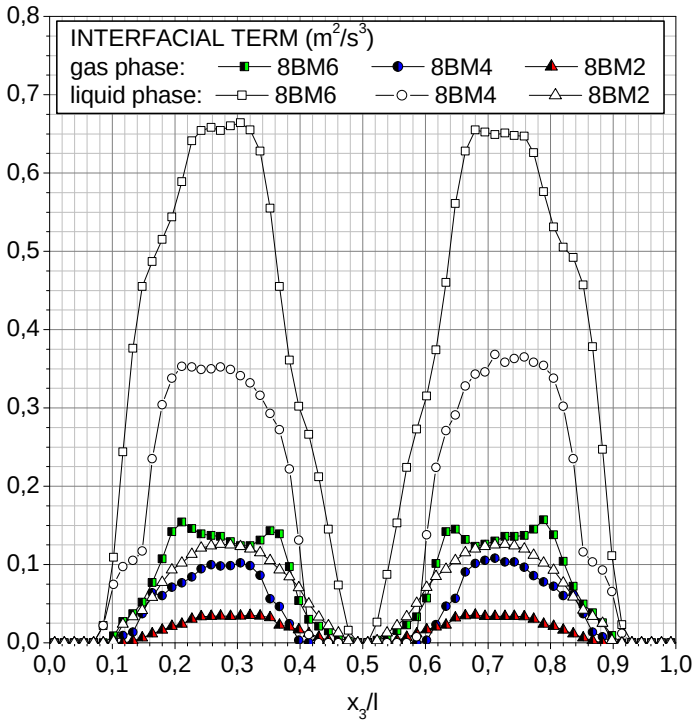

Figure 6.4: Interfacial generation of turbulence kinetic energy of the liquid and the gas phase evaluated on the basis of DNS data for bubble-array flow scenarios with different liquid viscosity.

When the drag contribution to the interfacial term is concerned in Table 6.1 it can be seen that, although the same physical effect is modelled, surprisingly many different approaches are reported. An attempt to group the various models is presented in the following.

1. Υ^d is evaluated on the basis of mean flow properties.

- Υ^d is equal to the total work of the drag force, $\Upsilon^d = W^d$.
  - Model D1 [50] [78]: Work of the drag force is expressed in terms of the mean relative velocity between the phases, $\overline{\overline{\mathbf{u}}}_r$, as:

$$W^d = \mathbf{F}^d \cdot \overline{\overline{\mathbf{u}}}_r, \tag{6.11}$$

    where the drag force exerted to the liquid phase by bubbles is given by:

$$\mathbf{F}^d = \frac{3}{4} C_d \varrho_l \frac{\alpha_g}{d_b} |\overline{\overline{\mathbf{u}}}_r| \overline{\overline{\mathbf{u}}}_r. \tag{6.12}$$

    The drag coefficient is evaluated from the 'standard' relation:

$$C_d = \frac{2}{3}\sqrt{\mathrm{E\ddot{o}}_b} \underbrace{\frac{1 + 17.67\alpha_l^{1.3}}{18.67\alpha_l^{1.5}}}_{f_\alpha}, \tag{6.13}$$

    where $\mathrm{E\ddot{o}}_b$ represents bubble Eötvos number and f_α takes into account multiple bubble effects.

- Υ^d is equal to a portion, C_b, of the total work of the drag force,$\Upsilon^d = C_b W^d$.

  In models D2, D3 and D4 the definition 6.11 is used to express W^d while $\mathbf{F}^d$ is given by 6.12. The values specified for C_b and applied formulations for the drag coefficient are as follows.

  - Model D2 [6]: $C_b = 0.05\alpha_l$ and

$$\begin{aligned} C_d &= 16/\mathrm{Re}_b \quad \text{for } \mathrm{Re}_b < 0.49 \\ &= 20.68/\mathrm{Re}_b^{0.643} \quad \text{for } 0.49 < \mathrm{Re}_b < 100 \\ &= 6.3/\mathrm{Re}_b^{0.385} \quad \text{for } \mathrm{Re}_b \gg 100 \\ &= 8/3 \quad \text{for } \mathrm{Re}_b \gg 100 \text{ and } \mathrm{We}_b > 8 \\ &= \mathrm{We}_b/3 \quad \text{for } \mathrm{Re}_b \gg 100 \text{ and } \mathrm{Re}_b > 2065.1/\mathrm{We}_b^{2.6}, \end{aligned} \tag{6.14}$$

    where Re_b represents bubble Reynolds number and We_b stands for bubble Weber number.

– Model D3 [54]: $C_b = 0.75$ and

$$C_d = \frac{2}{3}\sqrt{\mathrm{E\ddot{o}}_b}(1 - \langle\alpha_g\rangle)^p, \tag{6.15}$$

where $\langle\alpha_g\rangle$ represents the overall gas volumetric fraction and p is an integer dependent on the bubble diameter and gas superficial velocity (for conditions of bubble-array flows considered here p takes the value of 0).

– Model D4 [56]: $C_b = 1.44\alpha_l$ and $C_d = 0.44$ (valid for flow around a rigid sphere at Reynolds number $Re > 1000$).

– Model D5 [34] [33]: Contrary to the above presented models where drag effects are expressed in terms of the mean relative velocity between the phases, $\overline{\overline{\mathbf{u}}}_r$, in this model the terminal velocity of a single bubble is used:

$$u_t = 1.414\left[\frac{\sigma|\mathbf{g}|(\varrho_l - \varrho_g)}{\varrho_l^2}\right]^{1/4}, \tag{6.16}$$

where $\mathbf{g}$ represents the gravity and σ stands for the surface tension. In this context, the drag force, $\mathbf{F}^d$, and the work of the drag force, W^d, are defined replacing[2] $\overline{\overline{\mathbf{u}}}_r$ by u_t in 6.12 and 6.11, respectively. The coefficient of the drag force, C_d, is determined by 6.13, while

$$C_b = 0.075\left(1 - e^{-\frac{yu_f}{26\nu_l}}\right), \tag{6.17}$$

where y represents the distance from the channel wall and u_f denotes the friction velocity.

- Work of the drag force is not explicitly contained in Υ^d.

  – Model D6 [38]:

$$\Upsilon^d = C_p\alpha_l\alpha_g\left(1 + C_d^{\frac{4}{3}}\right)\frac{\overline{\overline{\mathbf{u}}}_r^3}{d_b}, \tag{6.18}$$

where $C_p = 0.25$ and the correlation for C_d is not reported. In here performed computations C_d is evaluated by equation 6.13.

2. Υ^d is formulated taking into account both mean and turbulent quantities.

- Only liquid turbulence quantities are taken into account.

[2]Doing so one should keep in mind that u_t is a scalar and $\overline{\overline{\mathbf{u}}}_r$ is a vector.

– Model D7 [70]:

$$\Upsilon_l^d = C_{k2}\frac{3}{4}\varrho_l C_d \frac{\alpha_g}{d_b}|\overline{\overline{\mathbf{u}}}_r|k_l, \tag{6.19}$$

where k_l represents the liquid turbulence kinetic energy and the constant $C_{k2} = 0.6$. The correlation for the drag coefficient, C_d, is not reported. In here performed computations C_d is evaluated by 6.13.

- Turbulence quantities of both, the gas and the liquid phase, are accounted for.

  – Model D8 [26]

$$\Upsilon^d = \frac{3}{4}\frac{C_d}{d_b}|\overline{\overline{\mathbf{u}}}_r|\left[2\alpha_g\varrho_l(C_t-1)k_l - \frac{\nu_l^{k\varepsilon}}{\alpha_l\alpha_g}\overline{\overline{\mathbf{u}}}_r\cdot\nabla\alpha_g\right], \tag{6.20}$$

where $\nu_l^{k\varepsilon}$ represents the eddy viscosity evaluated by 2.25 and the drag coefficient, C_d is computed from 6.13. The ratio of gas turbulence intensity to the liquid one is given by:

$$C_t = \left(\frac{9+\beta_0\beta}{1+\beta_0\beta}\right)^{\frac{1}{2}} \quad \text{with} \tag{6.21}$$

$$\beta_0 = 0.8 \quad \text{and} \quad \beta = \frac{12}{\pi d_b}\frac{\varrho_l}{\mu_l}\frac{3}{4}C_d\frac{\alpha_g}{d_b}|\overline{\overline{\mathbf{u}}}_r|\left(\frac{l_e}{d_b}\right)^2\frac{1}{\mathrm{Re}_t}, \tag{6.22}$$

where μ_l stands for the liquid viscosity. The turbulence length scale and Reynolds number are, respectively, defined as:

$$l_e = \frac{k_l^{\frac{2}{3}}}{\varepsilon_l} \quad \text{and} \quad \mathrm{Re}_t = \frac{l_e}{\nu_l}\sqrt{\frac{2}{3}\overline{\overline{k}}_l}, \tag{6.23}$$

where ε_l stands for the dissipation rate of the liquid turbulence kinetic energy.

– Model D9 [53]: The procedure analogous to the one in Model D8 is applied, but the coefficient C_t is, instead of using the equation 6.21, formulated as:

$$C_t = \frac{3+\beta}{1+\beta+2\varrho_g/\varrho_l}. \tag{6.24}$$

The non-drag contributions to the interfacial term are taken into account only by a few authors. In the following these models are outlined.

- Υ^{nd} is equal to the work of the added mass force, $\mathbf{F}^{am}$:

  – Model ND1 [50]:

$$\Upsilon^{nd} = \underbrace{C_{am}\frac{1+2\alpha_g}{1-\alpha_g}\alpha_g\varrho_l\left(\frac{D_g\overline{\overline{\mathbf{u}}}_g}{D\vartheta} - \frac{D_l\overline{\overline{\mathbf{u}}}_l}{D\vartheta}\right)}_{\mathbf{F}_l^{am}}\cdot\overline{\overline{\mathbf{u}}}_r, \tag{6.25}$$

where $D/D\vartheta$ indicates the material derivative and $C_{am} = 0.5$ is the added mass coefficient.

- Υ^{nd} takes into account turbulence reduction by bubble interfaces
  - Model ND2 [34] [33]:

$$\Upsilon^{nd} = \alpha_g \varrho_l \frac{k_l^{2/3}}{d_b}. \tag{6.26}$$

- Υ^{nd} is related to the energy transfer between the mean and fluctuating liquid flow.
  - Model ND3 [70]:

$$\Upsilon^{nd} = C_{k1} \alpha_g \alpha_l \Pi_l, \tag{6.27}$$

where Π_l represents the liquid turbulence production by mean shear and the constant $C_{k1} = 2.5$.

The performance [3] of all the presented closure assumptions is tested for the bubble-array flow scenario 8BM6 (see Figure 6.5). The comparison of obtained results with the exact interfacial term, Υ, revealed the following:

- Models M3, M6, M8, M9 and M10 totally failed predicting almost zero magnitudes of interfacial term, Υ. For this reason, these closure assumptions are eliminated from further considerations.
- Models M4, M5 and M7 underestimated the magnitudes of the exact interfacial term, Υ.
- Models M1 and M2 resulted in acceptable discrepancies and seem to be the promising approach in interfacial term modelling.

[3] Models for interfacial term are presented in the form as they are published in references. However, in order to be compatible with its exact formulation (equation 5.18), normalization with liquid density is performed where necessary when performance of interfacial term modelling is examined.

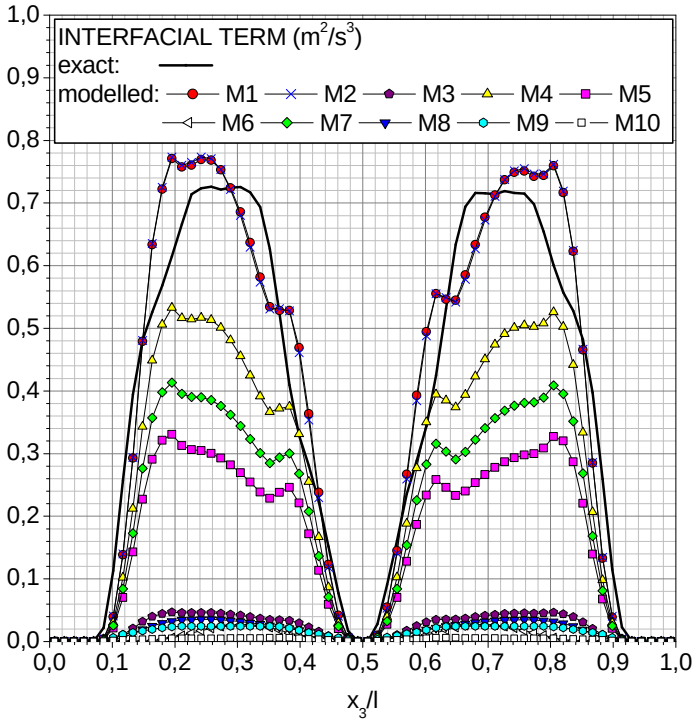

Figure 6.5: Performance of closure assumptions for the interfacial turbulence transfer for bubble-array flow scenario 8BM6.

An inspection of models M1 and M2 shows that the good agreement with the exact results seen in Figure 6.5) is achieved by a quite simple approach where the interfacial term Υ is identified with the work of the drag force[4]. In this context, it is interesting to see how such an approach performs for bubble-array flow scenarios 8BM2 and 8BM4. Figure 6.6 shows that the obtained results do not look optimistic at all: pronounced underestimation of the exact interfacial term is seen in scenario 8BM4 and total suppression of interfacial effects in the scenario 8BM2.

Taking into account significantly different flow conditions in scenarios 8BM2 and 8BM4 the situation presented in Figure 6.6 is not surprising. In relation to this it is supposed that the better performance of models M1 and M2 can be achieved by use of advanced correlations for the drag coefficient. In this context, the following analysis are performed.

[4]The evaluation of the work of the added mass force in Model 1 revealed its negligible contribution to the interfacial term Υ.

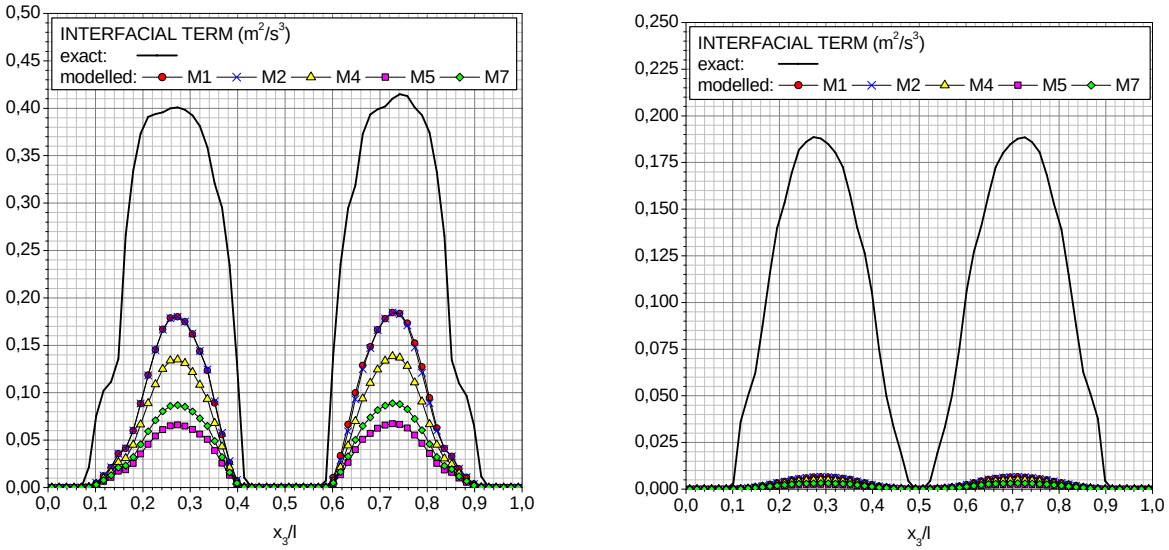

(a) scenario 8BM4 (b) scenario 8BM2

Figure 6.6: Performance of closure assumptions for the interfacial turbulence transfer for bubble-array flow scenarios with increased liquid viscosity.

Since the correlation for the drag coefficient given by expression 6.13 is developed for the most often used two-phase mixture of air bubbles in water, its applicability to bubble-array flows 8BM4 and especially 8BM2 is seriously limited due to increased liquid viscosity. On the other side, using direct numerical simulations to investigate balance of forces acting on bubbles Tomiyama [77] derived constitutive equations for the drag coefficient, that have experimentally been verified within a wide range of fluid properties (bubble Eötvos number $\mathrm{E\ddot{o}}_b = 10^{-2} - 10^3$, Morton number, $\mathrm{M} = 10^{-14} - 10^7$ and bubble Reynolds number, $\mathrm{Re}_b = 10^{-3} - 10^5$). For a pure gas-liquid system the following drag coefficient relation has been proposed:

$$C_d = max\left[min\left(\frac{16}{\mathrm{Re}_b}(1 + 0.15\mathrm{Re}_b^{0.687}), \frac{48}{\mathrm{Re}_b}\right), \frac{8}{3}\frac{\mathrm{E\ddot{o}}_b}{\mathrm{E\ddot{o}}_b + 4}\right]. \tag{6.28}$$

In the context of aforementioned the following analysis is performed. The interfacial terms as defined in models M1 and M2 are evaluated using the drag coefficient formulation 6.28 instead of 6.13. The comparison of obtained results for the interfacial term with the exact ones presented in Figure 6.7 reveals the importance of the proper drag coefficient formulation. Therefore, although discrepancies between the modelled and the exact profiles are not negligible, modelling concept for the interfacial term adopted in models M1 and M2,

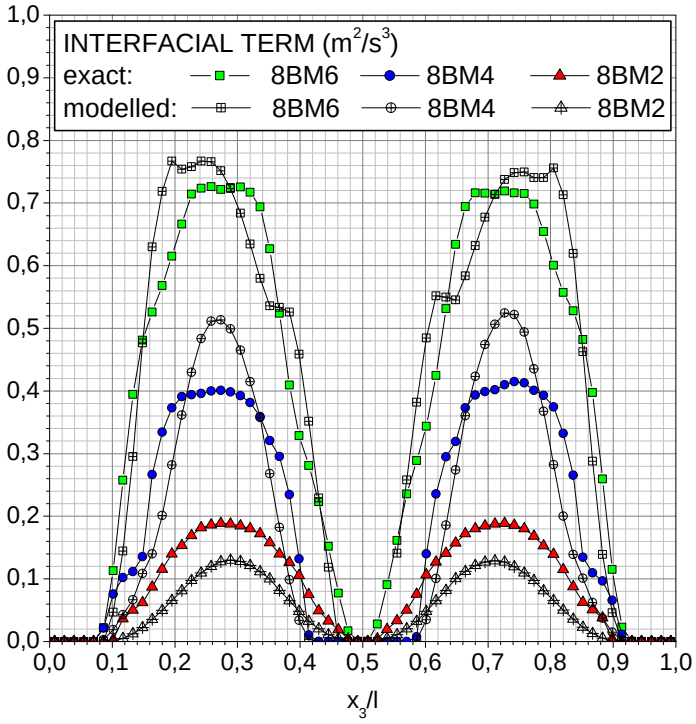

Figure 6.7: Improvement of closure assumptions for interfacial turbulence transfer (models M1 and M2) by use of the advanced drag coefficient relation 6.7.

where the bubbly flows are assumed to be drag dominated, may be judged as correct. Further, when one takes into account that in Figure 6.7 results computed by a semi-empirical engineering approach are drawn versus ones evaluated on the basis of rigid mathematical formulations for an extremely wide range of bubbly flow parameters, it may be stated that modelling of the interfacial turbulence effects by models M1 and M2 is acceptable.

Chapter 7

Summary and conclusions

This work presents investigations of liquid phase turbulence in dilute bubble-driven flows. The investigations are based on statistical analyses of liquid velocity fluctuations, where the liquid turbulence kinetic energy is considered as the fundamental turbulence quantity. The main goal of the performed analyses was to improve understanding of mechanisms in which bubbles alter generation, redistribution and dissipation of turbulence kinetic energy in the liquid phase. A secondary goal concerns assessment of closure assumptions commonly used in engineering liquid turbulence models.

Input data for the aforementioned liquid turbulence analysis are provided by direct numerical simulations (DNS) of bubbly flows. The simulated flow pattern, called bubble-array flow, represents an approximation of steady developed flow regime in flat bubble columns. A total of five numerical runs are performed, where the rise of moderately large bubbles within cubic channel with two lateral walls (ratio of bubble diameter to the channel size, $d_b/l = 0.25$) is computed. All the simulations are conducted for the same phase density ratio ($\Gamma_\varrho = 0.5$), phase viscosity ratio ($\Gamma_\mu = 1$) and bubble Eötvös number, (Eö $= 3.065$). In order to consider effects of suspended gas content, $\langle\alpha_g\rangle$, motion of monodisperse bubble swarms consisting of only one bubble ($\langle\alpha_g\rangle = 0.818\%$, five bubbles ($\langle\alpha_g\rangle = 4.088\%$) and eight bubbles ($\langle\alpha_g\rangle = 6.544\%$) is simulated. In these simulations Morton number $\mathrm{M} = 3.06 \cdot 10^{-6}$ is specified. In order to analyze the influence of bubble shape and bubble rise velocity on characteristics of generated liquid flow, two additional simulations are performed, where the rise of bubble swarms consisting of 8 bubbles through the liquids with viscosity increased by a factor of $\sqrt{10}$ i.e. 10 is considered (corresponding values of Morton number are $\mathrm{M} = 3.06 \cdot 10^{-4}$ and $\mathrm{M} = 3.06 \cdot 10^{-2}$).

The DNS data show significant differences in motion of simulated bubble-arrays. A stable bubble rise velocity and a rectilinear bubble trajectory characterizes the steady state of fixed bubble-array flow (configuration with one bubble within the computational domain). The motion of individual bubbles in multiple bubble scenarios with low liquid viscosity is

accompanied with a pronounced unsteadiness of bubble rise velocity and significant lateral deviations of bubble paths. In the simulation scenario with 8 bubbles an approximatively symmetric bubble distribution is observed with two distinctive bubble populations rising at constant distance from the channel walls. In the numerical experiment with 5 bubbles a more or less uniform bubble distribution over channel cross-section with no distinctive pattern with respect to the channel walls is found. Despite the significant differences in the dynamics of the considered bubble-array flows, bubbles generally took an approximatively identical ellipsoidal shape (bubble axis aspect ratio $\kappa \sim 1.5$) in all the simulation scenarios of bubble-array flows with low liquid viscosity.

The motion of aforementioned bubble-arrays with 8 bubbles through the liquid with viscosity increased by a factor of $\sqrt{10}$ resulted in slightly ellipsoidal bubbles (bubble axis aspect ratio $\kappa = 1.132$) and significantly suppressed lateral deviations of individual bubble paths, whereas the liquid viscosity increase of 10 times made the bubbles rise almost rectilinearly keeping the initial spherical shape.

An inspection of the instantaneous liquid flow has revealed that the rise of bubble-arrays induces complex perturbations of the liquid phase. In the following main results of performed investigations of these bubble-induced liquid velocity fluctuations are summarized and conclusions are drawn.

Performed statistical analyses have shown the following characteristics of the fluctuating liquid flow generated by rise of mono-disperse bubble-arrays:

1. Computed probability density functions have revealed a significant amplification of liquid velocity fluctuations in multiple bubble systems. The velocity fluctuations in vertical direction strongly dominate the horizontal ones implying a significant degree of the liquid turbulence anisotropy in all the considered bubble-array flows.

2. The distribution of liquid turbulence kinetic energy (k_l) in bubble-array flows is, principally, dictated by bubble distribution - in domains where bubbles rise high values of k_l are observed, while in single-phase regions perturbations of the liquid phase are significantly lower.

3. Effects of the gas volumetric fraction on magnitudes of the liquid turbulence kinetic energy are found to be as follows.

   (a) In very dilute two-phase mixtures an almost proportional increase of the liquid turbulence kinetic energy with the gas volumetric fraction is observed, what means that the total agitation of the liquid phase can be represented as a linear superposition of perturbations performed by the motion of individual bubbles.

   (b) In low viscosity mixtures with the dense bubble packing, where bubble-bubble distances are short, the increase of the liquid turbulence kinetic energy with

the gas content is stronger due to mutual hydrodynamic interactions of bubble wakes through which a greater amount of the kinetic energy is supplied to the fluctuating liquid flow.

4. An increase of the liquid viscosity causes a drastic decrease of the liquid turbulence kinetic energy. Three flow parameters have been identified as reasons for such a behaviour of the liquid turbulence kinetic energy: the decrease of bubble rise velocity, the change of bubble shape from ellipsoidal to spherical (reflected through the decrease of added mass) and the suppression of vortical structures in bubble wakes.

The aforementioned results are in agreement with observations reported in other experimental and/or DNS based studies of bubble-driven liquid flows. It is, however, noted that the comparisons with measured data could be done only on the level of general trends observed in behaviour of liquid turbulence quantities. This situation is caused by dramatically different physical properties of gas-liquid mixtures used in experimental investigations (usually air-water systems) from the ones that, due to computational restrictions, have to be specified in this study. Comparisons with corresponding DNS based analyses are also limited for two reasons. The first one is related to quite different parameters of gas-liquid systems considered in DNS studies of other authors. The second one concerns the peculiarity of DNS performed in this work, where bubble-column-like flows with included effects of columns walls are simulated. Since no simulation of multiple bubble systems within confined geometries are reported so far, even parameters concerning the motion of bubbles and the bubble-induced liquid flow could not be verified.

The quantitative analysis of balance equation for liquid turbulence kinetic energy performed in this work represents a conceptually new approach to investigating turbulence phenomena in bubbly flows. In relation to this, hereafter presented results can be considered as original and represent the most important findings of the presented research by which some light is shed on complex physical mechanisms in which bubbles alter the liquid turbulence.

The evaluation and analysis of balance terms in equation for liquid turbulence kinetic energy on the basis of their rigorous mathematical definitions have revealed the following.

1. The transfer of kinetic energy between the mean and fluctuating flow of the liquid phase (so-called production term) plays an appreciable role only for the very academic case of fixed bubble-array flow, where it behaves as a sink, while in other investigated cases of free bubble-array flows is very low and may, therefore, be neglected.

2. The viscous dissipation of the liquid turbulence kinetic energy non-linearly increases with the magnitude of suspended gas content. The intensification of the dissipation rate is, especially, pronounced in the simulation scenario with the densest bubble population, where eddies generated in the wake of an individual bubble decay faster owing to the shear stress associated with the motion of other bubbles. An engineering

based analysis has shown that the viscous dissipation of kinetic energy of liquid velocity fluctuations generated by the rise of identical bubble-arrays through liquids with different viscosity scales well with the relative phase velocity.

3. The generation of liquid turbulence kinetic energy is continuously maintained by moving bubbles through the work of fluctuating liquid stress upon the bubble interfaces. An analysis based on DNS data has revealed that the interfacial generation of the liquid turbulence kinetic energy can, with reasonable accuracy, be represented as the work of interfacial forces in the relative motion of bubbles.

4. The evaluation of the diffusion term revealed an intensive transport of liquid turbulence kinetic energy from the domains where bubbles rise to the regions of the channel permanently occupied with the liquid phase. A detailed analysis of the diffusion subterms has shown that the molecular transport process plays an important role and may, therefore, not be neglected in bubble-driven liquid flows. The dominant form of the diffusive transport in all the bubble-array flows with low liquid viscosity turned out to be correlation including pressure fluctuations. Although in the very viscous bubble-array flow the redistribution of the liquid turbulence kinetic energy is, mainly, performed by the molecular diffusion, the pressure correlation still plays an important role. This result implies that the commonly used modelling approaches, where the diffusion due to pressure fluctuations is of minor importance, cannot provide a realistic description of transport processes in fluctuating bubble-driven liquid flows.

The above presented analyses of individual balance terms revealed that only the interfacial term is the source of liquid turbulence kinetic energy. Since this term has a local character determined by the distribution of bubbles, the local non-equilibrium between the turbulence generation and turbulence dissipation gives importance to the diffusion term that redistributes turbulence kinetic energy over the flow domain. The balance of liquid turbulence kinetic energy is, therefore, governed by the competition among three mechanisms: the viscous dissipation, the diffusive transport and the external generation by bubble interfaces.

The DNS based evaluations of balance terms in the basic equation for liquid turbulence kinetic energy are, further, used to estimate the accuracy of corresponding closure assumptions applied in engineering models for the liquid phase turbulence. The performed analyses have revealed the following:

1. Currently used closure assumptions failed to realistically predict both, the production term and the diffusion term - while the production term is strongly overestimated, the diffusion transport of liquid turbulence kinetic energy is strongly underestimated by all closure assumptions. The closure assumption for the dissipation term proposed in $k - l$ models is also found to be inappropriate - the magnitude of the dissipation

rate in channel regions with high gas volumetric fractions is underestimated, while in the domains with low gas content is strongly overestimated. These results imply that the reliable modelling of liquid phase turbulence in bubbly flows cannot be achieved by an extension of closure assumptions originally derived for the turbulence in single-phase flows. However, while the analyses performed in this work suggest neglecting the production term, only hints for the modelling of the diffusion term could be offered. A DNS based analysis of individual contributions to the diffusion term revealed that the proper modelling of liquid turbulence redistribution in bubbly flows with low Reynolds number requires improved assumptions for the diffusion transport by pressure fluctuations. The development of reliable closures for the pressure correlation term cannot be achieved by an experimental approach since current measuring techniques are inoperative in view of providing complete data for the pressure field. Such considerations must, therefore, fully rely on the use of DNS data and are proposed as a further challenging task in DNS based investigations of the liquid phase turbulence in bubbly flows.

2. While the most of the available closure assumptions resulted in a strong underestimation of the interfacial turbulence generation, predictions made by the model of Morel [50] are quite acceptable. An inspection of the results obtained by this modelling approach indicated that the interfacial term can be formulated as the work of the drag force. It is, however, emphasized, that a great caution has to be paid when the closure relation for the drag coefficient is specified. According to the analysis performed here, the use of drag coefficient relations proposed by Tomiyama [77] is suggested.

Finally, it is noted that the aforementioned analyses suffer from the lack of an extensive validation. As mentioned in Introduction, highly resolved data on three-dimensional flow field and phase-interface topology necessary for the quantitative analysis of balance equation for liquid turbulence kinetic energy cannot be provided with the current status of measuring techniques, so that an experimental validation of the results presented in this work was not possible. On the other side, a validation by numerical results of other authors could not be made since to the best knowledge of the author no DNS based analyses of mechanisms governing balance of liquid turbulence kinetic energy is reported so far.

Bibliography

[1] M. Afshar and B.R. Baliga. Numerical simulations of fully-developed turbulent bubbly two-phase flows in straight ducts of triangular cross-section. In *Proceedings of* 2^{nd} *International Symposium on Two-phase Flow Modelling and Experimentation*, volume II, page 1071, Pisa, Italy, May 23-26 1999.

[2] S. Becker, A. Sokolichin, and G. Eigenberger. Gas-liquid flow in bubble columns and loop reactors: Part II. Comparison of detailed experiments and flow simulations. *Chemical Engineering Science*, **49**:5747–5762, 1994.

[3] R. Bel F'Dhila and O. Simonin. Eulerian prediction of a turbulent bubbly flow downstream a sudden pipe expansion. In *Proceedings of* 6^{th} *Workshop on Two-phase Flow Predictions*, pages 264–273, Erlangen, Germany, April 11-14 1992. ISBN 3-89336-116-2.

[4] D. Bhaga and M. E. Weber. Bubbles in viscous liquids: shapes, wakes and velocities. *Journal of Fluid Mechanics*, **105**:61–85, 1981.

[5] A. Biesheuvel and L. Van Wijngaarden. Two-phase flow equations for a dilute dispersion of gas bubbles in liquid. *Journal of Fluid Mechanics*, **148**:301–318, 1984.

[6] N. Boisson and M.R. Malin. Numerical prediction of two-phase flow in bubble columns. *International Journal for Numerical Methods in Fluids*, **23**:1289–1310, 1996.

[7] C. Brücker. Structure and dynamics of the wake of bubbles and its relevance for bubble interaction. *Physics of Fluids*, **11**:1781–1796, 1999.

[8] D. Bröder, M. Sommerfeld, and S. Tisler. Analysis of the hydrodynamics in a bubble column by phase-doppler anemommetry. In *Proceedings of* 3^{rd} *International Conference on Multiphase Flow*, Lyon, France, June 8-12 1998. CD-ROM paper 601.

[9] B. Bunner and G. Tryggvason. Dynamics of homogeneous bubbly flows. Part 1. Rise velocity and microstructure of the bubbles. *Journal of Fluid Mechanics*, **466**:17–52, 2002.

[10] B. Bunner and G. Tryggvason. Dynamics of homogeneous bubbly flows. Part 2. Velocity fluctuations. *Journal of Fluid Mechanics*, **466**:53–84, 2002.

[11] B. Bunner and G. Tryggvason. Effect of bubble deformation on the properties of bubbly flows. *Journal of Fluid Mechanics*, **495**:77–118, 2003.

[12] A. Cartellier, O. Kashinsky, and L. Timkin. Experimental characterisation of pseudo-turbulence in Poiseuille bubbly flows. In *Proceedings of* 2^{nd} *International Conference on Multiphase Flow*, volume 2, pages IF1–27 – IF1–33, Kyoto, Japan, April 3-7 1998.

[13] J. Chahed, Colin C., and Masbernat L. Turbulence and phase distribution in bubbly pipe flow under microgravity condition. *Journal of Fluids Engineering*, **124**:951–956, 2002.

[14] J. Chahed, L. Masbernat, and V. Roig. Turbulence and void fraction prediction in a turbulent bubbly wake. In *Proceedings of* 3^{rd} *International Conference on Multiphase Flow*, Lyon, France, June 8-12 1998. CD-ROM paper 402.

[15] J. Chahed, V. Roig, and L. Masbernat. Eulerian-Eulerian two-fluid model for turbulent gas-liquid bubbly flows. *International Journal of Multiphase Flow*, **29**:23–49, 2003.

[16] W. Chedron, G. Grötzbach, M. Samstag, M. Sengpiel, and I. Tiseanu. Experimental investigation of air-water bubbly flow in vertical pipes. In *Proceedings of* 3^{rd} *International Conference on Multiphase Flow*, Lyon, France, June 8-12 1998. CD-ROM paper 404.

[17] R. Clift, J.R. Grace, and M.E. Weber. *Bubbles, drops and particles*. Academic Press, New York, 1978.

[18] E. Delinoij, F.A. Lammers, J.A.M. Kuipers, and W.M.P. Van Swaaij. Dynamic simulation of dispersed gas-liquid two-phase flow using a discrete bubble model. *Chemical Engineering Science*, **52**:1429–1458, 1997.

[19] D.A. Drew. Mathematical modelling of two-phase flow. *Ann. Rev. Fluid Mech*, **15**:261–291, 1983.

[20] T.B. Gataski and C.G. Speziale. On explicit algebraic stress models for complex turbulent flows. *Journal of Fluid Mechanics*, **254**:59–78, 1993.

[21] B.E. Ghidersa. *Finite Volume-based Volume−of−Fluid Method for the Simulation of Two-phase Flows in Small Rectangular Channels*. PhD thesis, Universität Karlsruhe (TH), FZKA 6478, 2003.

[22] J. Grienberger and H. Hofmann. Investigation and modelling of bubble columns. *Chemical Engineering Science*, **47**:2215–2220, 1992.

[23] J.S. Groen, R.G.C. Oldeman, R.F. Mudde, and H.E.A. Van Den Akker. Coherent structures and axial dispersion in bubble column reactors. *Chemical Engineering Science*, **51**:2511–2520, 1992.

[24] M.F. Göz, B. Bunner, M. Sommerfeld, and G. Tryggvason. Microstructure of a bidisperse swarm of spherical bubbles. In *Proceedings of 2002 ASME Fluids Engineering Division Summer Meeting*, Montreal, Canada, July 14-18 2002. Paper FEDSM2002-31395.

[25] Y.A. Hassan, J. Ortiz-Villafuerte, and W.D. Schmidl. Investigation of three-dimensional two-phase flow structure in a bubbly pipe flow. *Measurement Science Technology*, **9**:309–326, 1998.

[26] D.P. Hill, D.M. Wang, A.D. Gosman, and R.I. Issa. Numerical prediction of two-phase bubbly flow in a pipe. In *Proceedings of the* 2^{nd} *International Conference on Multiphase Flow*, volume 3, pages MO3–1 – MO3–6, Kyoto, Japan, April 3-7 1995.

[27] J.O. Hinze. *Turbulence. An introduction to its mechanism and theory.* McGraw-Hill Book Company, New York, 1959.

[28] J. Hua and C. Wang. Numerical simulation of bubble-driven liquid flows. *Chemical Engineering Science*, **55**:4159–4173, 2000.

[29] M. Ishii. *Thermo-fluid dynamic theory of two-phase flow.* Eyrolles, Paris, 1975.

[30] I. Kataoka. Local instant formulation of two-phase flow. *International Journal of Multiphase Flow*, **12**:745–758, 1986.

[31] I. Kataoka, D.C. Besnard, and A. Serizawa. Basic equations of turbulence and modelling of interfacial transfer terms in gas-liquid two-phase flow. *Chemical Engineering Communications*, **118**:221–236, 1992.

[32] I. Kataoka and A. Serizawa. Basic equations of turbulence in gas-liquid two-phase flow. *International Journal of Multiphase Flow*, **15**:843–855, 1989.

[33] I. Kataoka and A. Serizawa. Modelling and analysis of turbulence structure in bubbly flow. In *Proceedings of* 1^{st} *International Symposium on Two-phase Flow Modelling and Experimentation*, volume 1, pages 459–466, Rome, Italy, October 9-11 1995.

[34] I. Kataoka and A. Serizawa. Modelling and prediction of turbulence in bubbly two-phase flow. In *Proceedings of* 2^{nd} *International Conference on Multiphase Flow*, volume 3, pages MO2–11 – MO2–16, Kyoto, Japan, April 3-7 1995.

[35] I. Kataoka and A. Serizawa. Turbulence characteristics and their application to multi-dimensional analysis of two-phase flow. In *Proceedings of* 8^{th} *International Topical Meeting on Nuclear Reactor Thermal-Hydraulics*, volume 3, pages 1677–1683, Kyoto, Japan, September 30 - October 4 1997.

[36] I. Kataoka, A. Serizawa, and D.C. Besnard. Prediction of turbulence suppresion and turbulence modeling in bubbly two-phase flow. *Nuclear Engineering and Design*, **141**:145–158, 1993.

[37] T. Koso, H. Nakayama, Y. Kuniba, and H. Tokai. Turbulent mixing of matter by a rising bubble. In *Proceedings of* 5^{th} *International Conference on Multiphase Flow*, Yokohama, Japan, May 30 - June 4 2004. CD-ROM paper 525.

[38] R. T. Lahey Jr. and D. Drew. An analysis of two-phase flow and heat transfer using a multidimensional, multi-field, two-fluid computational fluid dynamics (CFD) model. presented at Japan/US Seminar on Two-Phase Flow Dynamics, Santa Barbara, California, USA, June 5-8 2000.

[39] R.T. Lahey Jr. Turbulence and phase distribution phenomena in two-phase flow. In *Proceedings of ICHMT Seminar on Transient Phenomena in Multiphase Flow, Hemisphere Press*, Dubrovnik, Yugoslavia, May 24-30 1987.

[40] R.T. Lahey Jr. The CFD analysis of multidimensional phenomena in multiphase flow. In *Proceedings of* 2^{nd} *International Conference on Multiphase Flow*, volume 3, pages MO2–1 – MO2–9, Kyoto, Japan, April 3-7 1995.

[41] R.T. Lahey Jr. and D. Drew. The analysis of two-phase flow and heat transfer using a multidimensional, four field two-fluid model. *Nuclear Engineering and Design*, **204**:29–44, 2001.

[42] R.T. Lahey Jr., M. Lopez de Bertodano, and O.C. Jones Jr. Phase distribution in complex geometry conduits. *Nuclear Engineering and Design*, **141**:177–201, 1993.

[43] M. Lance and J. Bataille. Turbulence in the liquid phase of a uniform bubbly air-water flow. *Journal of Fluid Mechanics*, **222**:95–118, 1981.

[44] M. Lance, J.L. Marie, and J. Bataille. Homogeneous turbulence in bubbly flows. *Journal of Fluids Engineering*, **113**:295–300, 1991.

[45] T.J. Liu and S.G. Bankoff. Structure of air-water bubbly flow in a vertical pipe - i local mean velocity and turbulence measurements. *Journal of Heat and Mass Transfer*, **36**:1049–1060, 1993.

[46] M. Lopez de Bertodano, R.T. Lahey Jr., and O.C. Jones. Development of a $k-\varepsilon$ model for bubbly two-phase flow. *Journal of Fluids Engineering*, **116**:128–134, 1994.

[47] M. Lopez de Bertodano, R.T. Lahey Jr., and O.C. Jones. Phase distribution in bubbly two-phase flow in vertical ducts. *International Journal of Multiphase Flow*, **20**:805–818, 1994.

[48] M. Lopez de Bertodano, S.J. Lee, R.T. Lahey Jr., and D.A. Drew. The prediction of two-phase turbulence and phase distribution phenomena using a Reynolds stress model. *Journal of Fluids Engineering*, **112**:107–113, 1990.

[49] I. Michiyoshi and A. Serizawa. Turbulence in two-phase bubbly flow. *Nuclear Engineering and Design*, **95**:253–267, 1986.

[50] C. Morel. Turbulence modelling and first numerical simulations in turbulent two-phase flows. In *Proceedings of* 11^{th} *Symposium on Turbulent Shear Flows*, pages P3–10 – P3–15, Grenoble, France, September 8-11 1997.

[51] R.F. Mudde, D.J. Lee, and L.S. Fan. Role of coherent structures on Reynolds stresses in a 2D bubble column. *AIChE Journal*, **55**:913–926, 1997.

[52] R.F. Mudde and H.E.A. Van Den Akker. 2D and 3D simulations of an internal airlift loop reactor on the basis of a two-fluid model. *Chemical Engineering Science*, **56**:6351–6358, 2001.

[53] R.S. Oey, R.F. Mudde, and H.E.A. Van Den Akker. Sensitivity study on interfacial closure laws in two-fluid bubbly flow simulations. *AIChE Journal*, **49**:1621–1636, 2003.

[54] E. Olmos, C. Gentric, and N. Midoux. Numerical description of flow regime transitions in bubble column reactors by a multiple gas phase model. *Chemical Engineering Science*, **58**:2113–2121, 2003.

[55] J. Ortiz-Villafuerte, W. D. Schmidl, and Y. A. Hassan. Three-dimensional PTV study of the surrounding flow and wake of a bubble rising in a stagnant liquid. *Experiments in Fluids*, Suppl.:202–210, 2000.

[56] D. Pfleger and S. Becker. Modelling and simulation of the dynamic flow behaviour in a bubble column. *Chemical Engineering Science*, **56**:1737–1747, 2001.

[57] D. Pfleger, S. Gomes, N. Gilbert, and H.G. Wagner. Hydrodynamic simulations of laboratory scale bubble columns fundamental studies of the Eulerian-Eulerian modelling approach. *Chemical Engineering Science*, **54**:5091–5099, 1999.

[58] M.S. Politano, P.M. Carrica, and J. Converti. A model for turbulent polydisperse two-phase flow in vertical channels. *International Journal of Multiphase Flow*, **29**:1153–1182, 2003.

[59] V.V. Ranade and Y. Tayalia. Modelling of fluid dynamics and mixing in shallow bubble column reactors: influence of sprager design. *Chemical Engineering Science*, **56**:1667–1675, 2001.

[60] F. Risso and K. Ellingsen. Velocity fluctuations in a homogeneous dilute dispersion of high-Reynolds-number rising bubbles. *Journal of Fluid Mechanics*, **453**:395–410, 2002.

[61] W. Rodi. *Turbulence models and their application in hydraulics - a state of the art review*. IAHR/AIRH Monograph, Delft, 1980.

[62] W. Sabisch. *Dreidimensionale numerische Simulation der Dynamik von aufsteigenden Einzelblasen und Blasenschwärmen mit einer Volume−of−Fluid−Methode*. PhD thesis, Universität Karlsruhe (TH), FZKA 6478, 2000.

[63] W. Sabisch, M. Wörner, G. Grötzbach, and D.G. Cacuci. 3D volume-of-fluid simulation of a wobbling bubble in a gas-liquid system of low Morton number. In *Proceedings of* 4^{th} *International Conference on Multiphase Flow*, New Orleans, USA, May 27-June 1 2001. CD-ROM paper 244.

[64] Y. Sato, M. Sadatomi, and K. Sekoguchi. Momentum and heat transfer in two-phase bubble flow - II. *Journal of Multiphase Flow*, **7**:179–190, 1981.

[65] M. Sato Y., Sadatomi and K. Sekoguchi. Momentum and heat transfer in two-phase bubble flow - I. *Journal of Multiphase Flow*, **7**:167–177, 1981.

[66] A. Serizawa, K. Huda, Y. Yamada, and I. Kataoka. Experiment and numerical simulation of bubbly two-phase flow across horizontal and inclined rod bundles. *Nuclear Engineering and Design*, **175**:131–146, 1997.

[67] A. Serizawa and I. Kataoka. Phase distribution in two-phase flow. In *Proc. of ICHMT Seminar on Transient Phenomena in Multiphase Flow, Hemisphere Press*, Dubrovnik, Yugoslavia, May 24-30 1987.

[68] A. Serizawa and I. Kataoka. Turbulence suppresion in bubbly two-phase flow. *Nuclear Engineering and Design*, **122**:1–16, 1990.

[69] A. Serizawa, I. Kataoka, and I. Michiyoshi. Turbulence structure of air-water bubbly flow - II. local properties. *Journal of Multiphase Flow*, **2**:235–246, 1975.

[70] Y.Y. Sheng and G.A. Irons. Measurements and modelling of turbulence in the gas-liquid two-phase zone during gas injection. *Mettalurgical Transactions B*, **24B**:695–705, 1993.

[71] A. Sokolochin and G. Eigenberger. Applicability of the standard k-epsilon turbulence model to the dynamic simulation of bubble columns. part I: Detailed numerical simulations. *Chemical Engineering Science*, **49**:5735–5746, 1993.

[72] A. Sokolochin, G. Eigenberger, and A. Lapin. Simulation of buoyancy driven bubbly flow: Established simplifications and open questions. *AIChE Journal*, **50**:24–45, 2004.

[73] P. Spicka, M.D. Dias, and J.C.B. Lopes. Gas-liquid flow in a 2D column: Comparison between experimental data and cfd modelling. *Chemical Engineering Science*, **56**:6367–6383, 2001.

[74] H.F. Svendsen, H.A. Jakobsen, and R. Torvik. Local flow structures in internal loop and bubble column reactors. *Chemical Engineering Science*, **47**:3297–3304, 1992.

[75] H. Tennekes and J.L. Lumley. *A first course in turbulence*. MIT Press, Cambridge, 1987.

[76] T.G. Theofanous and J. Sullivan. Turbulence in two-phase dispersed flows. *Journal of Fluid Mechanics*, **116**:343–362, 1982.

[77] A. Tomiyama. Strugle with computational bubble dynamics. In *Proceedings of* 3^{rd} *International Conference on Multiphase Flow*, Lyon, France, June 8-12 1995. CD-ROM paper 356.

[78] A.A. Troshko and Y.A. Hassan. A two-equation turbulence model of turbulent bubbly flows. *International Journal of Multiphase Flow*, **27**:1965–2000, 2001.

[79] L. Van Wijngaarden. On pseudo turbulence. *Theoretical and Computational Fluid Dynamics*, **10**:449–458, 1998.

[80] Ch. Vial, S. Poncin, G. Wild, and N. Midoux. Experimental and theoretical analysis of the hydrodynamics in the riser of an external loop airlift reactor. *Chemical Engineering Science*, **57**:4745–4762, 2002.

[81] S.K. Wang, S. J. Lee, Jr. O.C. Jones, and R.T. Lahey Jr. Statistical analysis of turbulent two-phase pipe flow. *Journal of Fluids Engineering*, **112**:89–96, 1990.

[82] D.C. Wilcox. *Turbulence modelling for CFD*. DCW Industries, La Canada, Calif., 1993.

[83] M. Wörner. The influence of gas-liquid density ratio on shape and rise velocity of an ellipsoidal bubble: A numerical study by 3D Volume-of-Fluid computations. In F.-P. Schlinder, editor, *VDI Forschritt-Berichte, Reihe 3, Nr. 738*, pages 67–84, VDI Verlag Düsseldorf, 2002. ISBN 3-18-373803-1.

[84] M. Wörner. Invariance of the velocity field induced by a bubble rising steadily through liquid under variation of the gas-liquid density ratio. In *Proceedings of the German-Japanesse Workshop on Multi-Phase Flow*, pages G10–G21, Karlsruhe, Germany, August 25-27 2002.

[85] M. Wörner, W. Sabisch, G. Grötzbach, and D.G. Cacuci. Volume-averaged conservation equations for Volume-of-Fluid interface tracking. In *Proceedings of* 4^{th} *International Conference on Multiphase Flow*, New Orleans, USA, May 27-June 1 2001. CD-ROM paper 245.

[86] J. Wu and K. Minemura. Numerical prediction of turbulent bubbly two-phase flow in a rotating complicated duct. *International Journal for Numerical Methods in Fluids*, **29**:811–826, 1999.

[87] L.X. Zhou, M. Yang, C.Y. Lian, L.S. Fan, and D.J. Lee. On the second-order moment turbulence model for simulating a bubble column. *Chemical Engineering Science*, **57**:3269–3281, 2002.

[88] I. Zun. Transverse migration of bubbles influenced by walls in vertical bubbly channel. *International Journal of Multiphase Flow*, **6**:583–585, 1980.

Appendix A

Bubble trajectories

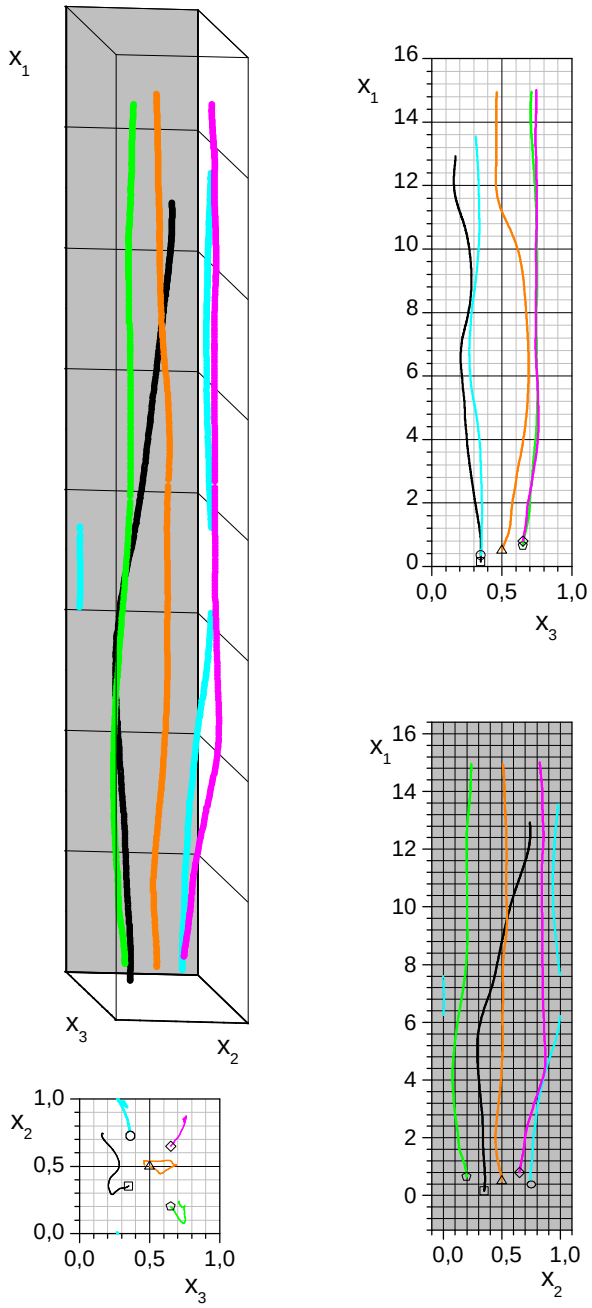

Figure A.1: Trajectories of individual bubbles for numerical run 5BM6. Symbols represent initial bubble centroid positions. Back channel wall is highlighted gray and the other one is considered to be transparent.

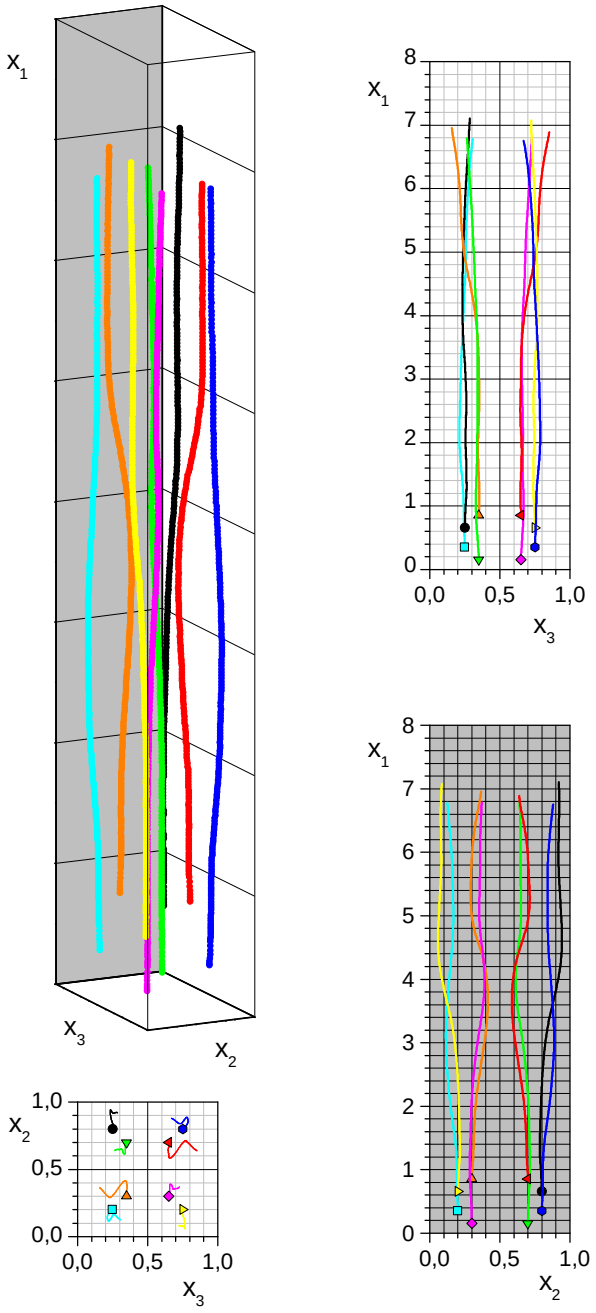

Figure A.2: Trajectories of individual bubbles for numerical run 8BM6. Symbols represent initial bubble centroid positions. Back channel wall is highlighted gray and the other one is considered to be transparent.

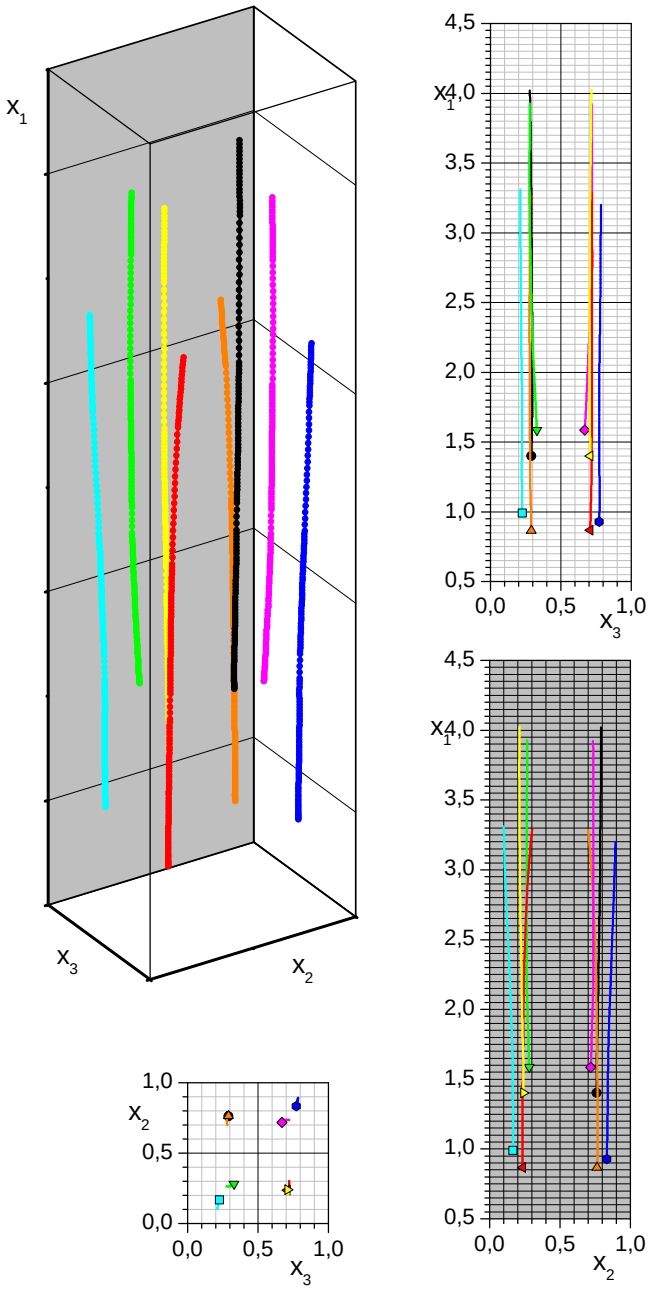

Figure A.3: Trajectories of individual bubbles for numerical run 8BM4. Symbols represent initial bubble centroid positions. Back channel wall is highlighted gray and the other one is considered to be transparent.

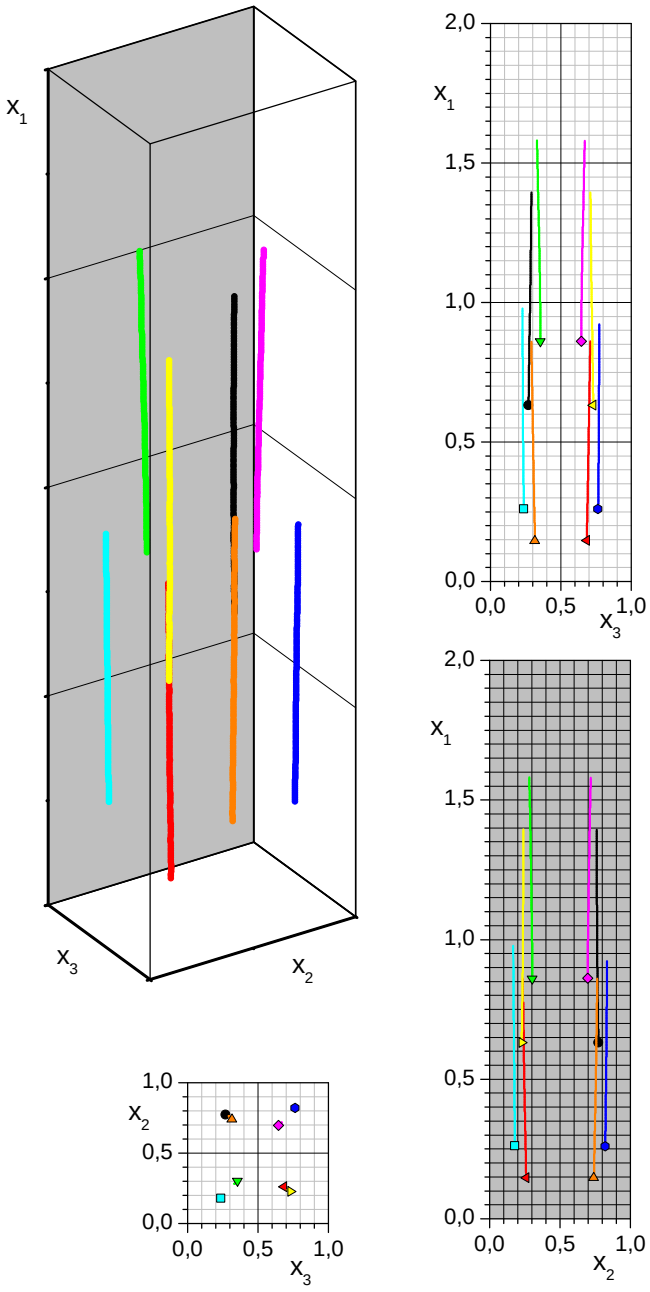

Figure A.4: Trajectories of individual bubbles for numerical run 8BM2. Symbols represent initial bubble centroid positions. Back channel wall is highlighted gray and the other one is considered to be transparent.

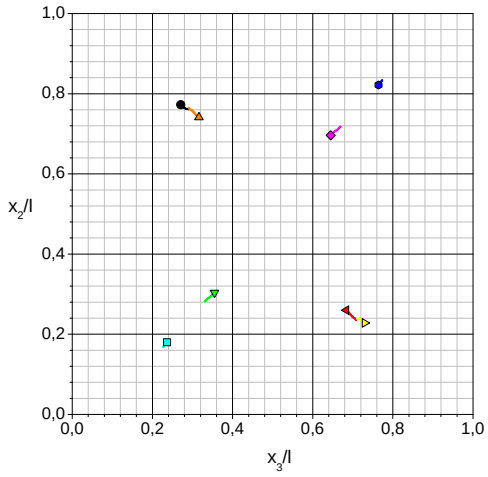

(a) scenario 8BM2

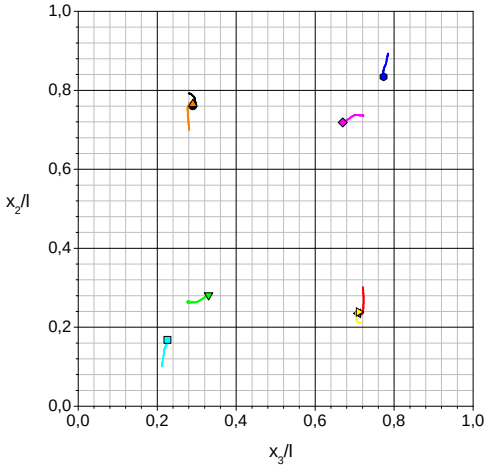

(b) scenario 8BM4

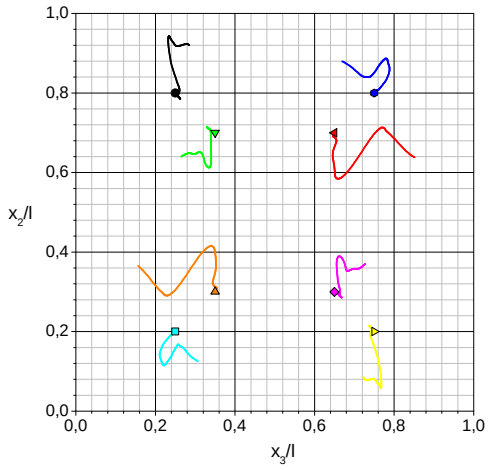

(c) scenario 8BM6

Figure A.5: Lateral movements of individual bubbles rising through the liquid with different viscosity. Symbols indicate initial bubble positions.

Appendix B

Distribution of mean gas volumetric fraction

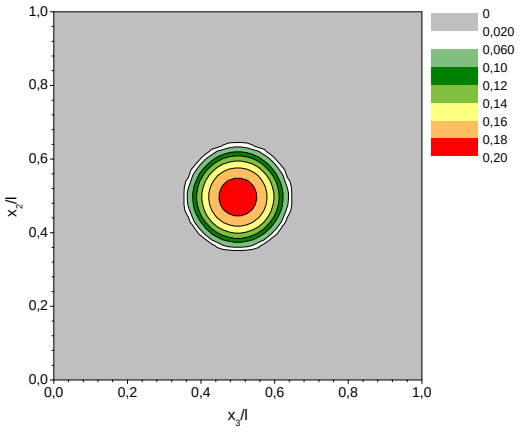

(a) scenario 1BM6

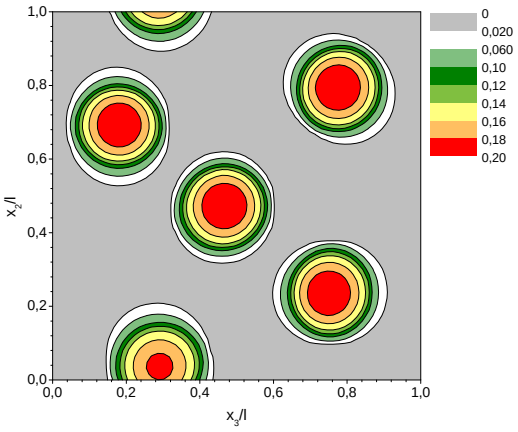

(b) scenario 5BM6

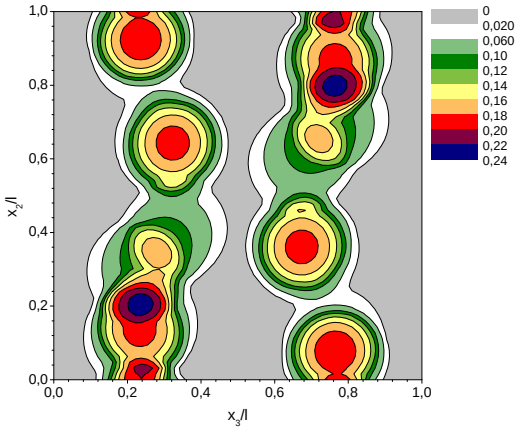

(c) scenario 8BM6

Figure B.1: Mean gas volumetric fraction in bubble-array flows with different number of bubbles.

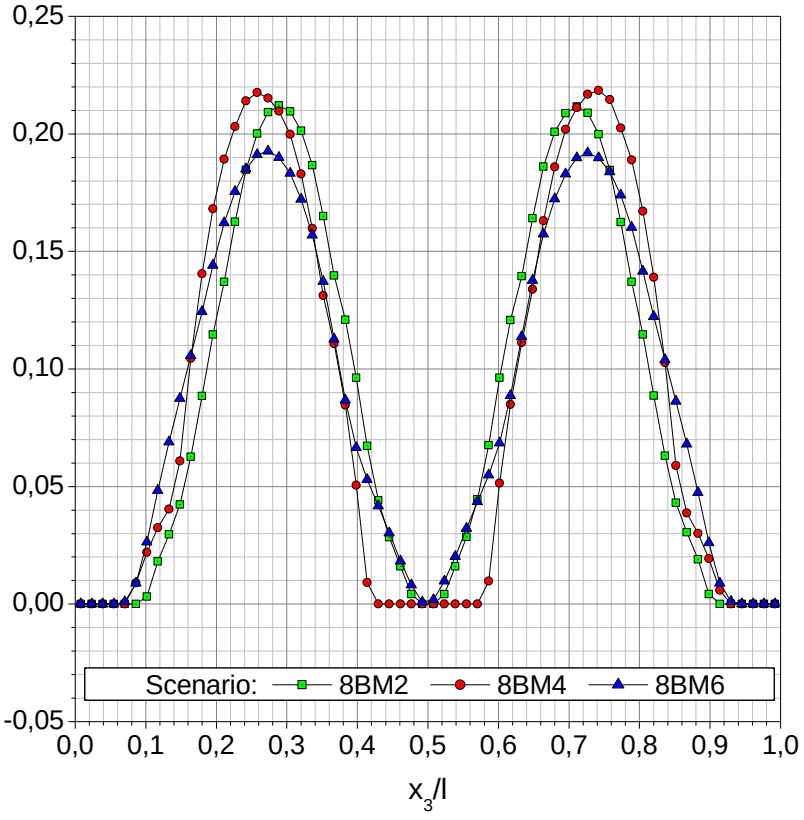

Figure B.2: Mean gas volumetric fraction in bubble-array flows with different liquid viscosity.

Appendix C

Root-mean-square of liquid velocity fluctuations

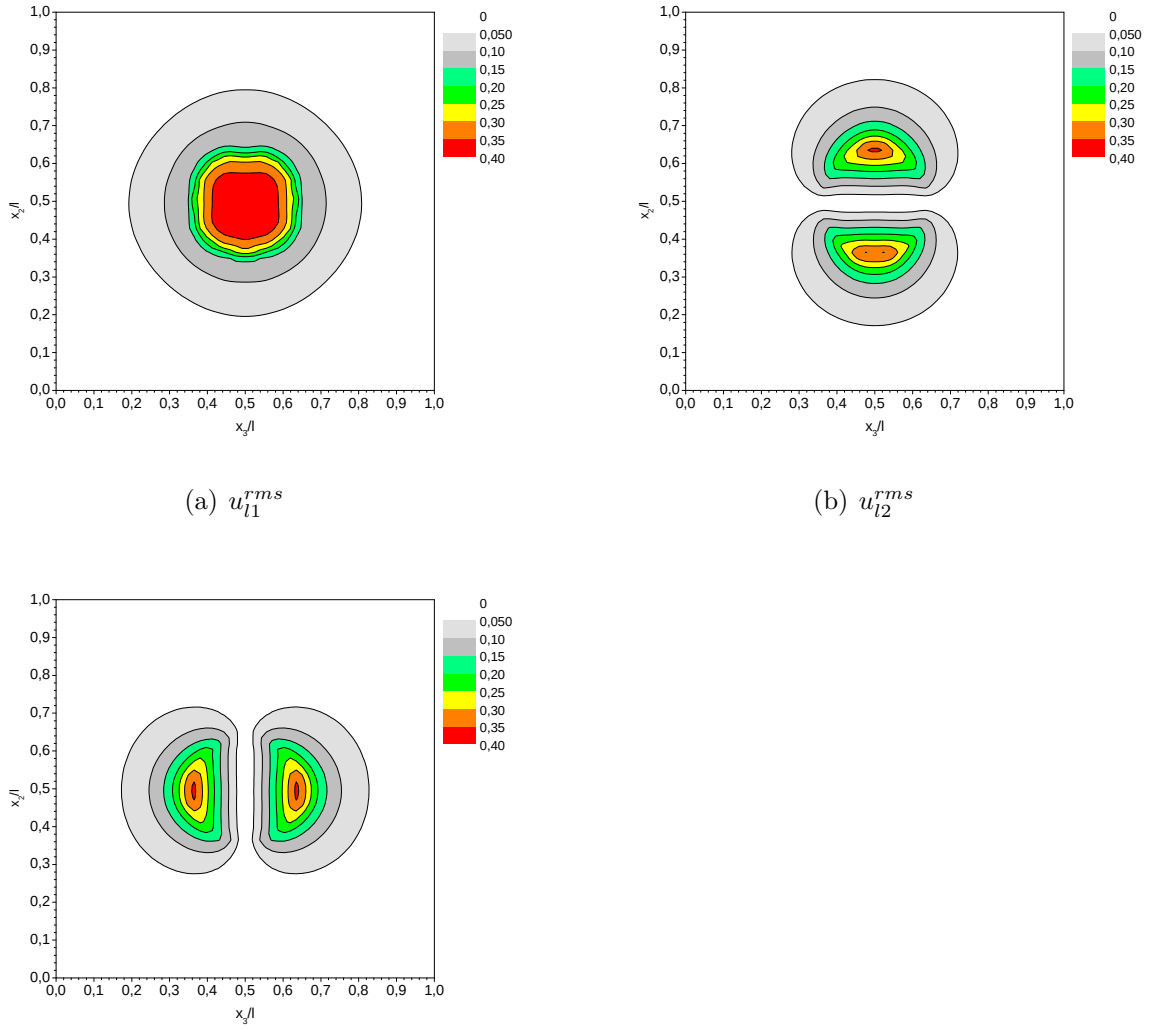

(a) u_{l1}^{rms} (b) u_{l2}^{rms}

(c) u_{l3}^{rms}

Figure C.1: Root-mean-square of liquid velocity fluctuations for fixed bubble-array flow (scenario 1BM6).

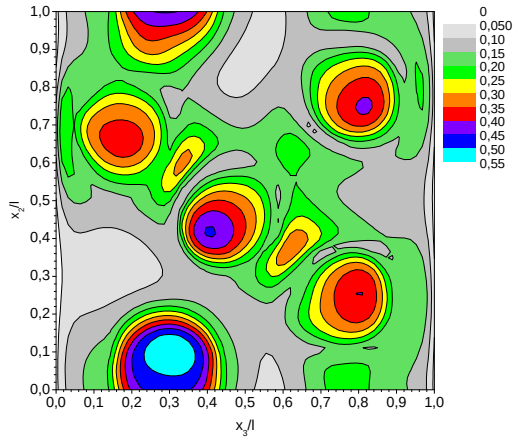

(a) u_{l1}^{rms}

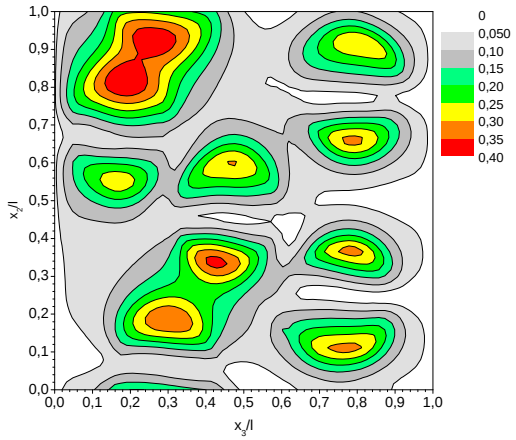

(b) u_{l2}^{rms}

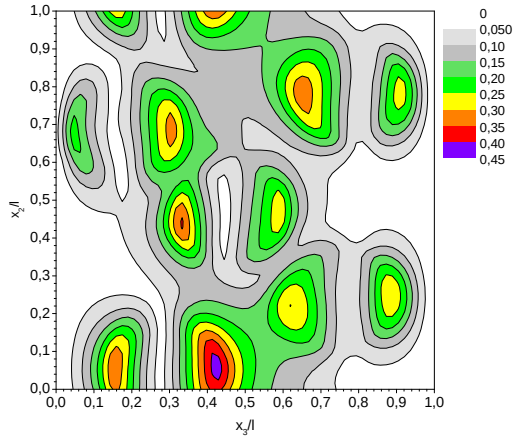

(c) u_{l3}^{rms}

Figure C.2: Root-mean-square of liquid velocity fluctuations for free bubble-array flow scenario 5BM6.

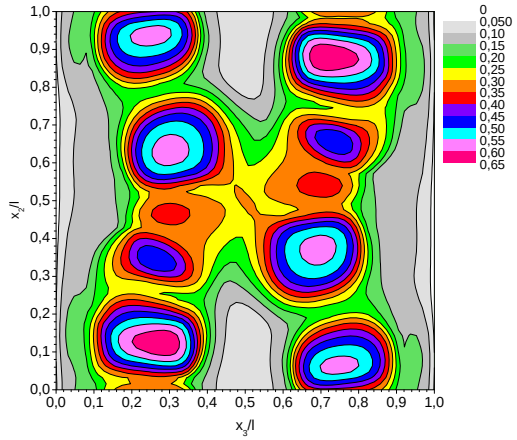

(a) u_{l1}^{rms}

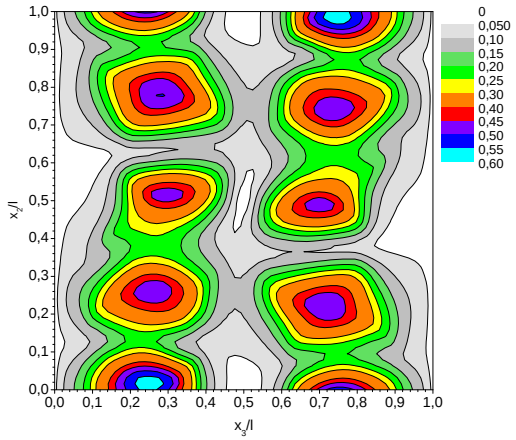

(b) u_{l2}^{rms}

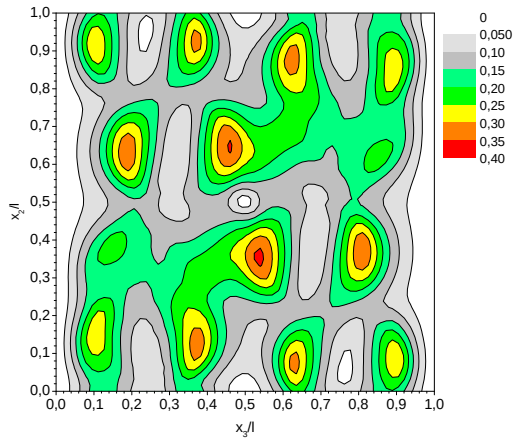

(c) u_{l3}^{rms}

Figure C.3: Root-mean-square of liquid velocity fluctuations for free bubble-array flow scenario 8BM6.

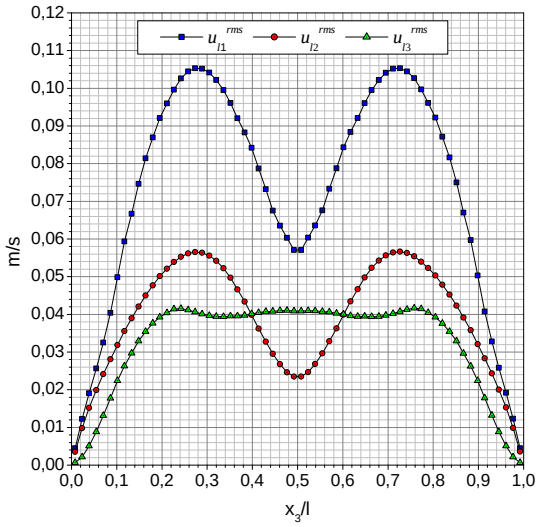

(a) scenario 8BM2

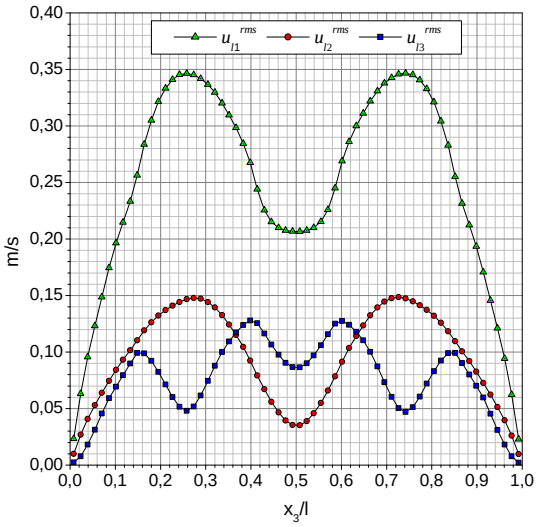

(b) scenario 8BM4

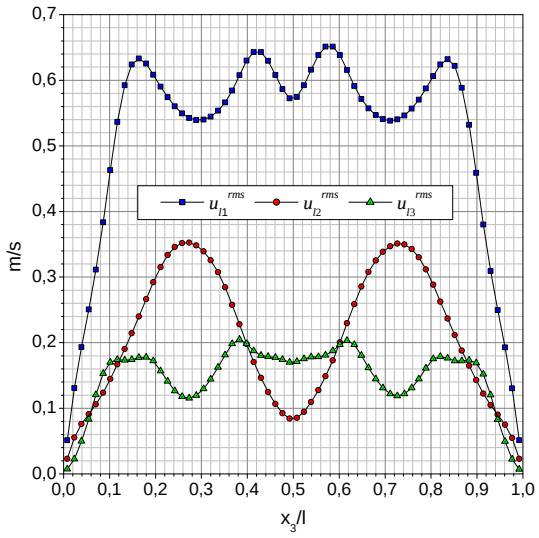

(c) scenario 8BM6

Figure C.4: Root-mean-square of liquid velocity fluctuations induced by motion of bubble-arrays through liquids with different viscosity.